ISTANBUL TECHNICAL UNIVERSITY ★ GRADUATE SCHOOL

MODELLING-CONTROL OF SHIMMY OSCILLATIONS IN AIRCRAFT LANDING GEAR AND APPLICATION DESIGN

M.Sc. THESIS

Kemal OKUYAN

Department of Defense Technologies

Autonomous Systems Subprogramme

JULY 2024

ISTANBUL TECHNICAL UNIVERSITY ★ GRADUATE SCHOOL

MODELLING-CONTROL OF SHIMMY OSCILLATIONS IN AIRCRAFT LANDING GEAR AND APPLICATION DESIGN

M.Sc. THESIS

Kemal OKUYAN
(514201017)

Department of Defense Technologies

Autonomous Systems Subprogramme

Thesis Advisor: Assoc. Prof. Seher EKEN

JULY 2024

ISTANBUL TEKNİK ÜNİVERSİTESİ ★ LİSANSÜSTÜ EĞİTİM ENSTİTÜSÜ

UÇAK İNİŞ TAKIMLARINDA SHIMMY TİTREŞİMİNİN MODELLENMESİ-KONTROLÜ VE UYGULAMA TASARIMI

YÜKSEK LİSANS TEZİ

Kemal OKUYAN
(514201017)

Savunma Teknolojileri Anabilim Dalı

Otonom Sistemler Alt Programı

Tez Danışmanı: Doç. Dr. Seher EKEN

TEMMUZ 2024

Kemal OKUYAN, a M.Sc. student of İTU Graduate School student ID 514201017, successfully defended the thesis/dissertation entitled “MODELLING-CONTROL OF SHIMMY OSCILLATIONS IN AIRCRAFT LANDING GEAR AND APPLICATION DESIGN”, which he prepared after fulfilling the requirements specified in the associated legislations, before the jury whose signatures are below.

Thesis Advisor : **Assoc. Prof. Seher EKEN** ....
İstanbul Technical University

Jury Members : **Assis. Prof. Dr. İsmail BAYEZIT** ....
Istanbul Technical University

Assis. Prof. Dr. Serhat YILMAZ ....
National Defence University

Date of Submission : 24 May 2024
Date of Defense : 05 July 2024

FOREWORD

I would like to thank my advisor, Associate Professor Seher EKEN, and my friend, Ismail Bozdag, for her guidance and support throughout my studies.

Mayıs 2024

Kemal OKUYAN
(Mechanical Engineer)

TABLE OF CONTENTS

Page

FOREWORD .... **vii**
TABLE OF CONTENTS .... **ix**
ABBREVIATIONS .... **xi**
SYMBOLS .... **xiii**
LIST OF TABLES .... **xv**
LIST OF FIGURES .... **xvii**
SUMMARY .... **xxiii**
ÖZET .... **xxv**
1. INTRODUCTION **1**
1.1 Literature Review 1
1.2 Methodology 2
2. LANDING GEAR SYSTEMS **5**
2.1 Landing Gear Configurations 5
2.2 Landing Gear Components 6
2.2.1 Shock absorbers 7
2.2.1.1 Solid spring 7
2.2.1.2 Steel spring 7
2.2.1.3 Rubber spring 7
2.2.1.4 Liquid spring 7
2.2.1.5 Air pneumatic 7
2.2.1.6 Oleo-Pneumatic 7
2.2.1.7 Spring force 8
2.2.1.8 Single gas chamber systems 9
2.2.1.9 Double gas chamber systems 10
2.2.1.10 Damper force 11
2.2.1.11 Oleo-pneumatic systems with metering pins 12
2.2.1.12 Oleo-pneumatic systems with poppet valf 14
2.2.2 Tire 15
3. LANDING GEAR SHIMMY OSCILLATIONS **19**
3.1 Eigenvalues and Characteristic Equation 20
3.2 Routh-Hurwitz Criterion 21
3.3 One DOF Third Order Landing Gear Shimmy Model 21
3.3.1 One DOF third order stable/unstable region 25
3.3.1.1 One DOF third order shimmy model e-V plane stability status 25
3.3.1.2 One DOF third order shimmy model F_z-V plane stability status 31
3.4 Two DOF Fifth Order Landing Gear Shimmy Model 36
3.4.1 Two DOF third order stable/unstable region 38
3.4.1.1 Two DOF third order shimmy model e-V plane stability status 38
3.4.1.2 Two DOF third order shimmy model F_z-V plane stability status 43
4. LANDING GEAR SHIMMY CONTROL **49**
4.1 Linear Quadratic Regulator (LQR) 49
4.1.1 LQR controller design for 1 DOF system 50

4.1.2 LQR controller design for 2 DOF system 55
5. LANDING GEAR SHIMMY APPLICATION DESIGN (LaGeSh) 61
6. CONCLUSION AND FUTURE WORK 65
6.1 Future Recommendations 65
7. REFERENCES 67
APPENDICES 69
APPENDIX A 70
CURRICULUM VITAE 77

ABBREVIATIONS

DOF **:** Degree of Freedom

LQR **:** Linear Quadratic Regulator

SYMBOLS

a	: Half contact length [m]
$C_{m\alpha}$	: Tire self-alligning moment derivative [m/rad]
$C_{f\alpha}$	: Tire side force derivative [1/rad]
c_{Ψ}	: Torsional damping constant [Nm/rad/s]
c_{δ}	: Lateral damping constant [Nm/rad/s]
e	: Caster length [m]
F_c	: Cornering Force [N]
F_z	: Vertical force [N]
I_x	: Lateral area moment of inertia [kgm^2]
I_z	: Rotational area moment of inertia [kgm^2]
K	: Tire longitudinal slip; tread width moment constant [Nm^2/rad]
k_{Ψ}	: Torsional spring rate [Nm/rad]
k_{δ}	: Lateral spring rate [Nm/rad]
lg	: Landing gear hight [m]
M_1	: Linear spring torque [Nm]
M_2	: Combined damping moment [Nm]
M_3	: Tire moment [Nm]
M_4	: Tire damping moment [Nm]
V	: Velocity of aircraft [m/s]
y_1	: Lateral displacement [m]
Ψ	: Yaw angle [rad]
α	: Slip angle [rad]
δ	: Lateral rotational displacement [rad]
Φ	: Rake angle[rad]
σ	: Relaxation length [m]

LIST OF TABLES

Page

Table 3.1 : 1 DOF 3 order shimmy model parameters. **24**
Table 3.2 : 1 DOF 3 order the effect of F_z change on e -V plane. **31**
Table 3.3 : 1 DOF 3 order the effect of e change on F_z -V plane. **36**
Table 3.4 : 2 DOF 5 order shimmy model parameters. **37**
Table 3.5 : 2 DOF 5 order the effect of F_z change on e-V plane. **43**
Table 3.6 : 2 DOF 5 order the effect of e change on F_z-V plane. **48**

LIST OF FIGURES

Page

Figure 2.1 : Landing gear comfigurations [13]. **5**
Figure 2.2 : Landing gear components [16]. **6**
Figure 2.3 : The efficiency of shock damper models [17]. **8**
Figure 2.4 : Single gas chamber oleo-pneumatic systems [17]. **9**
Figure 2.5 : Spring force-stroke curve in single gas chamber systems. **10**
Figure 2.6 : Double gas chamber oleo-pneumatic systems [17]. **11**
Figure 2.7 : Spring force-stroke curve in double gas chamber systems. **11**
Figure 2.8 : Oleo-pneumatic systems with metering pins [18]. **12**
Figure 2.9 : Poppet valve open status. **14**
Figure 2.10 : Poppet valve close status. **14**
Figure 2.11 : Tire (Normal pressure – Longitudinal stress) [20]. **15**
Figure 2.12 : Tire behaviour [19]. **16**
Figure 2.13 : Cornering Force – Slip Angle [15]. **17**
Figure 3.1 : Shimmy phenomenon [9]. **19**
Figure 3.2 : Shimmy dynamic model side view [12]. **22**
Figure 3.3 : Shimmy dynamic model top view [12]. **22**
Figure 3.4 : 1 DOF Stability region of e-V plane for k=100000 Nm/rad (Eigenvalue). **25**
Figure 3.5 : 1 DOF Stability region of e-V plane for k=100000 Nm/rad (Routh-Hurwitz). **25**
Figure 3.6 : 1 DOF Torsional stability for k=100000 & V=120 m/s & e=0.1325 m (unstable). **26**
Figure 3.7 : 1 DOF Torsional stability for k=100000 & V=85 m/s & e=0.1325 m (stable). **26**
Figure 3.8 : 1 DOF Stability region of e-V plane for k=75000 Nm/rad (Eigenvalue). **26**
Figure 3.9 : 1 DOF Stability region of e-V plane for k=75000 Nm/rad (Routh-Hurwitz). **27**
Figure 3.10 : 1 DOF Torsional stability for k=75000 & V=153 m/s & e=0.135 m (unstable). **27**
Figure 3.11 : 1 DOF Torsional stability for k=75000 & V=52 m/s & e=0.135 m (stable). **27**
Figure 3.12 : 1 DOF Stability region of e-V plane for k=50000 Nm/rad (Eigenvalue). **28**
Figure 3.13 : 1 DOF Stability region of e-V plane for k=50000 Nm/rad (Routh-Hurwitz). **28**
Figure 3.14 : 1 DOF Torsional stability for k=50000 & V=173 m/s & e=0.14 m (unstable). **28**
Figure 3.15 : 1 DOF Torsional stability for k=50000 & V=33 m/s & e=0.14 m (stable). **29**
Figure 3.16 : 1 DOF Stability region of e-V plane for k=25000 Nm/rad (Eigenvalue). **29**

Figure 3.17 : 1 DOF Stability region of e-V plane for k=25000 Nm/rad (Routh-Hurwitz). **29**
Figure 3.18 : 1 DOF Torsional stability for k=25000 & V=187 m/s & e=0.14 m (unstable). **30**
Figure 3.19 : 1 DOF Torsional stability for k=25000 & V=18 m/s & e=0.14 m (stable). **30**
Figure 3.20 : 1 DOF Stability region of F_z -V plane for k=100000 Nm/rad (Eigenvalue). **31**
Figure 3.21 : 1 DOF Torsional stability for k=100000 & V=30 m/s & Fz=19000 N (unstable). **32**
Figure 3.22 : 1 DOF Torsional stability for k=100000 & V=26 m/s & Fz=19000 N (stable). **32**
Figure 3.23 : 1 DOF Stability region of F_z -V plane for k=75000 Nm/rad (Eigenvalue). **32**
Figure 3.24 : 1 DOF Torsional stability for k=75000 & V=22 m/s & Fz=19000 N (unstable). **33**
Figure 3.25 : 1 DOF Torsional stability for k=75000 & V=20 m/s & Fz=19000 N (stable). **33**
Figure 3.26 : 1 DOF Stability region of F_z -V plane for k=50000 Nm/rad (Eigenvalue). **33**
Figure 3.27 : 1 DOF Torsional stability for k=50000 & V=15 m/s & Fz=19000 N (unstable). **34**
Figure 3.28 : 1 DOF Torsional stability for k=50000 & V=13 m/s & Fz=19000 N (stable). **34**
Figure 3.29 : 1 DOF Stability region of F_z-V plane for k=25000 Nm/rad (Eigenvalue). **34**
Figure 3.30 : 1 DOF Torsional stability for k=25000 & V=8 m/s & Fz=19000 N (unstable). **35**
Figure 3.31 : 1 DOF Torsional stability for k=25000 & V=6 m/s & Fz=19000 N (stable). **35**
Figure 3.32 : 2 DOF (Yaw and lateral) shimmy model [21]. **36**
Figure 3.33 : 2 DOF Stability region of e-V plane for k=100000 Nm/rad. **38**
Figure 3.34 : 2 DOF Torsional stability for k=100000 & V=103 m/s & e=0.125 m (unstable). **39**
Figure 3.35 : 2 DOF Torsional stability for k=100000 & V=85 m/s & e=0.125 m (stable). **39**
Figure 3.36 : 2 DOF Stability region of e-V plane for k=75000 Nm/rad. **39**
Figure 3.37 : 2 DOF Torsional stability for k=75000 & V=140 m/s & e=0.13 m (unstable). **40**
Figure 3.38 : 2 DOF Torsional stability for k=75000 & V=47 m/s & e=0.13 m (stable). **40**
Figure 3.39 : 2 DOF Stability region of e-V plane for k=50000 Nm/rad. **40**
Figure 3.40 : 2 DOF Torsional stability for k=50000 & V=154 m/s & e=0.13 m (unstable). **41**
Figure 3.41 : 2 DOF Torsional stability for k=50000 & V=30 m/s & e=0.13 m (stable). **41**
Figure 3.42 : 2 DOF Stability region of e-V plane for k=25000 Nm/rad. **41**
Figure 3.43 : 2 DOF Torsional stability for k=25000 & V=160 m/s & e=0.13 m (unstable). **42**

Figure 3.44 : 2 DOF Torsional stability for k=25000 & V=14 m/s & e=0.13 m (stable). **42**
Figure 3.45 : 2 DOF Stability region of F_z-V plane for k=100000 Nm/rad.......... **43**
Figure 3.46 : 2 DOF Torsional stability for k=100000 & V=24 m/s & Fz=19000 N (unstable). **44**
Figure 3.47 : 2 DOF Torsional stability for k=100000 & V=22 m/s & Fz=19000 N (stable). **44**
Figure 3.48 : 2 DOF Stability region of F_z-V plane for k=75000 Nm/rad.......... **44**
Figure 3.49 : 2 DOF Torsional stability for k=75000 & V=17 m/s & Fz=19000 N (unstable). **45**
Figure 3.50 : 2 DOF Torsional stability for k=75000 & V=17 m/s & Fz=19000 N (stable). **45**
Figure 3.51 : 2 DOF Stability region of F_z-V plane for k=50000 Nm/rad.......... **45**
Figure 3.52 : 2 DOF Torsional stability for k=50000 & V=7 m/s & Fz=19000 N (unstable). **46**
Figure 3.53 : 2 DOF Torsional stability for k=50000 & V=7 m/s & Fz=17000 N (stable). **46**
Figure 3.54 : 2 DOF Stability region of F_z-V plane for k=25000 Nm/rad.......... **46**
Figure 3.55 : 2 DOF Torsional stability for k=25000 & V=7 m/s & Fz=19000 N (unstable). **47**
Figure 3.56 : 2 DOF Torsional stability for k=25000 & V=8 m/s & Fz=7500 N (stable). **47**
Figure 4.1 : 1 DOF Stability region of e-V plane for k=100000 Nm/rad & V=120 m/s & e=0.1325 m (Roots). **51**
Figure 4.2 : 1 DOF Stability region of e-V plane for k=100000 Nm/rad & V=120 m/s & e=0.1325 m (System/LQR).......... **51**
Figure 4.3 : 1 DOF Stability region of e-V plane for k=100000 Nm/rad & V=120 m/s & e=0.1325 m (Actuator moment). **51**
Figure 4.4 : 1 DOF Stability region of e-V plane for k=50000 Nm/rad & V=173 m/s & e=0.14 m (Roots).......... **52**
Figure 4.5 : 1 DOF Stability region of e-V plane for k=50000 Nm/rad & V=173 m/s & e=0.14 m (System/LQR). **52**
Figure 4.6 : 1 DOF Stability region of e-V plane for k=50000 Nm/rad & V=173 m/s & e=0.14 m (Actuator moment). **52**
Figure 4.7 : 1 DOF Stability region of F_z-V plane for k=100000 Nm/rad & V=30 m/s & F=19000 N (Roots).......... **53**
Figure 4.8 : 1 DOF Stability region of F_z-V plane for k=100000 Nm/rad & V=30 m/s & F=19000 N (System/LQR). **53**
Figure 4.9 : 1 DOF Stability region of e-V plane for k=100000 Nm/rad & V=30 m/s & F=19000 N (Actuator moment).......... **53**
Figure 4.10 : 1 DOF Stability region of F_z-V plane for k=50000 Nm/rad & V=15 m/s & F=19000 N (Roots).......... **54**
Figure 4.11 : 1 DOF Stability region of F_z-V plane for k=50000 Nm/rad & V=15 m/s & F=19000 N (System/LQR). **54**
Figure 4.12 : 1 DOF Stability region of e-V plane for k=50000 Nm/rad & V=15 m/s & F=19000 N (Actuator moment).......... **54**
Figure 4.13 : 2 DOF Stability region of e-V plane for k=100000 Nm/rad & V=103 m/s & e=0.125 m (System/LQR).......... **55**
Figure 4.14 : 2 DOF Stability region of e-V plane for k=100000 Nm/rad & V=103 m/s & e=0.125 (Actuator moment).......... **56**

Figure 4.15 : 2 DOF Stability region of e-V plane for k=75000 Nm/rad & V=140 m/s & e=0.13 m (System/LQR). **56**
Figure 4.16 : 2 DOF Stability region of e-V plane for k=75000 Nm/rad & V=140 m/s & e=0.13 (Actuator moment). **56**
Figure 4.17 : 2 DOF Stability region of e-V plane for k=50000 Nm/rad & V=154 m/s & e=0.13 m (System/LQR). **57**
Figure 4.18 : 2 DOF Stability region of e-V plane for k=50000 Nm/rad & V=154 m/s & e=0.13 (Actuator moment). **57**
Figure 4.19 : 2 DOF Stability region of F_z-V plane for k=100000 Nm/rad & V=24 m/s & F_z=19000 N (System/LQR). **57**
Figure 4.20 : 2 DOF Stability region of F_z -V plane for k=100000 Nm/rad & V=24 m/s & F_z =19000 N (Actuator moment). **58**
Figure 4.21 : 2 DOF Stability region of F_z-V plane for k=75000 Nm/rad & V=17 m/s & F_z=19000 N (System/LQR). **58**
Figure 4.22 : 2 DOF Stability region of F_z -V plane for k=75000 Nm/rad & V=17 m/s & F_z =19000 N (Actuator moment). **58**
Figure 4.23 : 2 DOF Stability region of F_z-V plane for k=50000 Nm/rad & V=7 m/s & F_z=19000 N (System/LQR). **59**
Figure 4.24 : 2 DOF Stability region of F_z -V plane for k=50000 Nm/rad & V=7 m/s & F_z =19000 N (Actuator moment). **59**
Figure 5.1 : LaGeSh parameters table. **61**
Figure 5.2 : LaGeSh stable region table. **62**
Figure 5.3 : LaGeSh stability table. **63**
Figure 5.4 : LaGeSh 1 DOF Controller table. **64**
Figure 5.5 : LaGeSh 2 DOF Controller table. **64**
Figure A.1 : 1 DOF Stability region of e-V plane for k=75000 Nm/rad & V=153 m/s & e=0.135 m (Roots). **70**
Figure A.2 : 1 DOF Stability region of e-V plane for k=75000 Nm/rad & V=153 m/s & e=0.135 m (System/LQR). **70**
Figure A.3 : 1 DOF Stability region of e-V plane for k=75000 Nm/rad & V=153 m/s & e=0.135 m (Actuator moment). **70**
Figure A.4 : 1 DOF Stability region of e-V plane for k=25000 Nm/rad & V=187 m/s & e=0.14 m (Roots). **71**
Figure A.5 : 1 DOF Stability region of e-V plane for k=25000 Nm/rad & V=187 m/s & e=0.14 m (System/LQR). **71**
Figure A.6 : 1 DOF Stability region of e-V plane for k=25000 Nm/rad & V=187 m/s & e=0.14 m (Actuator moment). **71**
Figure A.7 : 1 DOF Stability region of F_z-V plane for k=25000 Nm/rad & V=8 m/s & F=19000 N (Roots). **72**
Figure A.8 : 1 DOF Stability region of F_z-V plane for k=25000 Nm/rad & V=8 m/s & F=19000 N (System/LQR). **72**
Figure A.9 : 1 DOF Stability region of e-V plane for k=25000 Nm/rad & V=8 m/s & F=19000 N (Actuator moment). **72**
Figure A.10 : 2 DOF Stability region of F_z-V plane for k=25000 Nm/rad & V=7 m/s & F_z=19000 N (System/LQR). **73**
Figure A.11 : 2 DOF Stability region of F_z -V plane for k=25000 Nm/rad & V=7 m/s & F_z =19000 N (Actuator moment). **73**
Figure A.12 : 1 DOF Stability region of F_z-V plane for k=75000 Nm/rad & V=22 m/s & F=19000 N (Roots). **73**

Figure A.13 : 1 DOF Stability region of F_z-V plane for k=75000 Nm/rad & V=22 m/s & F=19000 N (System/LQR). **74**
Figure A.14 : 1 DOF Stability region of e-V plane for k=75000 Nm/rad & V=22 m/s & F=19000 N (Actuator moment). **74**
Figure A.15 : 2 DOF Stability region of e-V plane for k=25000 Nm/rad & V=160 m/s & e=0.13 m (System/LQR). **74**
Figure A.16 : 2 DOF Stability region of e-V plane for k=25000 Nm/rad & V=160 m/s & e=0.13 (Actuator moment). **75**

MODELLING-CONTROL OF SHIMMY OSCILLATIONS IN AIRCRAFT LANDING GEAR AND APPLICATION DESIGN

SUMMARY

In aviation, the landing gear is a critical component that ensures the aircraft's stability and safety during ground operations. There are two fundamental types of landing gear configurations: Tail-Wheel and Tricycle. The Tail-Wheel setup consists of two main landing gears at the front and a single tail gear at the rear. Conversely, the Tricycle arrangement features a single nose landing gear complemented by two main landing gears at the rear.

One of the significant challenges in landing gear design is the phenomenon known as shimmy. Shimmy refers to an oscillatory motion that combines lateral and yaw movements of the landing gear. This motion results from the complex interaction between the tire dynamics and the structural characteristics of the landing gear. Both nose and main landing gears can exhibit shimmy oscillations; however, the nose gear in Tricycle configurations and the tail gear in Tail-Wheel setups are particularly susceptible.

The prevalence of shimmy oscillations has led to extensive research, with most studies concentrating on the nose or tail landing gears. Shimmy is characterized by self-excited oscillations propelled by the aircraft's forward movement. The oscillation amplitude can range from minor disturbances affecting comfort and visibility to intense vibrations that may cause structural damage or even catastrophic failure. To mitigate these risks, a comprehensive modelling and analysis of the landing gear's dynamic behavior and structural integrity are imperative. This approach enables the evaluation of the landing gear design and facilitates the implementation of necessary modifications at an early development stage.

For analytical purposes, a mathematical model of the landing gear is derived using the Lagrange equation. This model includes a third-order, 1-degree-of-freedom system representing the yaw motion, and a more complex fifth-order, 2-degree-of-freedom system accounting for both yaw and lateral movements. Subsequently, the Routh-Hurwitz criteria and the coefficients of the characteristic equation are employed to conduct a linear stability analysis. Following the derivation of the mathematical equations, various simulations are executed using MATLAB and Simulink. Once the mathematical models and simulation frameworks are established and validated, control strategies such as Linear Quadratic Regulator (LQR) controller design is applied to both models.

To streamline the analysis process, a specialized application named LaGeSh has been developed. This application allows for the adjustment of multiple parameters, including tire characteristics, slip angle, caster length, force, moments of inertia, and aircraft speed. These modifications enable a practical assessment of the aircraft's susceptibility to shimmy vibrations and facilitate the extraction of controller parameters based on the input values. Moreover, LaGeSh can generate comparative

graphs, such as caster length versus aircraft speed and force versus aircraft speed, to identify the most optimal parameter configurations.

As a result this study not only elaborates on the technical aspects of landing gear dynamics but also provides a comprehensive overview of the analytical methods and tools used in the study of shimmy oscillations.

UÇAK İNİŞ TAKIMLARINDA SHIMMY TİTREŞİMİNİN MODELLENMESİ-KONTROLÜ VE UYGULAMA TASARIMI

ÖZET

Havacılık endüstrisinde, bir uçağın güvenli bir şekilde havalanması, uçuşu sürdürmesi ve nihayetinde güvenli bir şekilde yere inmesi, uçağın farklı sistemlerinin bir arada sorunsuz bir şekilde çalışmasına bağlıdır. Bu sistemler arasında iniş takımı, özellikle yere iniş, kalkış ve taksi gibi kritik operasyonlar sırasında uçağın stabilite ve güvenliğini sağlayan en önemli bileşenlerden biri olarak ön plana çıkar. İniş takımı, sadece uçağın havacılık faaliyetlerini başarılı bir şekilde yerine getirmesi için değil, aynı zamanda yerdeki tüm operasyonlarının güvenli bir şekilde gerçekleştirilmesi için de tasarlanmış bir sistemdir. İniş takımı olmadan, bir uçağın yer operasyonlarını gerçekleştirmesi mümkün değildir, bu nedenle iniş takımı, havacılığın ayrılmaz bir parçası olarak kabul edilir.

İniş takımları, uçağın yerle temas ettiği ilk andan itibaren devreye girer. Uçağın ağırlığı, iniş sırasında büyük bir kuvvetle iniş takımları üzerine biner ve bu kuvvetlerin uçağın gövdesine zarar vermeden emilmesi gerekir. Ayrıca, iniş sırasında meydana gelebilecek herhangi bir dengesizlik, uçağın ciddi hasar almasına veya tehlikeli durumların oluşmasına neden olabilir. Bu nedenle, iniş takımları sadece uçağın ağırlığını taşımakla kalmaz, aynı zamanda bu yükü güvenli bir şekilde dağıtarak uçağın stabilitesini korur. İniş takımları, uçağın hareket halindeyken ya da yerde durduğu sürece sürekli olarak bu dengeyi sağlamak zorundadır.

Uçakların farklı kullanım amaçlarına ve tasarımlarına bağlı olarak, iniş takımlarının konfigürasyonları da çeşitlilik gösterir. Genel olarak, iki ana iniş takımı konfigürasyonu bulunmaktadır: Tail-Wheel (Kuyruk-Tekerlek) ve Tricycle (Üç Tekerlekli) konfigürasyonları. Tail-Wheel konfigürasyonu, uçağın ön kısmında iki ana iniş takımının ve arka kısmında tek bir kuyruk iniş takımının bulunduğu bir yapıya sahiptir. Bu yapı, özellikle hafif uçaklar, eski model uçaklar ve bazı helikopterler gibi daha küçük hava araçlarında tercih edilir. Kuyruk-Tekerlek konfigürasyonunun, uçağın kalkış ve iniş sırasında daha hassas bir denge gerektirmesi, bu tür uçakların pilotlarının dikkatini ve deneyimini önemli kılar. Kuyruk iniş takımının konumu, uçağın dengesinin korunmasında kritik bir rol oynar ve özellikle düzensiz zeminlerde iniş veya kalkış sırasında pilotların daha dikkatli olmasını gerektirir.

Bununla birlikte, modern havacılıkta yaygın olarak kullanılan Tricycle konfigürasyonu, uçağın burun kısmında bir burun iniş takımı ve arka kısmında iki ana iniş takımından oluşur. Bu konfigürasyon, günümüzün büyük yolcu uçakları ve askeri jetlerde standart bir hale gelmiştir ve bu uçakların yerde daha fazla stabilite ve manevra kabiliyeti sağlamasına olanak tanır. Tricycle konfigürasyonu, uçağın kalkış ve iniş işlemlerinin daha kolay ve güvenli bir şekilde gerçekleştirilmesini sağlar, bu da bu konfigürasyonu modern havacılıkta yaygın hale getiren en önemli faktörlerden biridir. Ayrıca, bu konfigürasyon, uçakların farklı yüzeylerde daha iyi performans

göstermesine yardımcı olur, bu da çeşitli hava koşullarında uçak operasyonlarının sorunsuz bir şekilde gerçekleştirilmesine katkıda bulunur.

Ancak, iniş takımı tasarımı ve konfigürasyonları, sadece uçağın stabilitesini ve güvenliğini sağlamakla kalmaz; aynı zamanda çeşitli fiziksel fenomenlere karşı da dayanıklı olmalıdır. Bu fenomenlerden biri olan shimmy, iniş takımlarında sıklıkla karşılaşılan ve özellikle uçakların yüksek hızlarda hareket ettiği durumlarda ciddi tehlikeler yaratabilen bir olgudur. Shimmy, iniş takımının yanal (lateral) ve yalpa (yaw) hareketlerini birleştirerek ortaya çıkan salınımlı bir hareketi ifade eder. Bu salınımlar, iniş takımı bileşenlerinin dinamik özellikleri ile lastiklerin yapısal özellikleri arasındaki karmaşık etkileşimlerin bir sonucudur. Shimmy salınımlarının şiddeti ve genliği, birçok faktöre bağlı olarak değişebilir ve bu salınımlar, uçak stabilitesini ciddi şekilde tehdit edebilir.

Shimmy fenomeni, özellikle yüksek hızlarda veya iniş sırasında meydana geldiğinde, uçak operasyonları için kritik bir risk oluşturur. Hem burun iniş takımı hem de ana iniş takımları shimmy salınımlarına maruz kalabilir; ancak, Tricycle konfigürasyonunda burun iniş takımı ve Tail-Wheel düzeninde kuyruk iniş takımı özellikle shimmyye karşı duyarlıdır. Bu tür salınımlar, iniş takımının yapısal bütünlüğünü tehlikeye atabilir, bu da uçağın güvenliğini riske sokabilir. Shimmy fenomeni, iniş takımında yapısal hasarlara, yolcular için rahatsız edici titreşimlere ve en kötü durumda uçak kazalarına yol açabilecek ciddi bir sorundur. Bu nedenle, shimmy salınımlarının kontrol altına alınması ve minimize edilmesi, iniş takımı tasarımında en önemli hedeflerden biri olarak kabul edilir.

Shimmy fenomeninin geniş çaplı bir sorun olması, mühendisler ve araştırmacılar tarafından yoğun olarak çalışılmasına yol açmıştır. Bu çalışmaların büyük bir kısmı, shimmy salınımlarını anlamak ve önlemek için matematiksel modelleme, analitik inceleme ve simülasyon tekniklerine dayanmaktadır. Shimmy, uçağın ileriye doğru hareketiyle tetiklenen ve lastik deformasyonları, iniş takımının elastik özellikleri ve yüzey düzensizlikleri gibi faktörlerin etkisi altında gelişen kendiliğinden uyarılan salınımlar olarak tanımlanır. Bu salınımlar, küçük rahatsızlıklardan yapısal hasarlara kadar uzanan geniş bir etki spektrumuna sahip olabilir. Shimmy fenomeninin bu denli karmaşık ve tehlikeli olması, iniş takımı tasarımında kapsamlı bir analiz ve modelleme gerektirir.

Shimmy fenomenini incelemek için kullanılan analitik yöntemler, iniş takımlarının dinamik davranışını ve yapısal bütünlüğünü modellemek amacıyla kapsamlı ve detaylı matematiksel yaklaşımlar gerektirir. Bu tür analizlerde, iniş takımlarının karmaşık dinamik yapısını tam olarak temsil edebilmek için genellikle Lagrange denklemi temel alınır. Lagrange denklemleri, enerjinin korunumu ilkelerine dayanan güçlü bir matematiksel araç olarak, fiziksel sistemlerin hareket denklemlerini türetmekte kritik bir rol oynar. Bu denklemler, bir sistemin potansiyel ve kinetik enerjisini dikkate alarak, sistemi tanımlayan diferansiyel denklemleri oluşturur.

Özellikle shimmy fenomeninin anlaşılmasında, bu yöntemler büyük önem taşır. Shimmy, iniş takımlarında, genellikle yüksek hızlarda karşılaşılan ve kontrol edilmezse uçuş güvenliğini tehdit edebilecek tehlikeli bir salınım türüdür. Bu fenomeni analiz etmek amacıyla geliştirilen matematiksel modeller arasında, farklı derecelerde serbestlik içeren sistemler bulunmaktadır. Örneğin, shimmy davranışını temsil eden basit bir model, üçüncü dereceden, bir serbestlik dereceli bir sistem olabilir. Bu tür bir model, yaw (sapma) hareketini temsil eder ve shimmy salınımlarının temel dinamiklerini incelemek için yeterlidir. Bununla birlikte, daha karmaşık durumları analiz etmek için, hem yaw hem de lateral (yanal) hareketleri kapsayan beşinci dereceden, iki serbestlik dereceli sistemler de kullanılabilir. Bu daha gelişmiş modeller, iniş takımının hareketinin daha geniş bir spektrumunu kapsar ve shimmy fenomeninin daha kapsamlı bir şekilde incelenmesine olanak tanır.

Bu modellerin temel amacı, shimmy salınımlarının dinamik özelliklerini anlamak ve bu salınımların iniş takımına ve dolayısıyla uçuş güvenliğine olan potansiyel etkilerini değerlendirmektir. Shimmy'nin ortaya çıkması ve büyümesi, iniş takımının yapısal bütünlüğünü tehdit edebilir ve bu nedenle bu fenomenin önceden tespit edilmesi ve kontrol altına alınması hayati öneme sahiptir. Bu bağlamda, sistemlerin stabilitesini incelemek, shimmy riskini değerlendirmenin önemli bir parçasıdır. Stabilite analizlerinde, sistemin karakteristik denkleminin köklerini ve bu köklerin gerçek eksen üzerindeki konumlarını değerlendirmek için Routh-Hurwitz kriterleri gibi yöntemler kullanılır. Routh-Hurwitz kriterleri, sistemin stabil olup olmadığını belirlemek için matematiksel olarak sağlam bir temel sağlar. Sistem köklerinin gerçek eksende olup olmadığı, shimmy fenomeninin başlaması ya da büyümesi açısından kritik bir gösterge olup, bu köklerin kompleks düzlemdeki konumu, sistemin uzun vadeli davranışını belirler.

Matematiksel modellerin türetilmesinden sonra, bu modeller üzerinde çeşitli simülasyonlar gerçekleştirilir. Simülasyonlar, MATLAB ve Simulink gibi gelişmiş yazılımlar kullanılarak yapılır. Bu simülasyonlar, iniş takımı dinamiklerini ve shimmy fenomenini daha iyi anlamak için önemli veriler sağlar. Simülasyonların yanı sıra, modellere Linear Quadratic Regulator (LQR) kontrolcü tasarımı gibi kontrol stratejileri uygulanır. LQR kontrolcüleri, sistemin performansını optimize etmek amacıyla geri besleme kazançlarını belirler ve böylece shimmy salınımlarını minimize eder. Bu kontrol stratejileri, shimmy fenomenini kontrol altına almak ve minimize etmek için etkili bir çözüm sunar.

Bu tür analiz süreçlerini daha pratik ve kullanıcı dostu hale getirmek için, shimmy fenomenini incelemek üzere LaGeSh adlı özel bir uygulama geliştirilmiştir. LaGeSh, lastik özellikleri, kayma açısı, caster uzunluğu, tekerlek kuvveti, atalet momentleri ve uçak hızı gibi parametrelerin kolayca ayarlanmasına olanak tanır. Bu parametreler üzerinde yapılan değişiklikler, uçağın shimmy titreşimlerine karşı duyarlılığını değerlendirmeyi sağlar ve kontrolcü parametrelerinin optimize edilmesine yardımcı olur. Ayrıca, LaGeSh, çeşitli parametreler arasındaki ilişkileri görselleştirmek için karşılaştırmalı grafikler oluşturabilir. Bu grafikler, caster uzunluğu ve uçak hızı veya tekerlek kuvveti ve uçak hızı gibi ilişkileri daha iyi anlamak için kritik bir araç sunar. LaGeSh'in sunduğu bu görsel ve analitik araçlar, shimmy fenomeninin daha derinlemesine incelenmesi ve bu fenomeni kontrol altına almak için etkili çözümler geliştirilmesi açısından büyük bir değer taşır.

Sonuç olarak, shimmy fenomeni, iniş takımı tasarımında dikkate alınması gereken karmaşık ve tehlikeli bir olgudur. Uçakların güvenli bir şekilde iniş yapması ve yerde manevra yapması için shimmy fenomeninin etkilerinin minimize edilmesi büyük bir önem taşır. Bu amaçla geliştirilen matematiksel modeller, simülasyonlar ve kontrol stratejileri, shimmy fenomeninin anlaşılmasına ve etkili bir şekilde kontrol altına alınmasına katkı sağlar. LaGeSh gibi özel uygulamalar ise bu süreçleri daha kullanıcı dostu ve erişilebilir hale getirir. Bu sayede, mühendisler, uçakların iniş takımlarını daha güvenli ve verimli bir şekilde tasarlayabilir, uçak operasyonlarının güvenliğini artırabilir.

1. INTRODUCTION

The shimmy phenomenon refers to a self-excited oscillatory motion commonly observed in aircraft. This phenomenon manifests as intense angular vibrations during movement, posing significant safety risks. Although the main causes of shimmy appear to be the tire and wheel, it depends on various parameters such as caster length, aircraft speed, and moment of inertia. Shimmy is particularly dangerous in the tail landing gear of tail-wheel type landing gears and the nose landing gear of tricycle type landing gears. If not properly controlled, it can lead to severe structural damage. To understand and mitigate this phenomenon, comprehensive models are required that consider various parameters, including tire dynamics, suspension systems, and the interaction between the vehicle and the road surface.

1.1 Literature Review

The phenomenon of shimmy has long been analyzed by researchers and engineers in the aviation industry. Early studies focused on modeling the dynamic behavior of tires. Some of these early tire models, developed by Von Schlippe in 1941 [1] and Moreland in 1954 [2], are still in use today. Building on the work of Von Schlippe and Moreland, Smiley developed a summary theory in 1956. Smiley and Horne conducted experiments on different aircraft tire sizes and parameters, proposing empirical formulas for calculating tire parameters. In 1966, Pacejka [3] expanded the Von Schlippe tire model with a straightforward tangential approach and suggested nonlinear models. In 1974, Rogers [4] developed an empirical tire model based on measured transfer functions. Grossman [5] demonstrated the use of linearization techniques to simplify nonlinear analysis in 1980. More recent work by Somieski [6] in 1997 applied well-known linear and nonlinear methods to analyze the nonlinear model of landing gear and tire mechanics, including eigenvalue calculations, analytical solutions of stability boundaries, and limit cycle determination. Additionally, typical tire and landing gear parameters for a 10-ton small aircraft were provided.

Besselink [7] analyzed twin-wheel cantilever aircraft landing gear in 2000. Simple linear and nonlinear models available in the literature, along with empirical formulas for calculating tire parameters, were summarized. The impact of different landing gear parameters on shimmy was investigated. In 2006, Long [8] developed an active control strategy to suppress shimmy oscillations. The stability changes of shimmy with varying casting length and speed were analyzed for a linear system, and a new control strategy was formed by combining RMPC control law with linear parameter-varying polytope design. Atabay [9] performed shimmy analysis of torsional nose landing gear using the model and parameters provided by Somieski [6]. The effect of parameters such as caster length and tire's semi-contact length on stability was investigated. An MR damper using the current-dependent Bouc-Wen model was incorporated into the torsional landing gear model with and without clearance in 2012.

Although the primary application of shimmy analysis is in airplanes, shimmy vibrations can also occur in helicopters. Helicopter-specific studies have been conducted by Kogan and Butts [10] and Grossini et al. [11]. Kogan and Butts [10] developed a full aircraft shimmy model for the CH-53K and compared the results with an independent model using nonlinear analysis software, VI-Aircraft. Given the previous aircraft test experience with the CH-53A, the full aircraft model provided a better understanding of the shimmy phenomenon in 2010. Grossini et al. [11] modeled the landing gear of the A109 helicopter using two multibody models with two and five degrees of freedom.

1.2 Methodology

A mathematical model of a third-order, single-degree-of-freedom system representing yaw motion and a more complex fifth-order, two-degrees-of-freedom system accounting for both yaw and lateral motions are derived. These equations are formulated in state-space form. The stability analyses of these systems, written in this form, are examined using the Routh-Hurwitz criteria and eigenvalue evaluations. After deriving the mathematical equations, various simulations are performed using MATLAB and Simulink. Once the mathematical models and simulation frameworks are established and validated, control strategies such as Linear Quadratic Regulator (LQR) controller design is applied to both models. To facilitate the analysis process, a specialized application called LaGeSh has been developed. This application allows for the adjustment of multiple parameters, including tire characteristics, slip angle, caster length, force, moments of inertia, and aircraft speed. With this application, various results such as the stability status of the system in stable and unstable regions and controller design can be obtained. Comparative graphs can be generated, such as aircraft speed versus caster length and aircraft speed versus force, to determine the optimal parameter configurations. The generated graphs can be examined for a single condition, and controller design for unstable conditions is also possible. In the controller design, LQR (Linear Quadratic Regulator) method has been utilized.

2. LANDING GEAR SYSTEMS

2.1 Landing Gear Configurations

In terms of landing gear, aircraft have various types such as single main, taildragger (tail-wheel), quadricycle, bicycle, tricycle, and multi-bogey. These aircraft configuration types can be seen in Figure 2.1. Among these, the most important types are the tricycle and taildragger (tail-wheel) landing gear. Each type has its own advantages and disadvantages. In tricycle landing gear, the main landing gears are located behind the center of gravity (CG), which increases stability during taxiing. However, in tail-wheel landing gear, the main landing gears are in front of the CG, resulting in lower stability during taxiing compared to tricycle landing gear.

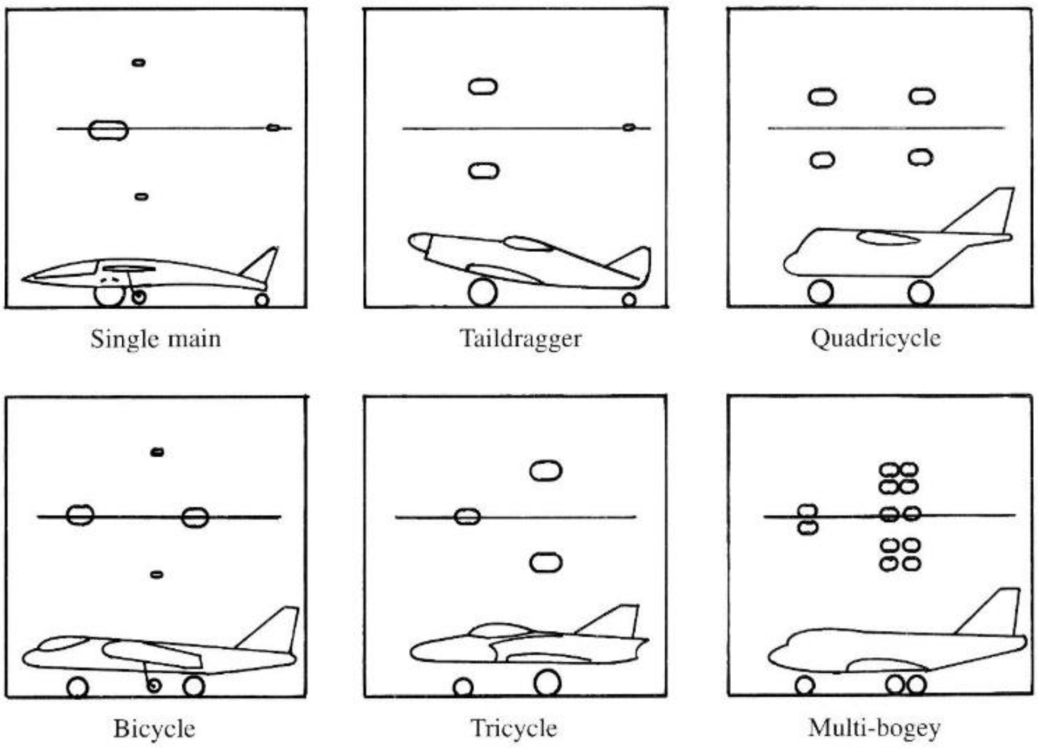

Figure 2.1 : Landing gear comfigurations [13].

2.2 Landing Gear Components

Landing gear is crucial for an aircraft, serving as a vital component for safe takeoffs and landings. As seen in Figure 2.2, the landing gear contains many components. This system comprises various components, each playing an essential role in its functionality. The primary parts of the landing gear system include the cylinder, piston, axle, brake, wheel, and tire. For aircraft with retractable landing gear, additional components such as extension/retraction actuators are necessary. Depending on the type of aircraft, if the front or rear landing gears are non-steerable, equipment like centering cams and center lock actuators may also be present.

One of the most critical elements of the landing gear is the shock absorber. The shock absorber consists of various parts housed within the piston and cylinder, designed to absorb and dissipate the kinetic energy from landing impacts. Additionally, the selection of components like the wheel and tire is of paramount importance, as they directly influence the aircraft's performance and safety during landing and takeoff.

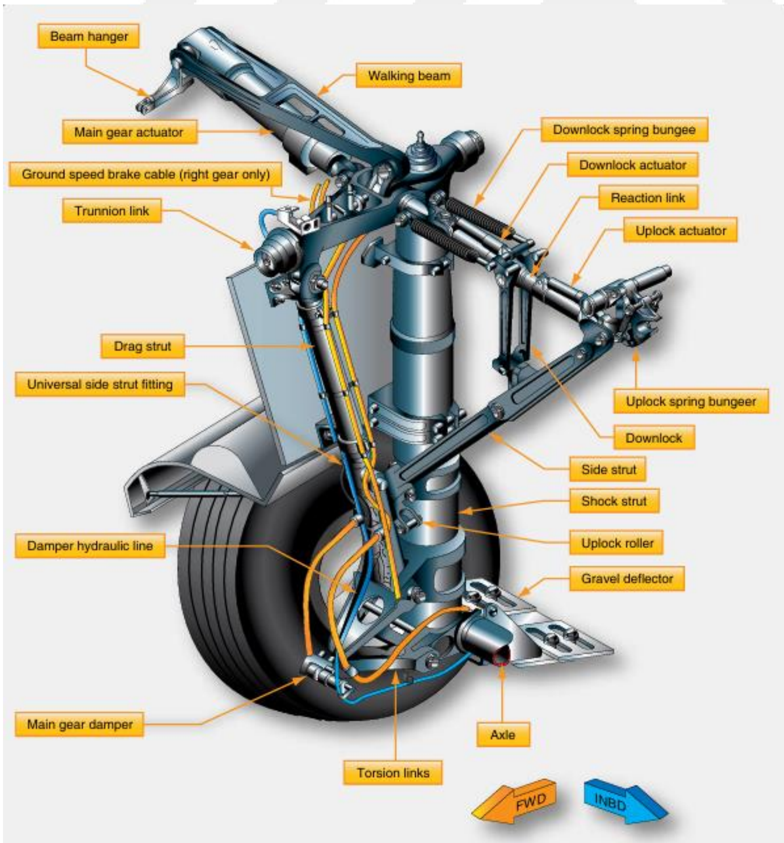

Figure 2.2 : Landing gear components [16].

2.2.1 Shock absorbers

Shock absorbers play the most crucial role in absorbing energy during landing. It can be said that shock absorbers are the most complex and relatively high-cost components of landing gear. However, there are some simple types of shock absorbers used for light, ultra-light, small, and home-built aircraft or helicopters. In this section, the types of shock absorbers will be briefly introduced and compared. Figure 2.3 shows a comparison of the efficiency of different landing gear shock absorber types. [17]

2.2.1.1 Solid spring

These types of shock absorbers are preferred due to their simplicity and low cost.

2.2.1.2 Steel spring

Steel springs are often useful due to their simplicity and ease of maintenance. They are commonly preferred for light aircraft.

2.2.1.3 Rubber spring

It is a type of shock absorber that utilizes the high damping properties of rubber. However, it is not preferred today due to its lack of control, mechanical weaknesses, and inability to withstand high temperatures.

2.2.1.4 Liquid spring

Fluid damping systems were used from World War II until the 1980s. Although they resemble oleo-pneumatic systems, their need for high fluid pressure and sensitivity to temperature changes in the fluid make them very heavy and inefficient.

2.2.1.5 Air pneumatic

Pneumatic dampers are heavier and less efficient compared to oleo-pneumatic dampers. As a result, pneumatic systems are not used today.

2.2.1.6 Oleo-Pneumatic

Modern aircraft and rotorcraft use oleo-pneumatic shock absorbers in their landing gear. Oleo-pneumatic shock absorbers consist of a gas spring and a hydraulic damper. The gas springs can be designed as single-stage or double-stage. The nitrogen-filled gas chamber acts as a spring during landing, while the oil passing through the orifice between chambers to balance the pressure changes in the fluid creates a damping effect. Additionally, design solutions such as metering pin and poppet valves are available for the damper.

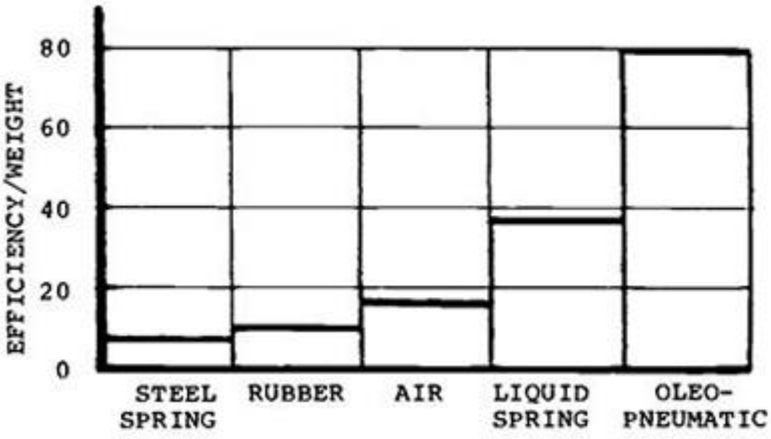

Figure 2.3 : The efficiency of shock damper models [17].

The shock absorber systems in landing gear consist of two interrelated components: the gas spring and the damper. The gas springs can be single or double chamber, while the dampers include mechanisms such as metering pin and poppet valves. The operating principle of shock absorber systems is that during the vertical descent of the aircraft to the ground with a certain acceleration and speed, the gas compresses between the piston and the oil, increasing its pressure. This compression forces the fluid through the orifice, creating the damping force. The gas spring operates based on the ideal gas principle, calculated using the F_spring formula. The damper force for the poppet valve is defined by mathematical equations, while the behavior curve of the adjustment rod mechanism is determined through dynamic analysis. The parameters used during the design process and the resulting spring and damper curves are shown below with mathematical relations. In hydraulic force calculations, one important parameter is the orifice discharge coefficient (C_d), which depends on the dimensional parameters and vertical speed of the landing gear.

2.2.1.7 Spring force

The spring force in oleo-pneumatic systems is generated by the compression and subsequent expansion of nitrogen gas and oil. Since oil is a liquid, its compression is negligible. The spring force in oleo-pneumatic systems is created in two different configurations: single-chamber systems and double-chamber systems. The following formula is used as a reference for both configurations.

$$F_{spring} = P_2 A \left(\frac{y_1}{1 - \frac{y_1}{y_0}} \right)^n \tag{2.1}$$

Nitrogen Gas Pressure (P_2): The pressure value generated by nitrogen gas is calculated by considering the state of the system at full extension. It is obtained by multiplying the constant pressure value by the expansion ratio.

Pneumatic Area (A): Calculated from the piston diameter.

Stroke Position (y_1): A variable length that can move as much as the stroke length due to the movement of the piston.

Piston Length (y_0): A fixed length that must be greater than the stroke length.

2.2.1.8 Single gas chamber systems

Figure 2.4 shows an example of a single gas chamber oleo-pneumatic system. In these types of systems, the spring force is provided by nitrogen gas compressed in a chamber. When the aircraft piston begins to compress, the oil applies pressure to the air chamber, causing it to compress. This compression continues until the equation of equilibrium is reached. Once this equilibrium is achieved, the compression of the air chamber stops. The air chamber then starts to push the oil back, indicating that the compression phase has ended and the expansion phase has begun. Figure 2.5 shows the spring force-stroke curve of the single gas chamber oleo-pneumatic system

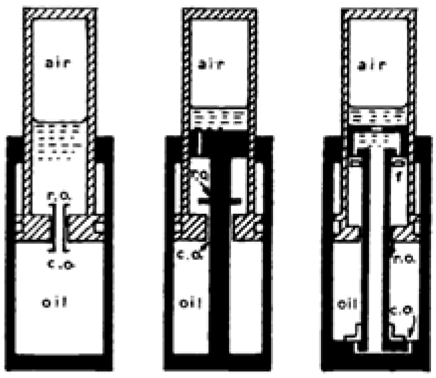

Figure 2.4 : Single gas chamber oleo-pneumatic systems [17].

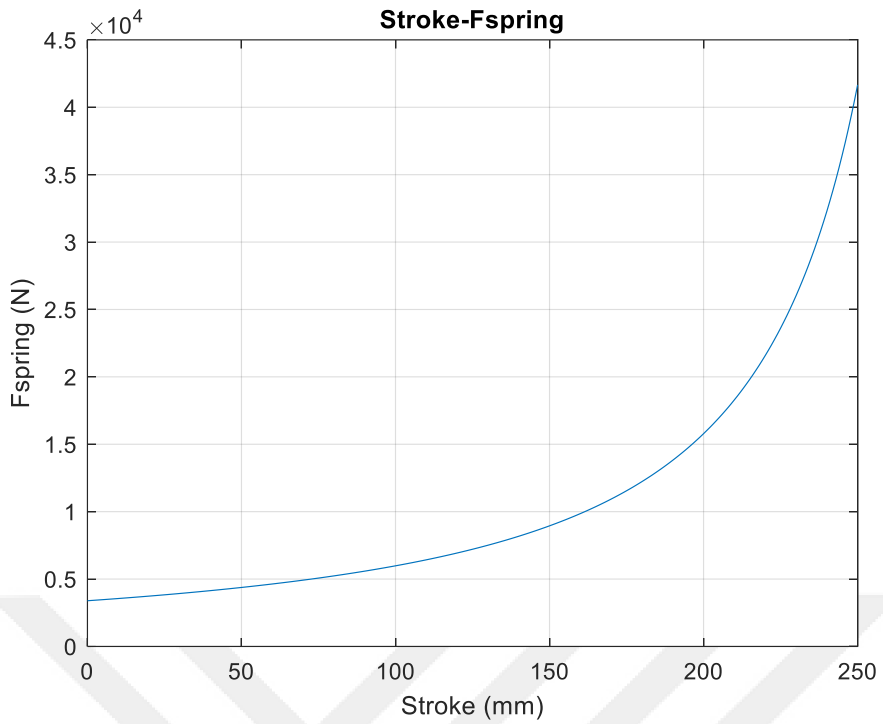

Figure 2.5 : Spring force-stroke curve in single gas chamber systems.

2.2.1.9 Double gas chamber systems

These systems generate more spring force compared to single-chamber systems due to the presence of multiple chambers that can be compressed. The spring force in such systems is generally calculated using the F_{spring} formula. While the number of chambers can be increased, production typically favors a two-chamber design. This is because the cost increases with each additional chamber, and the benefits diminish beyond the first addition. Figure 2.6 shows an example of a double gas chamber oleo-pneumatic system, and Figure 2.7 presents its spring force-stroke curve.

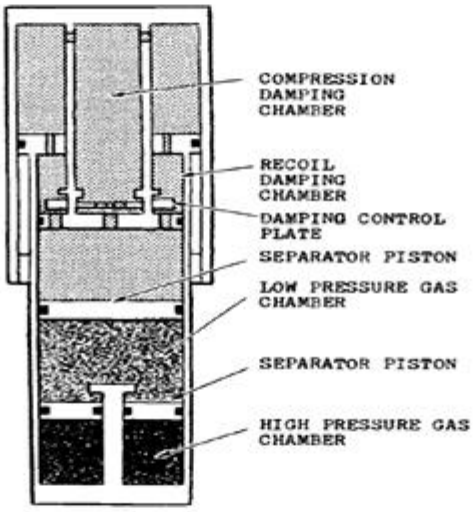

Figure 2.6 : Double gas chamber oleo-pneumatic systems [17].

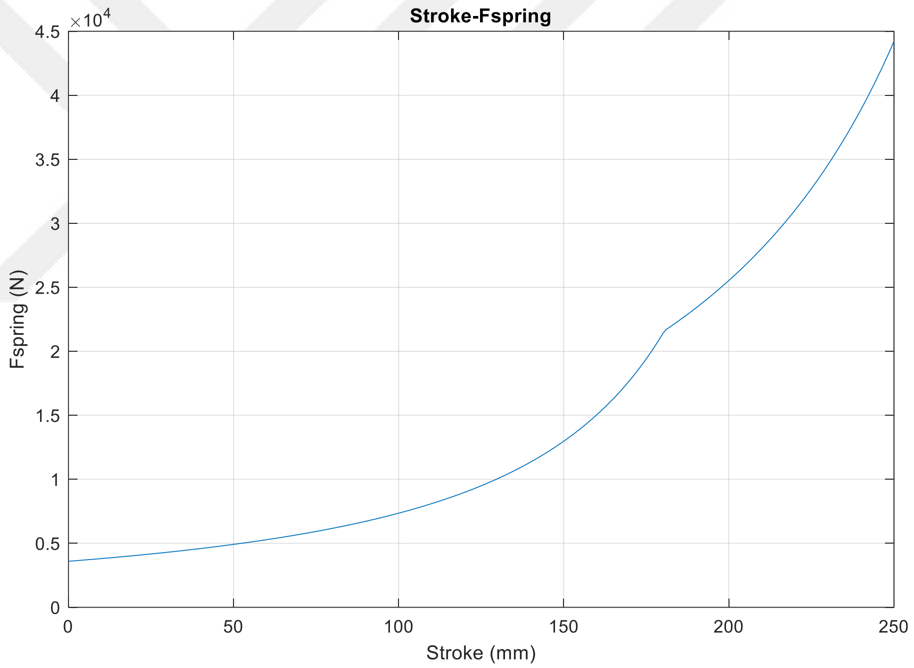

Figure 2.7 : Spring force-stroke curve in double gas chamber systems.

2.2.1.10 Damper force

The damper force is the force generated to balance the spring force. It can be increased or decreased as needed. In pinned oleo-pneumatic systems, the presence of the stroke speed value in the damper force equation allows for the determination of damper force values by establishing a dynamic model. In contrast, for systems with poppet valves, the damper force-speed curve can be determined without a dynamic model, as the design of the poppet takes speed value.

$$F_{damper} = \frac{1}{2}\rho\frac{{A_1}^3|\dot{y}|\dot{y}}{{C_d}^2{A_0}^2} \tag{2.2}$$

Hydraulic Area (A_1): This is calculated by subtracting the area of the pin from the main orifice area. Due to the geometry of the pin, it varies according to the stroke position and is used in determining the damper force.

Discharge Coefficient (C_d): This is the most important parameter in calculating the damper force. The discharge coefficient represents the flow rate through the orifice and, therefore, has a maximum value of 1.

Orifice Area (A_0): This is the sum of the fixed orifices, expansion orifices, and main orifice areas. Expansion orifices are only considered during the expansion phase.

2.2.1.11 Oleo-pneumatic systems with metering pins

Figure 2.8 shows the main components of the landing gear.

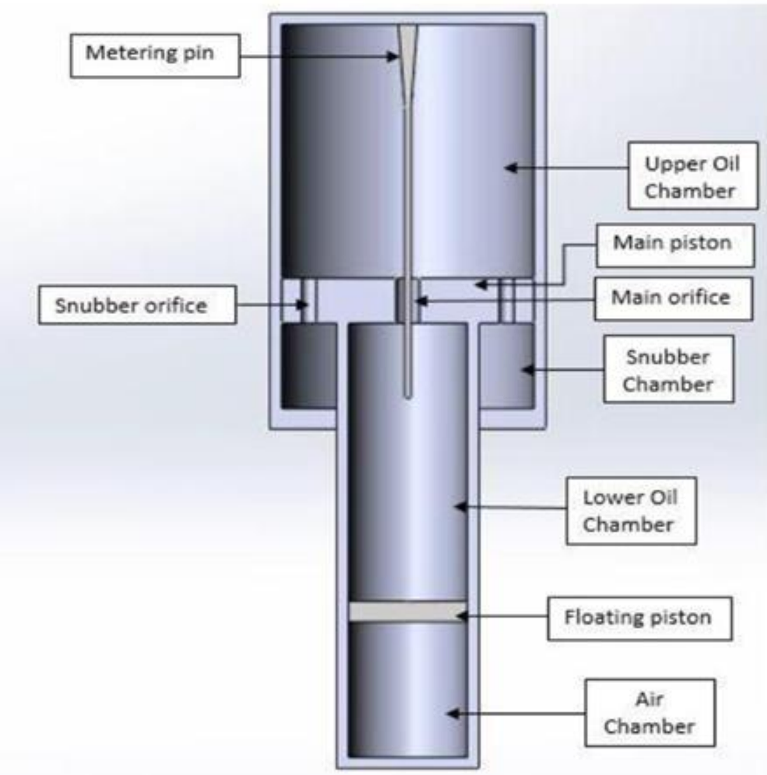

Figure 2.8 : Oleo-pneumatic systems with metering pins [18].

Air Chamber: This is the section containing nitrogen gas (N_2) and generates the system's spring energy. The spring force is calculated using the formula above.

Floating Piston: This component separates the nitrogen gas from the oil. The oil passes through the orifice and applies pressure to the piston. Therefore, the piston is designed considering the maximum pressure.

Lower Oil Chamber: During compression, this chamber compresses the air chamber with the oil passing through the orifice until the pressure-volume relationship equalizes ($P_1V_1^n = P_2V_2^n$). When this equilibrium is reached, the system stops. It is one of the components that provide damping force to the system.

Snubber Orifice and Snubber Chamber: These are optional components. These components are used to reduce the damping force.

Main Orifice: This is the section through which the metering pin passes. As the pin has variable diameters in different sections, the orifice diameter should be determined considering the widest part of the pin and the vibration during compression.

Main Piston: This part contains the orifice holes. It moves, causing the hydraulic area to change due to the pin having variable diameters in different sections.

Upper Oil Chamber: This chamber houses the metering pin and most of the oil. During compression, it sends oil to the lower chamber, and during expansion, it collects the oil again.

Metering Pin: This is the most critical component determining the damping force generated to dampen the system. The pin has variable diameters along its length.

2.2.1.12 Oleo-pneumatic systems with poppet valf

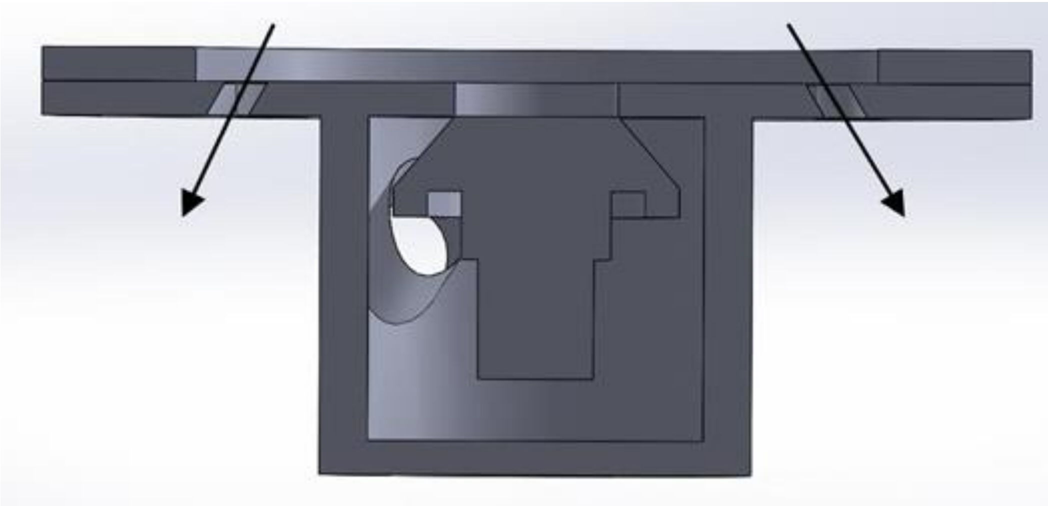

Figure 2.9 : Poppet valve open status.

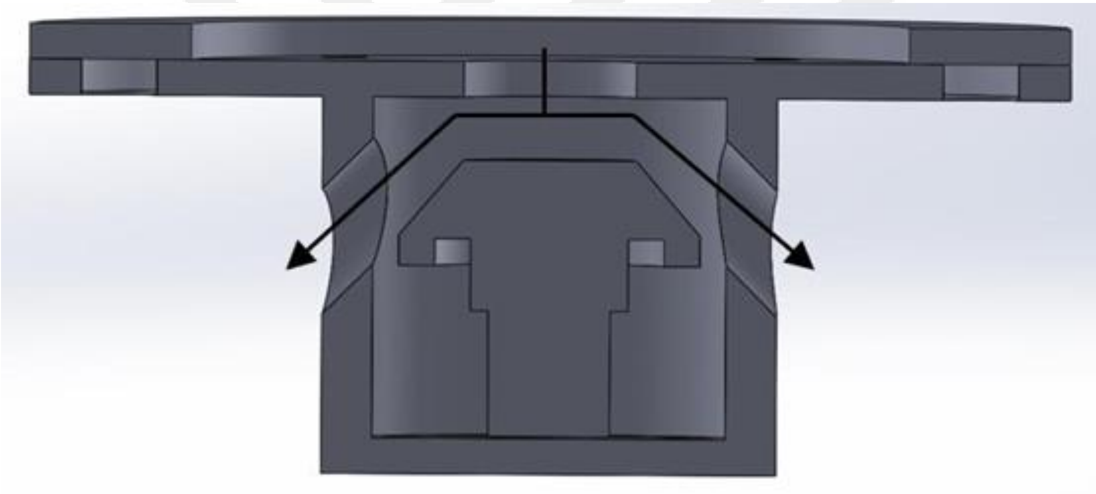

Figure 2.10 : Poppet valve close status.

In shock absorber systems with poppet valves, the variability of the fluid flow area depends on the poppet. While the orifice holes in a metering pin are fixed, the orifice holes in a poppet valve change according to speed and pressure. The poppet valve has taxi holes that are always open. At the center of the system is the poppet valve itself, which opens to increase the orifice area based on changes in speed. This reduces the increase in pressure difference, thereby increasing the damping force. This opening and closing are passively controlled by a spring that connects the poppet valve to the mechanism. Figures 2.9 and 2.10 show the poppet valve component in its open and closed states.

2.2.2 Tire

Most aircraft are used with pneumatic tires. With technological advancements, pneumatic tires have become a lightweight and effective solution compared to other options. The primary functions of these tires include generating adequate friction with the ground, distributing the applied load over a contact area, and providing shock absorption. Figure 2.11 shows the normal pressure and longitudinal stress curves corresponding to the forces applied to the tire.

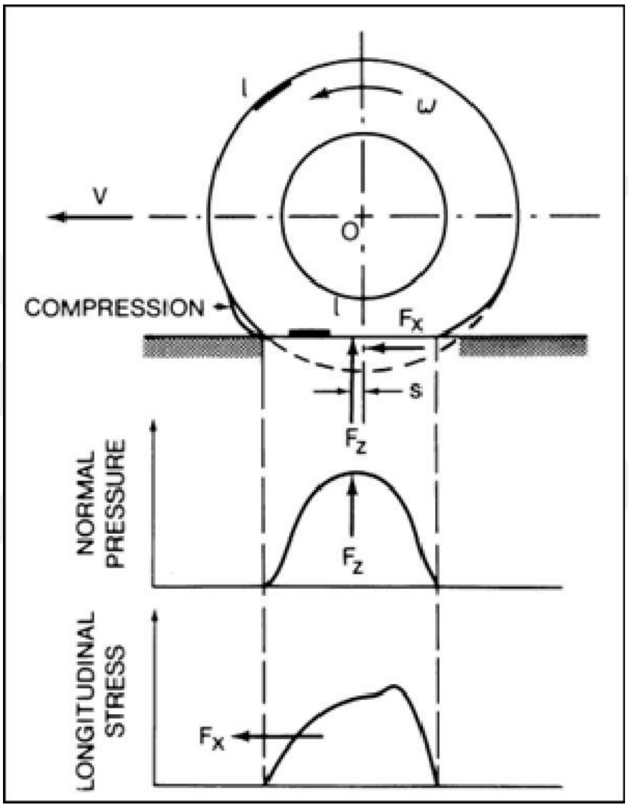

Figure 2.11 : Tire (Normal pressure – Longitudinal stress) [20].

Most aircraft are used with pneumatic tires. With technological advancements, pneumatic tires have become a lightweight and effective solution compared to other options. The primary functions of these tires include generating adequate friction with the ground, distributing the applied load over a contact area, and providing shock absorption. When a force is applied perpendicular to the wheel plane, the tire moves along the wheel plane. In contrast, when a lateral force is applied, it generates a lateral force in the contact area, causing the tire to move along a path at an angle to the wheel plane. This angle is known as the slip angle. At small slip angles, the cornering force on the ground plane typically lags behind the applied lateral force, resulting in a torque that aligns the wheel plane with the direction of motion. This torque is known as the self-aligning torque and is the primary moment that returns the tire to its original position after a turn. The distance between the lateral force and the cornering force is referred to as the pneumatic trail, and the product of the cornering force and the pneumatic trail produces the self-aligning torque. Figure 2.12 shows the factors affecting tire behavior. [19][20]

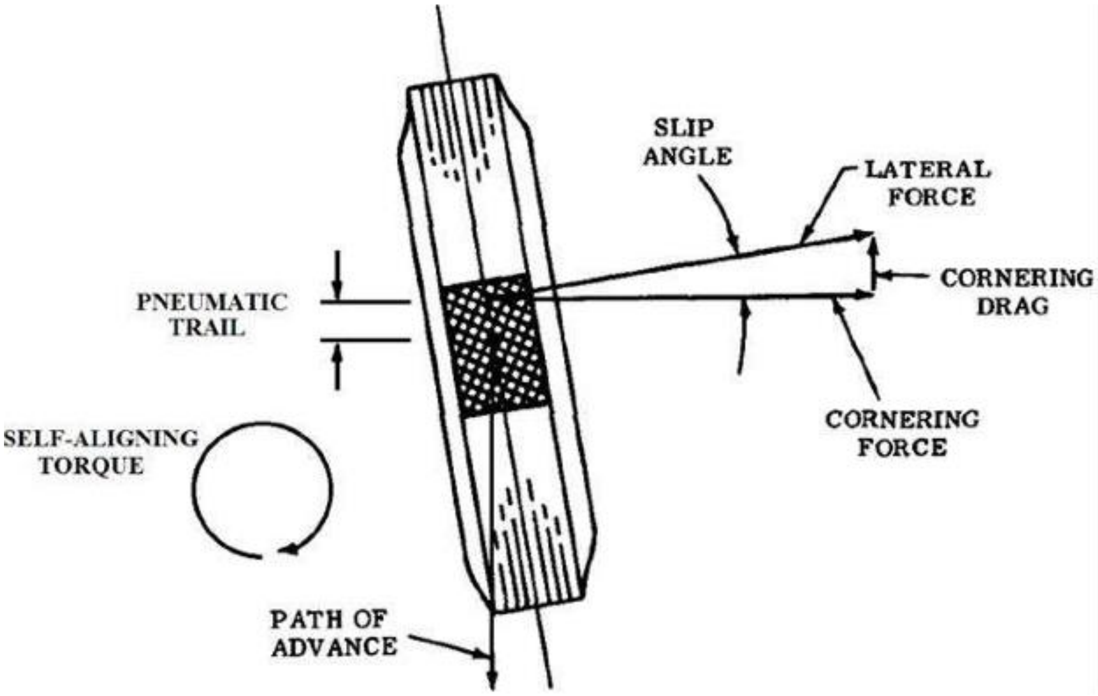

Figure 2.12 : Tire behaviour [19].

This thesis focuses on the analytical tire model. There are primarily two types of analytical tire models: the straight tangent approximation and the elastic string tire model. In this study, the elastic tire model will be used. The following formula illustrates this approach:

$$\dot{y}_1 = -\frac{V}{\sigma} y_1 + V sin(\Psi) + (e - a)\dot{\Psi} \cos(\Psi) \cos(\Phi) + l_g \dot{\delta} \cos{(\delta)} \tag{2.3}$$

The term y_1 represents the lateral displacement in the y-axis at the leading contact point. V denotes the velocity of the aircraft, σ is the relaxation length of the tire, Ψ is the yaw angle e is the caster length, 2a is the total contact length, and Φ is the rank angle. In this thesis, the rake angle of the landing gear is assumed to be 0 degrees. After linearization and substituting the necessary values, the following equation is obtained:

$$\sin(\Psi) = \Psi \tag{2.4}$$

$$\cos(\Psi) = 1 \tag{2.5}$$

$$\cos(\Phi) = \cos(0) = 1 \tag{2.6}$$

As a result, the equation,

$$\dot{y}_1 = -\frac{V}{\sigma} y_1 + V\Psi + (e-a)\dot{\Psi} \tag{2.7}$$

This equation will be used in the shimmy model.

As shown in Figure 2.13, the relationship between cornering force and slip angle is provided. Beyond a certain angle, the relationship between slip angle and cornering stiffness becomes nonlinear. Therefore, a low slip angle value has been chosen for this thesis.

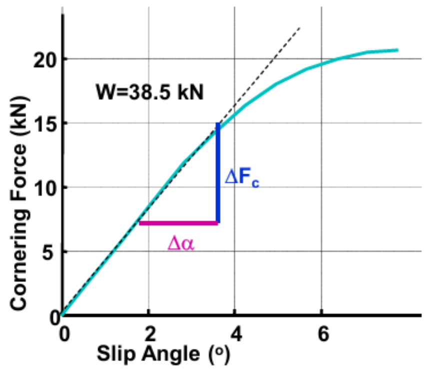

Figure 2.13 : Cornering Force – Slip Angle [15].

3. LANDING GEAR SHIMMY OSCILLATIONS

Shimmy is a rapid, oscillatory motion that occurs in an aircraft's landing gear, primarily during taxiing, takeoff, or landing. This phenomenon is caused by several factors, including imbalances in the wheels, loose or worn components, and misalignment. When the wheels are not balanced, they can cause vibrations similar to those experienced when a car's wheels are out of balance. Loose or worn parts such as bearings and bushings can exacerbate these vibrations, while improper alignment can cause uneven movement and additional stress on the landing gear. The speed of the aircraft and the surface it is moving over can also influence the occurrence of shimmy, with rough surfaces and certain speeds being more prone to inducing this oscillation. Shimmy can lead to increased wear and tear on the landing gear, necessitating more frequent maintenance and repairs. Figure 3.1 shows the shimmy phenomenon. It can also affect passenger comfort and, in severe cases, compromise the pilot's ability to control the aircraft during critical phases of flight. To prevent shimmy, regular maintenance is essential, including balancing the wheels and inspecting for worn parts. Proper alignment of the landing gear and the use of shock absorbers can also help mitigate the effects of shimmy, ensuring a smoother and safer operation of the aircraft.

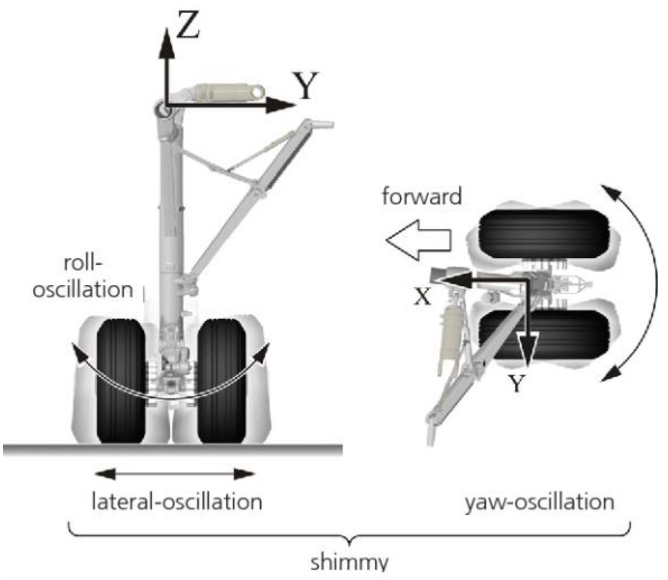

Figure 3.1 : Shimmy phenomenon [9].

3.1 Eigenvalues and Characteristic Equation

Eigenvalues and the characteristic equation are crucial in the aviation industry for analyzing and ensuring the stability and performance of aircraft systems. Eigenvalues are special numbers that arise from solving the characteristic equation of a matrix that represents a system. The characteristic equation,

$$\det(A - \lambda I) = 0 \tag{3.1}$$

where I is the identity matrix, is a polynomial equation whose roots are the eigenvalues of the matrix A. The eigenvalues of the system matrix in flight dynamics determine the stability of an aircraft; negative real parts of eigenvalues indicate a stable system, while positive real parts suggest instability.

As an example, if we derive the characteristic equation of the state space form of a 1 DOF third order shimmy model:

$$\mathrm{A} = \begin{bmatrix} 0 & 1 & 0 \\ c_1 & c_2 & c_3 \\ V & c_4 & c_5 \end{bmatrix} \tag{3.2}$$

$$\lambda \mathrm{I} = \begin{bmatrix} \lambda & 0 & 0 \\ 0 & \lambda & 0 \\ 0 & 0 & \lambda \end{bmatrix} \tag{3.3}$$

$$\det\left(\mathrm{A} - \lambda \mathrm{I}\right) = \begin{vmatrix} \lambda & 1 & 0 \\ c_1 & c_2 - \lambda & c_3 \\ V & c_4 & c_5 - \lambda \end{vmatrix} \tag{3.4}$$

$$\lambda(c_2 - \lambda)(c_5 - \lambda) + 0 + \mathrm{V}c_3 - (0 + c_3 c_4 \lambda + ((c_5 - \lambda)c_1)) = 0 \tag{3.5}$$

$$\lambda^3 - (c_2 + c_5)\lambda^2 + (c_2 c_5 - c_1 - c_3 c_4)\lambda + (c_1 c_5 - \mathrm{V}c_3) = 0 \tag{3.6}$$

The roots of the derived characteristic equation provide the eigenvalues and determine the stability condition. Similarly, the characteristic equation of the 2 DOF fifth order shimmy model is derived, and stability analysis is performed using the eigenvalues.

3.2 Routh-Hurwitz Criterion

The Routh-Hurwitz Criterion is a mathematical method used in the aviation industry to determine the stability of dynamic systems without solving for the eigenvalues explicitly. This criterion provides a systematic procedure to assess whether all the roots of a characteristic polynomial lie in the left half of the complex plane, which corresponds to stable behavior. In aviation, ensuring the stability of control systems and dynamic models is critical for safe operation. The Routh-Hurwitz Criterion involves constructing the Routh array from the coefficients of the characteristic polynomial. By examining the first column of this array, one can determine the number of roots with positive real parts. If there are no sign changes in the first column, the system is stable.

3.3 One DOF Third Order Landing Gear Shimmy Model

The research work mentioned in Section 1.1, present the developed landing gear and tire models. Among the mentioned research work Somieski [6] provides a modeling approach of coupling simple mechanical model and the elastic tire model, the equations are also linearized and typical values of the landing gear system parameters of a small aircraft are provided. Therefore, the modeling approach by Somieski is widely used by other researchers [8][9]. The same approach shall be used in the current analysis, the detailed explanation of tire and landing gear mechanical models are can be found in some doctoral thesis [7] [[8][9] . The simple trailing wheel model seen in Figure 3.2 and Figure 3.3 are used to evaluate the shimmy instability.

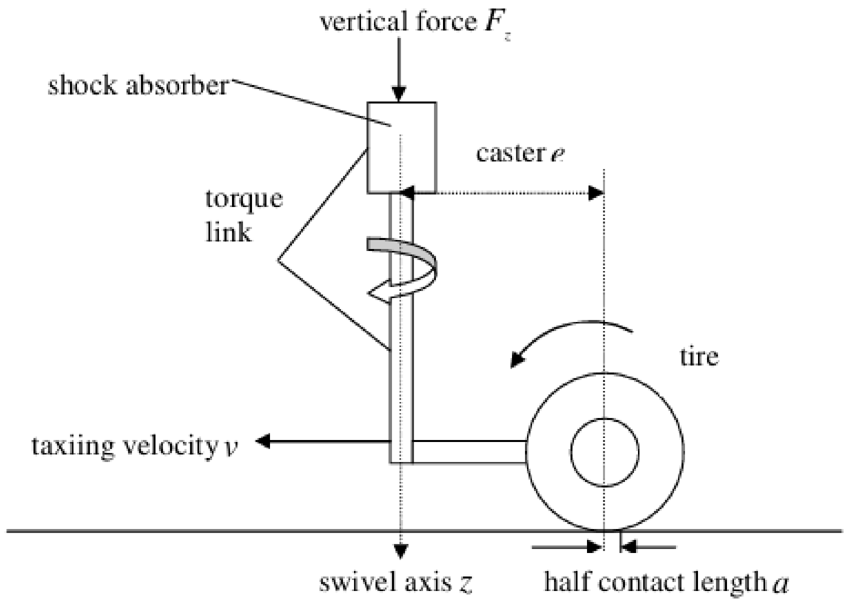

Figure 3.2 : Shimmy dynamic model side view [12].

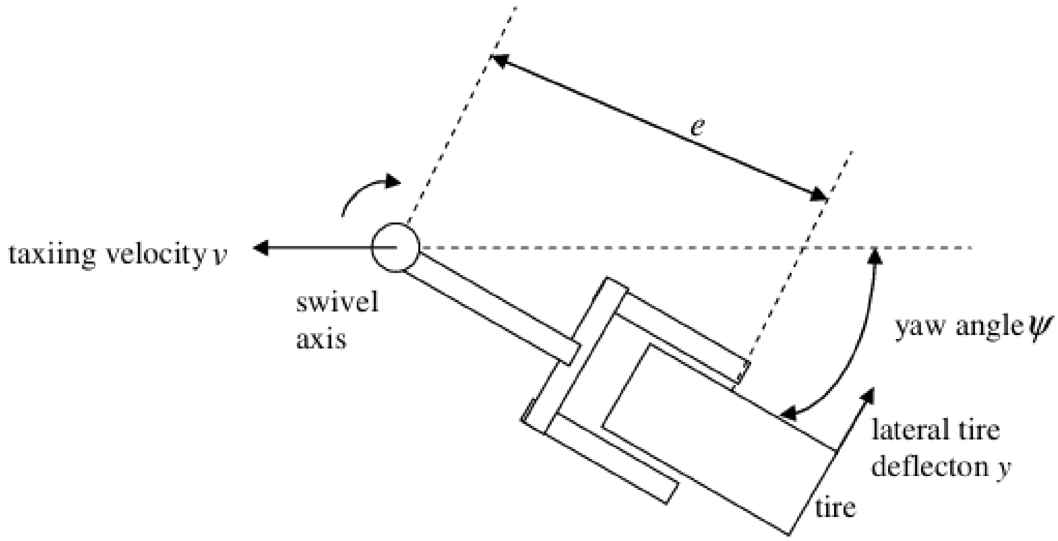

Figure 3.3 : Shimmy dynamic model top view [12].

The torsional dynamics of the lower parts of the landing gear is described by the following equation [6]:

$$I_z\ddot{\Psi} = M_1 + M_2 + M_3 + M_4 \tag{3.7}$$

Where Iz is the moment of inertia about the z-axis. M_1 is the linear spring torque provided by the turning tube and the torque link and M_2 is a combined damping moment from the viscous friction in the bearings of the oleo-pneumatic shock absorber. M_3 is the tire moment due to tire lateral deformation and M_4 is the tire damping moment due to tire tread width. In the following equations, the notation of stiffness and damping has been changed from the original equations [6] similar to Atabay [9], such that the stiffness is represented by k_Ψ and the damping by c_Ψ.

$$M_1 = k_\Psi \Psi \tag{3.8}$$

$$M_2 = c_\Psi \dot{\Psi} \tag{3.9}$$

$$M_3 = M_z - eF_y \tag{3.10}$$

$$M_4 = \frac{K}{V}\dot{\Psi} \tag{3.11}$$

M_z is aligning torque and F_y is the cornering force. The constant K is defined as [6],[9]:

$$K = -0.15a^2 C_{F\alpha} F_z \tag{3.12}$$

F_y and M_z depend on the vertical force F_z and slip angle α.

$$F_y = \begin{cases} C_{F\alpha}\alpha F_z, & \alpha \le \delta \\ C_{F\alpha}\delta F_z sign(\alpha), & \alpha > \delta \end{cases} \tag{3.13}$$

$$\frac{M_z}{F_z} = \begin{cases} C_{M\alpha}\dfrac{\alpha_g}{180}\sin\left(\dfrac{180}{\alpha_g}\alpha\right), & \alpha \le \alpha_g \\ 0, & \alpha > \alpha_g \end{cases} \tag{3.14}$$

Where δ is the limiting slip angle of tire force (5 degrees) and α_g is the limiting angle of tire moment (10 degrees). The lateral deflection of the tire is;

$$\dot{y}_1 + \frac{V}{\sigma} y_1 = V\Psi + (e-a)\dot{\Psi} \tag{3.15}$$

From y_1 an equivalent slip angle is formed as:

$$\alpha \approx \arctan \alpha = \frac{y_1}{\sigma} \tag{3.16}$$

The equations given above are linearized and summerized in state-space form with states;

$$\begin{bmatrix} \dot{\Psi} \\ \ddot{\Psi} \\ \dot{y}_1 \end{bmatrix} = \begin{bmatrix} 0 & 1 & 0 \\ -\frac{k_\Psi}{I_z} & -\frac{c_\Psi}{I_z} + \frac{K}{VI_z} & \frac{F_z(C_{M\alpha} - eC_{F\alpha})}{I_z\sigma} \\ V & e-a & -\frac{V}{\sigma} \end{bmatrix} \begin{bmatrix} \Psi \\ \dot{\Psi} \\ y_1 \end{bmatrix} \tag{3.17}$$

Table 3.1 : 1 DOF 3 order shimmy model parameters.

Description	Parameter	Value	Unit
k_Ψ	torsional spring rate	100000	Nm/rad
c_Ψ	torsional damping constant	50	Nm/rad/s
I_z	rotational area moment of inertia	1	kgm^2
K	tire longitudinal slip; tread width moment constant	-270	Nm^2/rad
F_z	vertical force	9000	N
$C_{m\alpha}$	tire self-alligning moment derivative	-2	m/rad
$C_{f\alpha}$	tire side force derivative	20	1/rad
a	half contact length	0.1	m
e	caster length	0.05	m
V	velocity of aircraft	100	m/s

3.3.1 One DOF third order stable/unstable region

In this study, stability analysis was performed both by calculating the eigenvalues and by using the Routh-Hurwitz criteria. The e-V plane can only be used during the design phase, while the F_z-V plane can also be used during the operational phase.

3.3.1.1 One DOF third order shimmy model e-V plane stability status

In this section, caster length (e) and aircraft speed (V) are defined as variables. The stability and instability conditions of the system will be investigated based on these variations. While plotting the e-V plane, for different rotational stiffness coefficient (k_Ψ) values are used. The other parameter values are taken from Table 3.1.

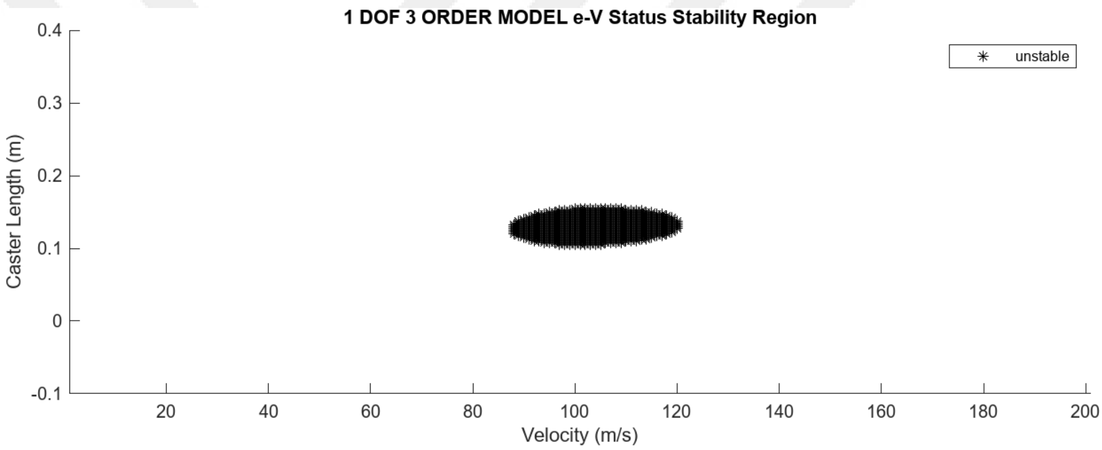

Figure 3.4 : 1 DOF Stability region of e-V plane for k=100000 Nm/rad (Eigenvalue).

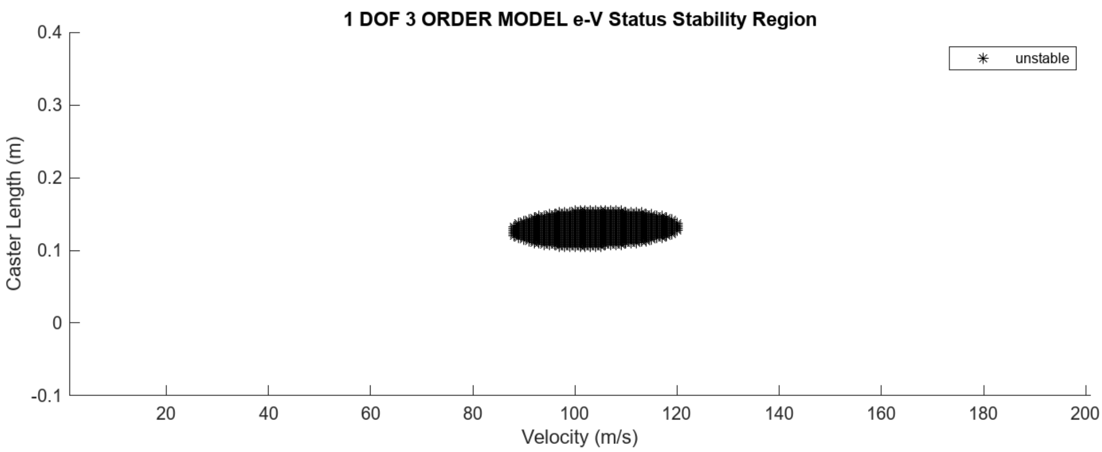

Figure 3.5 : 1 DOF Stability region of e-V plane for k=100000 Nm/rad (Routh-Hurwitz).

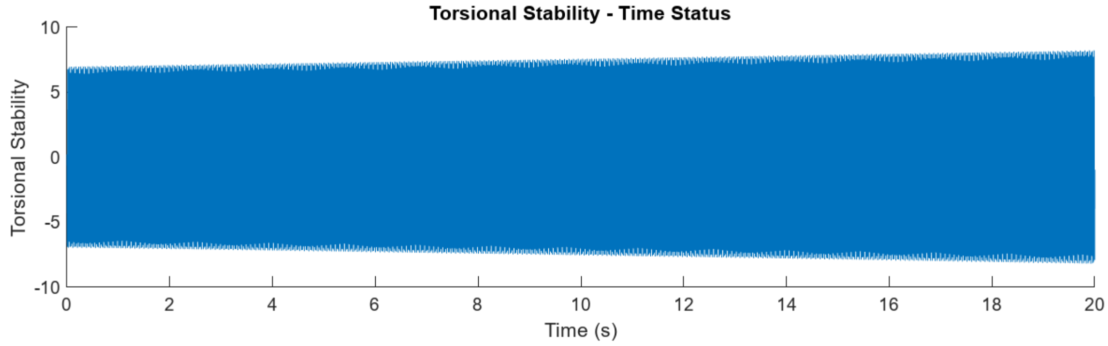

Figure 3.6 : 1 DOF Torsional stability for k=100000 & V=120 m/s & e=0.1325 m (unstable).

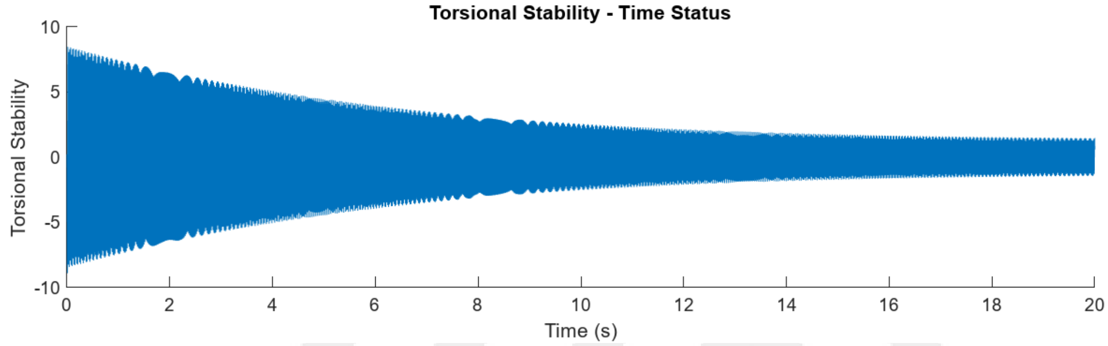

Figure 3.7 : 1 DOF Torsional stability for k=100000 & V=85 m/s & e=0.1325 m (stable).

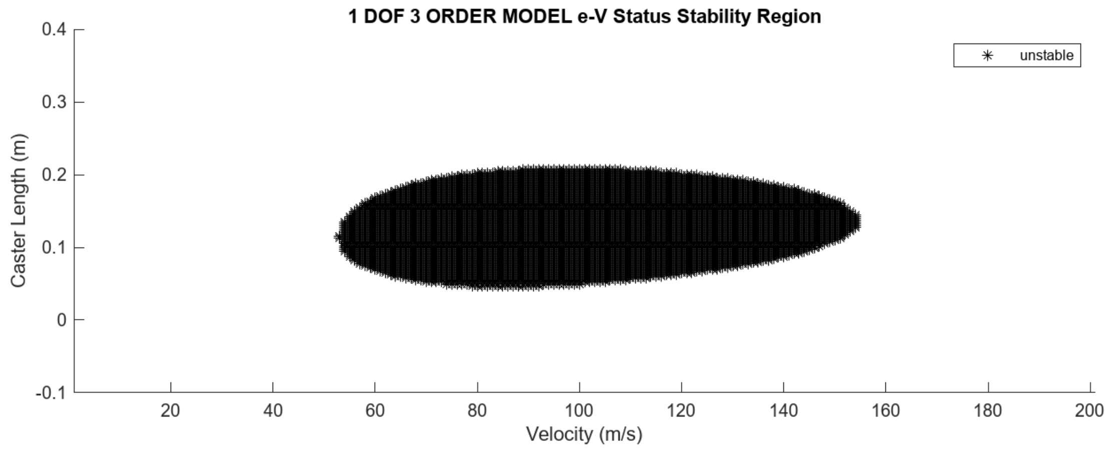

Figure 3.8 : 1 DOF Stability region of e-V plane for k=75000 Nm/rad (Eigenvalue).

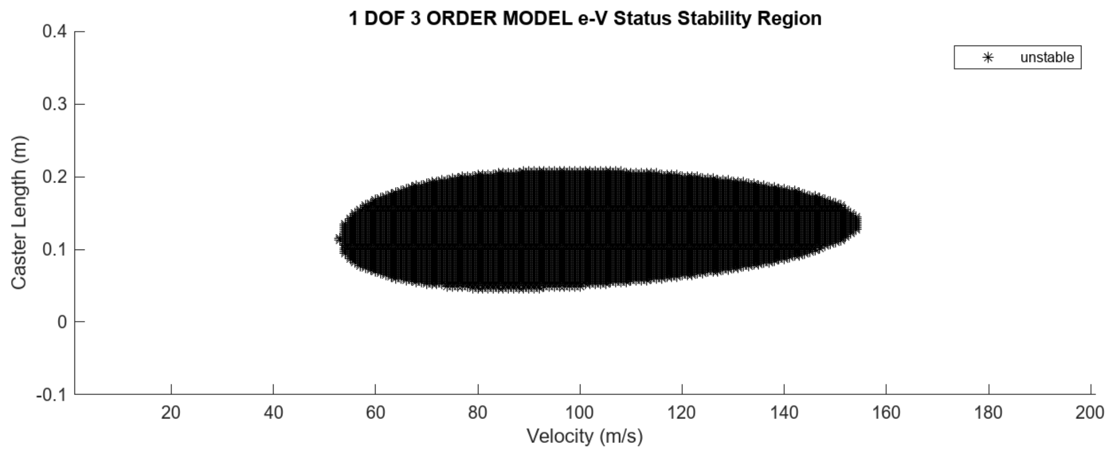

Figure 3.9 : 1 DOF Stability region of e-V plane for k=75000 Nm/rad (Routh-Hurwitz).

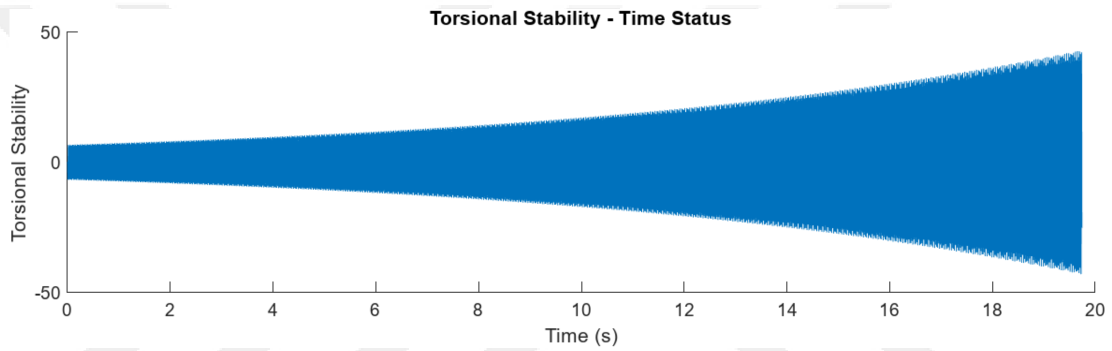

Figure 3.10 : 1 DOF Torsional stability for k=75000 & V=153 m/s & e=0.135 m (unstable).

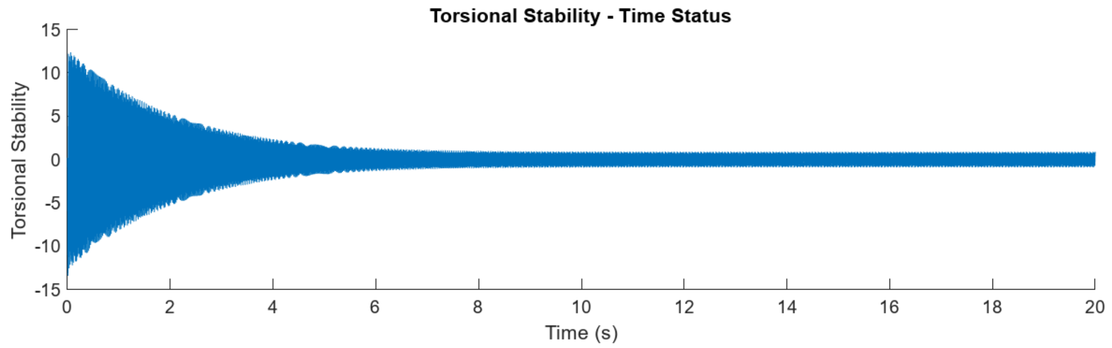

Figure 3.11 : 1 DOF Torsional stability for k=75000 & V=52 m/s & e=0.135 m (stable).

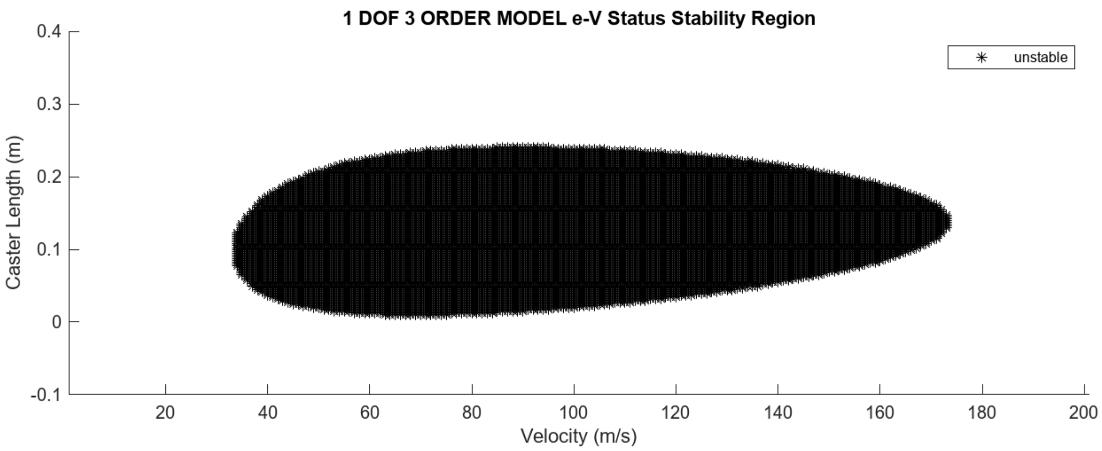

Figure 3.12 : 1 DOF Stability region of e-V plane for k=50000 Nm/rad (Eigenvalue).

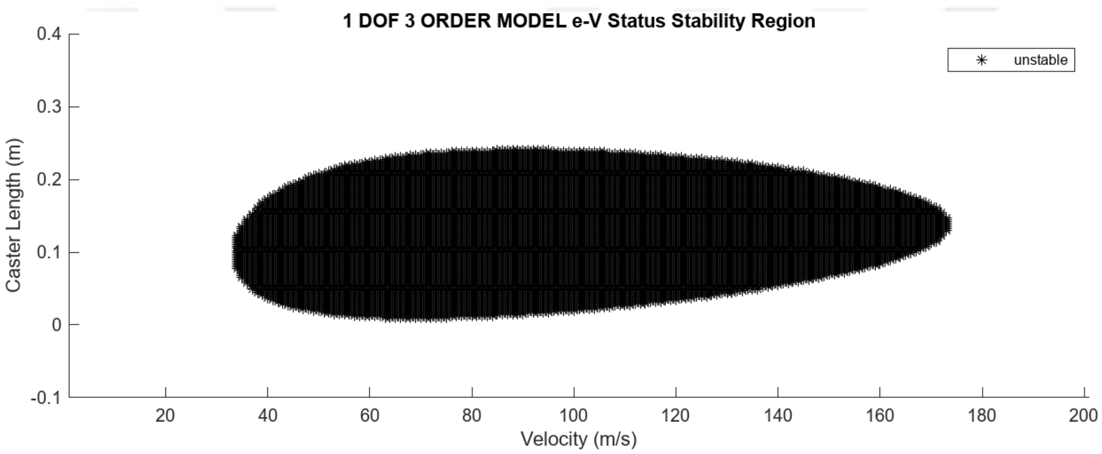

Figure 3.13 : 1 DOF Stability region of e-V plane for k=50000 Nm/rad (Routh-Hurwitz).

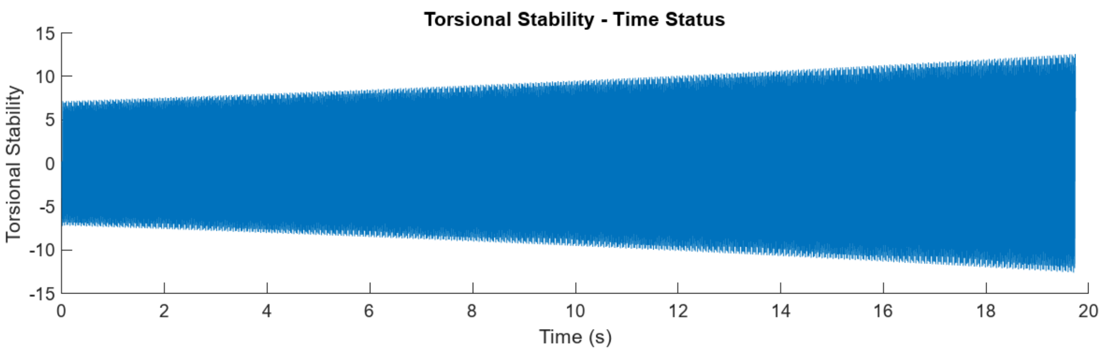

Figure 3.14 : 1 DOF Torsional stability for k=50000 & V=173 m/s & e=0.14 m (unstable).

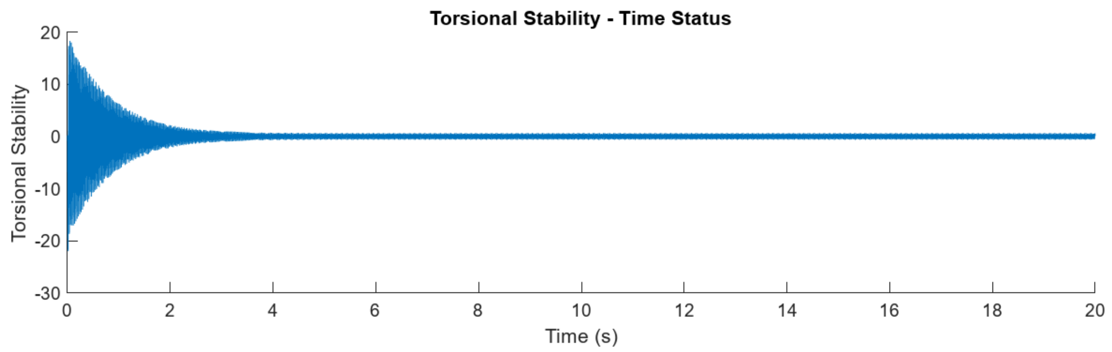

Figure 3.15 : 1 DOF Torsional stability for k=50000 & V=33 m/s & e=0.14 m (stable).

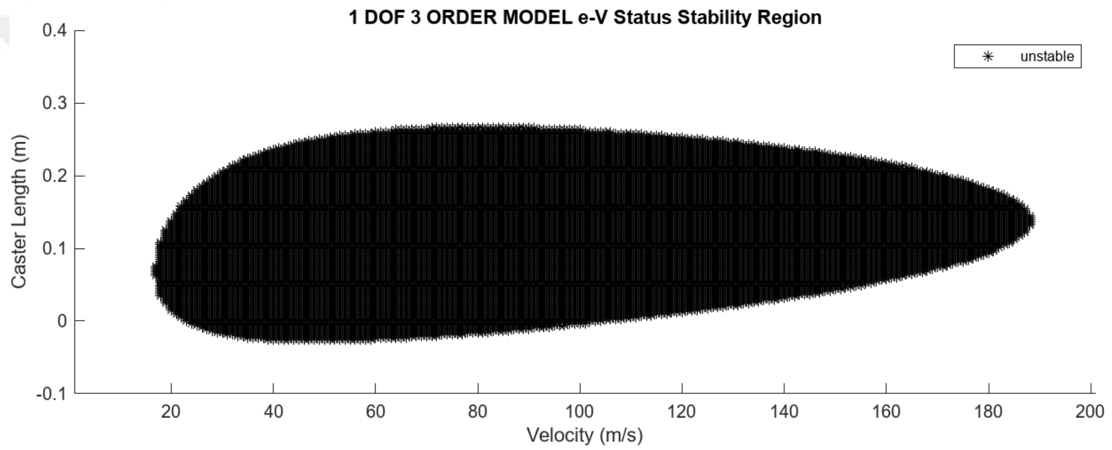

Figure 3.16 : 1 DOF Stability region of e-V plane for k=25000 Nm/rad (Eigenvalue).

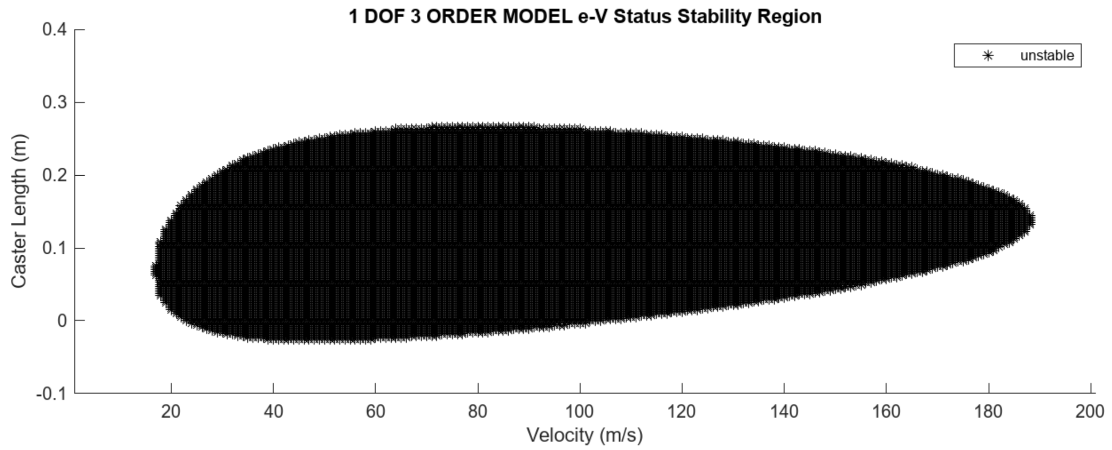

Figure 3.17 : 1 DOF Stability region of e-V plane for k=25000 Nm/rad (Routh-Hurwitz).

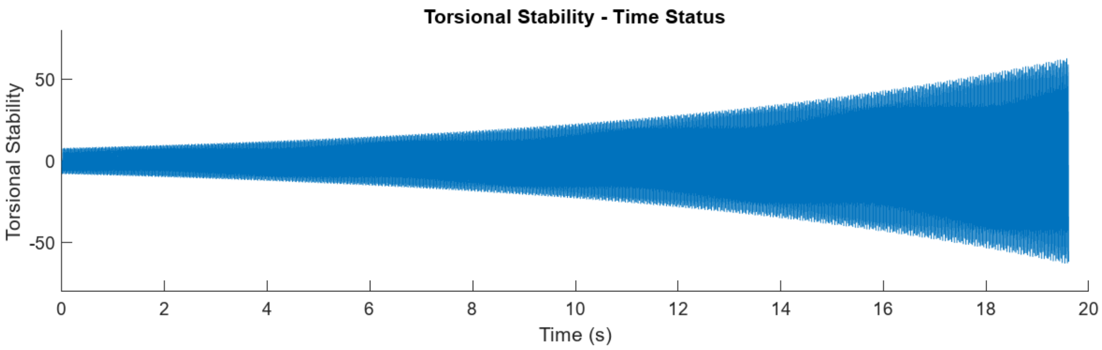

Figure 3.18 : 1 DOF Torsional stability for k=25000 & V=187 m/s & e=0.14 m (unstable).

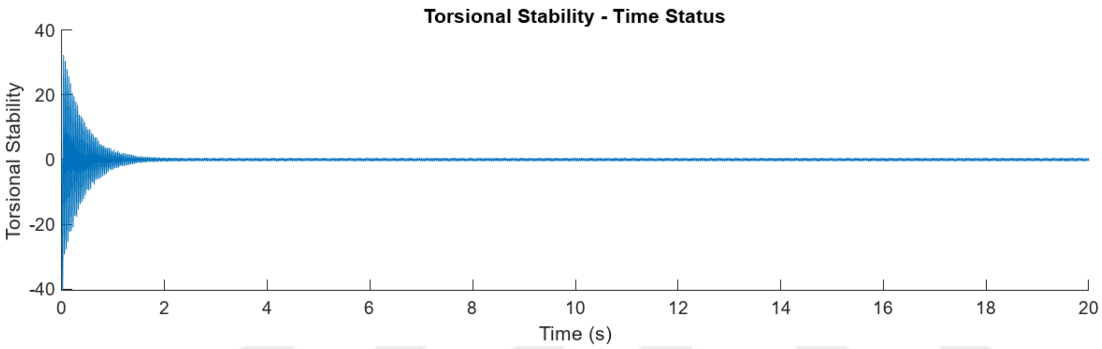

Figure 3.19 : 1 DOF Torsional stability for k=25000 & V=18 m/s & e=0.14 m (stable).

Conclusion;

- As seen in Figures 3.4-3.5, 3.8-3.9, 3.12-3.13, and 3.16-3.17, the system was solved using both the eigenvalue method and the Routh-Hurwitz method, resulting in identical graphs. Therefore, only one method will be used in the subsequent graphs.
- As seen in Figures 3.6-3.7, 3.10-3.11, 3.14-3.15, and 3.18-3.19, both stable and unstable conditions were created. Closely spaced values were selected to examine the critical conditions while generating the curves.
- Table 4.2 shows that as the normal tire force increases, stability decreases. Conversely, as the rotational stiffness coefficient increases, stability also increases.

Table 3.2 : 1 DOF 3 order the effect of F_z change on e -V plane.

e=-0.1-0.4 m	Rotational Stiffness Coefficient			
V=1-200 m/s	k=100000 Nm/rad	k=75000 Nm/rad	k=50000 Nm/rad	k=25000 Nm/rad
Fz=10000 N	87.09 % stable	76.48 % stable	65.38 % stable	54.47 % stable
	55.32 % increment	51.42 % increment	46.76 % increment	43.08 % increment
Fz=12500 N	66.16 % stable	59.23 % stable	51.95 % stable	44.00 % stable
	17.99 % increment	17.26 % increment	16.61 % increment	15.58 % increment
Fz=15000 N	56.07 % stable	50.51 % stable	44.55 % stable	38.07 % stable
Fz=17500 N	49.5 % stable	44.75 % stable	39.69 % stable	34.04 % stable
	11.72 % decrement	11.40 % decrement	10.91 % decrement	10.59 % decrement
Fz=20000 N	44.8 % stable	40.64 % stable	36.13 % stable	31.16 % stable
	20.10 % decrement	19.54 % decrement	18.9 % decrement	18.15 % decrement

3.3.1.2 One DOF third order shimmy model F_z-V plane stability status

In this section, normal tire force (F_z) and aircraft speed (V) are defined as variables. The stability and instability conditions of the system will be investigated based on these variations. While plotting the F_z-V plane, for different rotational stiffness coefficient (k) values are used. The other parameter values are taken from Table 3.1.

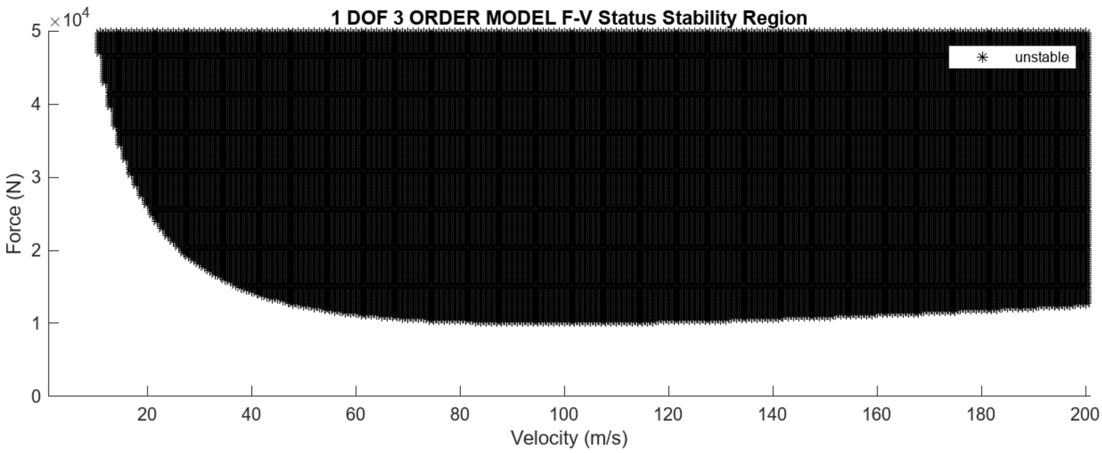

Figure 3.20 : 1 DOF Stability region of F_z -V plane for k=100000 Nm/rad (Eigenvalue).

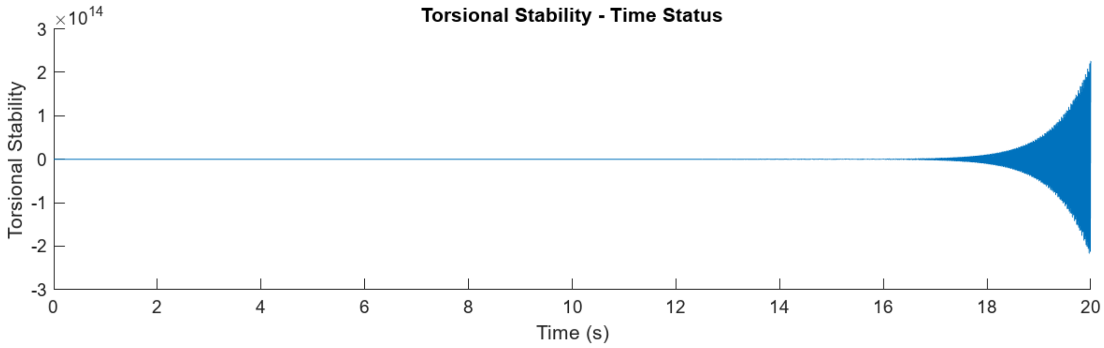

Figure 3.21 : 1 DOF Torsional stability for k=100000 & V=30 m/s & Fz=19000 N (unstable).

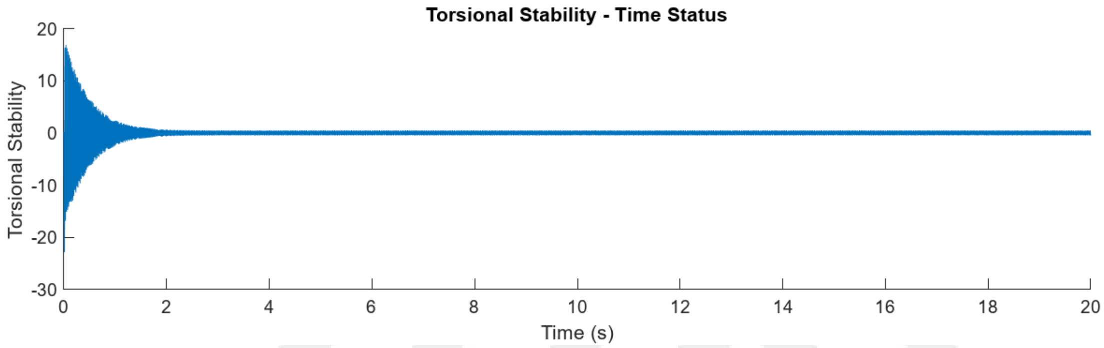

Figure 3.22 : 1 DOF Torsional stability for k=100000 & V=26 m/s & Fz=19000 N (stable).

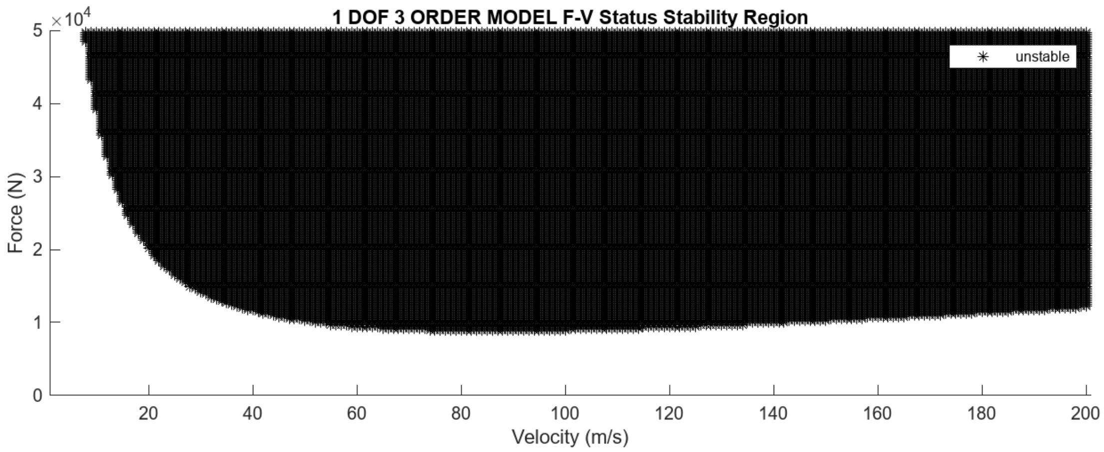

Figure 3.23 : 1 DOF Stability region of F_z -V plane for k=75000 Nm/rad (Eigenvalue).

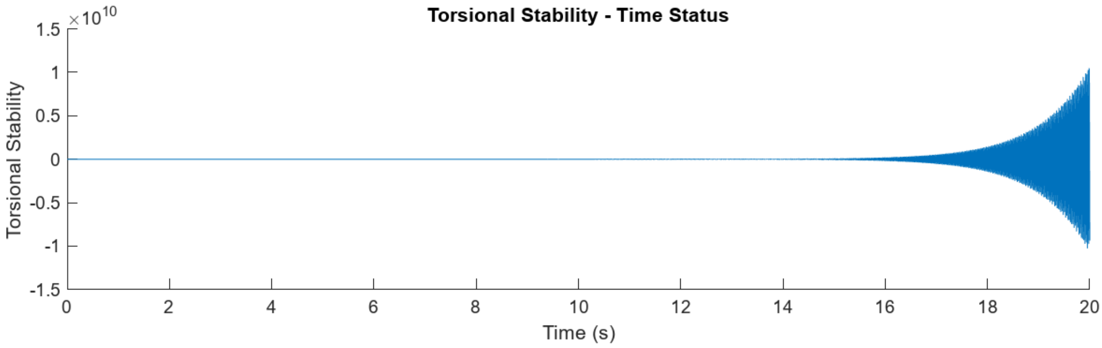

Figure 3.24 : 1 DOF Torsional stability for k=75000 & V=22 m/s & Fz=19000 N (unstable).

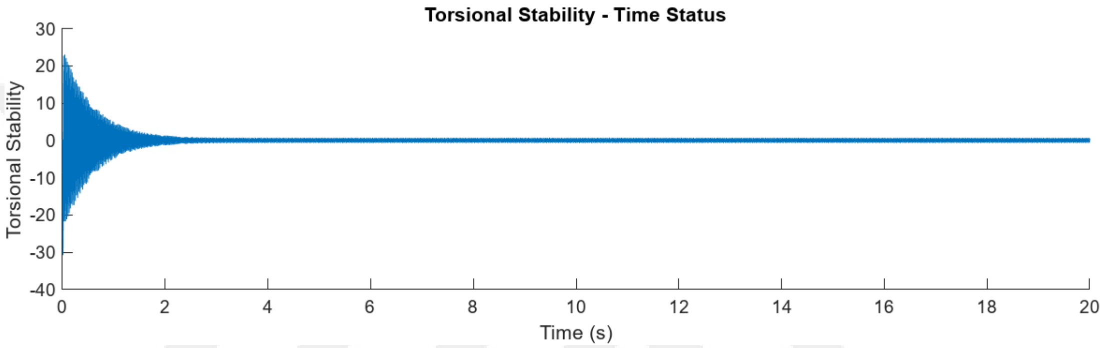

Figure 3.25 : 1 DOF Torsional stability for k=75000 & V=20 m/s & Fz=19000 N (stable).

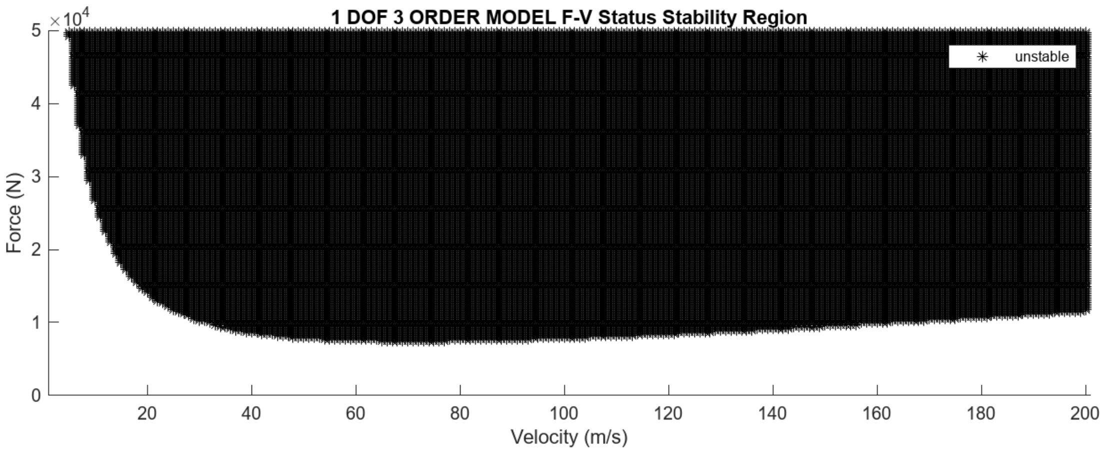

Figure 3.26 : 1 DOF Stability region of F_z -V plane for k=50000 Nm/rad (Eigenvalue).

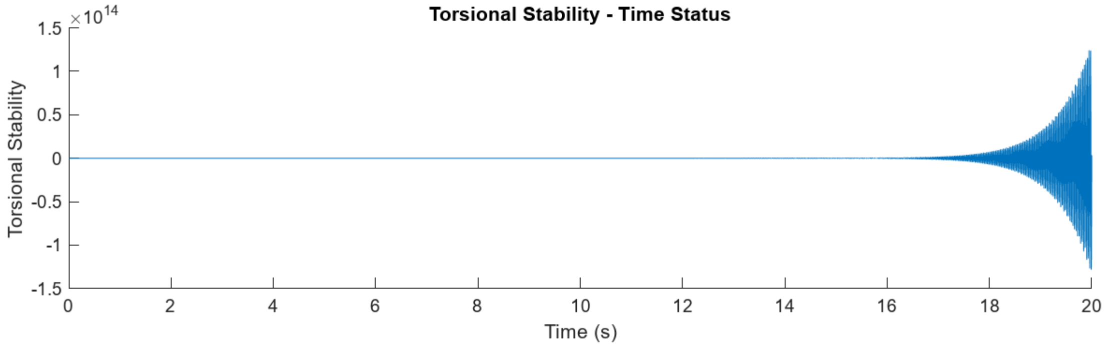

Figure 3.27 : 1 DOF Torsional stability for k=50000 & V=15 m/s & Fz=19000 N (unstable).

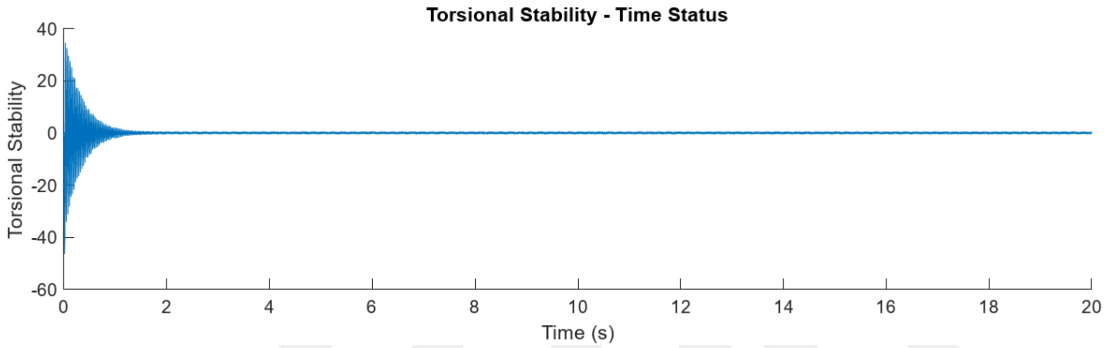

Figure 3.28 : 1 DOF Torsional stability for k=50000 & V=13 m/s & Fz=19000 N (stable).

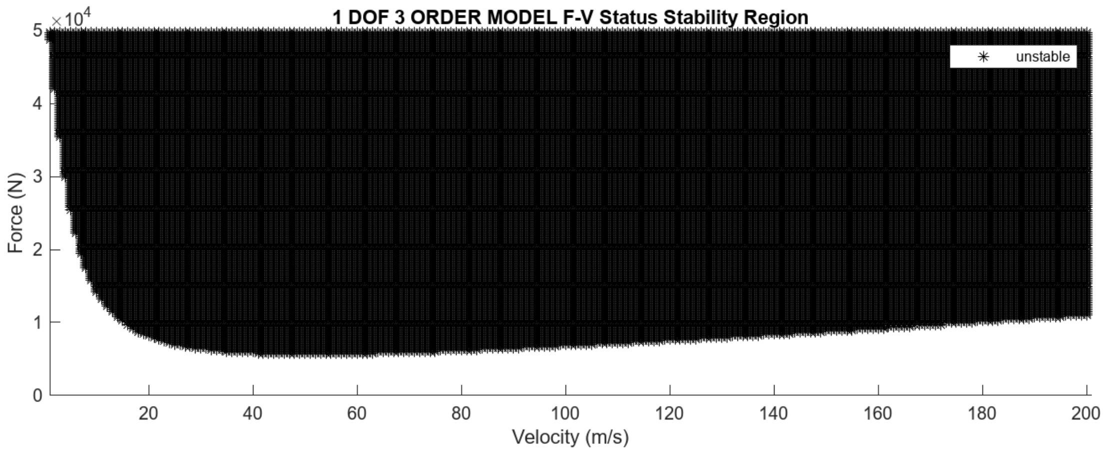

Figure 3.29 : 1 DOF Stability region of F_z-V plane for k=25000 Nm/rad (Eigenvalue).

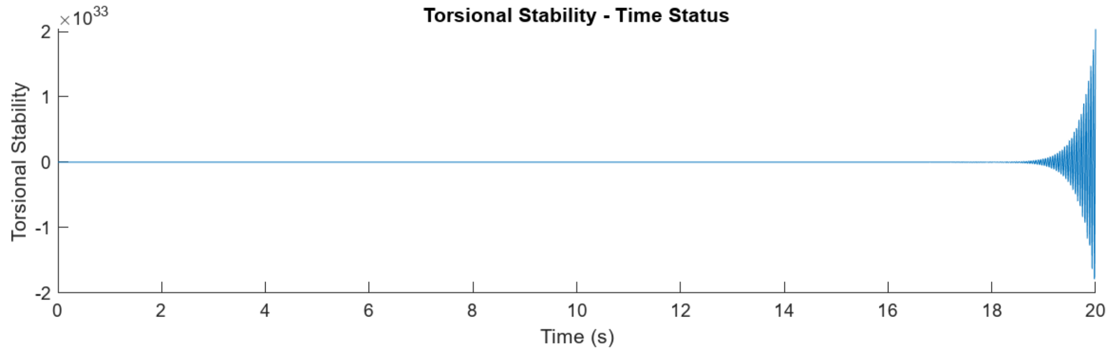

Figure 3.30 : 1 DOF Torsional stability for k=25000 & V=8 m/s & Fz=19000 N (unstable).

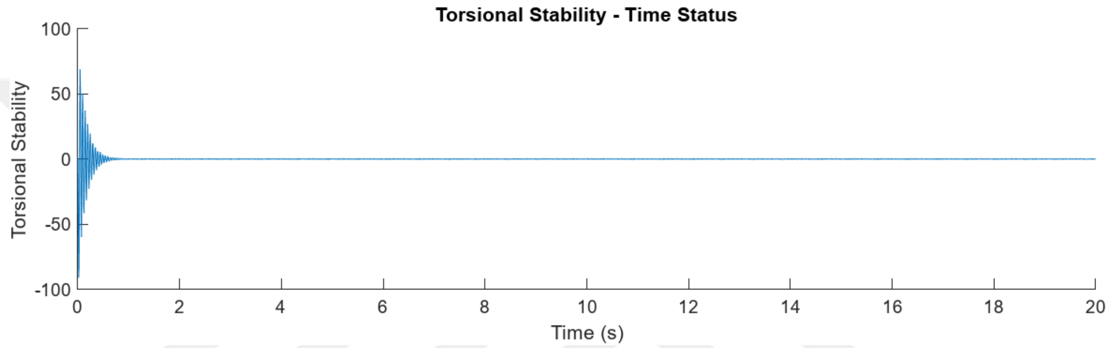

Figure 3.31 : 1 DOF Torsional stability for k=25000 & V=6 m/s & Fz=19000 N (stable).

Conclusion;

- In Figures 3.20, 3.23, 3.26, and 3.29, the stable region is observed. In these graphs, the variables are normal tire force and aircraft speed..
- As seen in Figures 3.21-3.22, 3.24-3.25, 3.27-3.28, and 3.30-3.31, both stable and unstable conditions were created. Closely spaced values were selected to examine the critical conditions while generating the curves.
- Examining Table 4.3, it is evident that an increase in caster length (e) expands the stability region. Similarly, an increase in the rotational stiffness coefficient also expands the stability region.

Table 3.3 : 1 DOF 3 order the effect of e change on F_z -V plane.

Fz=0-50000 N	Rotational Stiffness Coefficient			
V=1-200 m/s	k=100000 Nm/rad	k=75000 Nm/rad	k=50000 Nm/rad	k=25000 Nm/rad
e=0.26 m	42.93 % stable	39.6 % stable	35.95 % stable	31.79 % stable
	25.59 % increment	26.92 % decrement	28.56 % decrement	30.71 % decrement
e=0.28 m	49.00 % stable	45.57 % stable	41.80 % stable	37.5 % stable
	15.06 % decrement	15.91 % decrement	16.95 % decrement	18,27 % decrement
e=0.30 m	57.69 % stable	54.19 % stable	50.32 % stable	45.88 % stable
e=0.32 m	70.64 % stable	67.17 % stable	63.33 % stable	58.94 % stable
	22.45 % increment	23.95 % increment	25.85 % increment	28.47 % increment
e=0.34 m	89.99 % stable	87.3 % stable	84.18 % stable	80.50 % stable
	55.99 % increment	61.01 % increment	67.29 % increment	75.46 % increment

3.4 Two DOF Fifth Order Landing Gear Shimmy Model

In addition to the One DOF third-order shimmy model presented in Section 3.3, a lateral DOF has been added. Consequently, the system becomes, as seen in Figure 3.32, 2 DOF fifth-order model, considering the tire order. The system used by Arreza [14] will be applied.

Figure 3.32 : 2 DOF (Yaw and lateral) shimmy model [21].

The equations with the addition of the lateral degree of freedom to the torsional degree of freedom system are as follows:

$$I_z\ddot{\Psi} + k_\Psi \Psi + c_\Psi \dot{\Psi} + F_y e + M_z + M_k - F_Z e sin(\Psi) \sin(\Phi) = 0 \quad (3.18)$$

$$I_x\ddot{\delta} + k_\delta\delta + c_\delta\dot{\delta} + l_g F_y \cos(\Psi) - F_z e \sin(\Psi) = 0 \tag{3.19}$$

I_x represents the lateral area moment of inertia of the landing gear, k_δ represents the landing gear lateral stiffness coefficient, c_δ represents the landing gear lateral damping coefficient, and l_g represents the landing gear height.

The equations given above are linearized and summerized in state-space form with states;

$$\begin{bmatrix} \dot{\Psi} \\ \ddot{\Psi} \\ \dot{\delta} \\ \ddot{\delta} \\ \dot{y}_1 \end{bmatrix} = \begin{bmatrix} 0 & 1 & 0 & 0 & 0 \\ -\frac{k_\Psi}{I_z} & -\frac{c_\Psi}{I_z} + \frac{K}{VI_z} & 0 & 0 & \frac{F_z(C_{M\alpha} - eC_{F\alpha})}{I_z\sigma} \\ 0 & 0 & 0 & 1 & 0 \\ \frac{F_z e}{I_x} & 0 & -\frac{k_\delta}{I_x} & -\frac{c_\delta}{I_x} & -\frac{l_g F_z C_{F\alpha}}{I_x\sigma} \\ V & e-a & 0 & l_g & -\frac{V}{\sigma} \end{bmatrix} \begin{bmatrix} \Psi \\ \dot{\Psi} \\ \delta \\ \dot{\delta} \\ y_1 \end{bmatrix} \tag{3.20}$$

Table 3.4 : 2 DOF 5 order shimmy model parameters.

Description	Parameter	Value	Unit
k_Ψ	torsional spring rate	100000	Nm/rad
c_Ψ	torsional damping constant	50	Nm/rad/s
I_z	rotational area moment of inertia	1	kgm2
K	tire longitudinal slip; tread width moment constant	-270	Nm2/rad
F_z	vertical force	9000	N
$C_{m\alpha}$	tire self-alligning moment derivative	-2	m/rad
$C_{f\alpha}$	tire side force derivative	20	1/rad
a	half contact length	0.1	m
e	caster length	0.05	m
V	velocity of aircraft	100	m/s
k_δ	lateral spring rate	6100000	Nm/rad
c_δ	lateral damping constant	300	Nm/rad/s
I_x	lateral area moment of inertia	600	kgm2
l_g	landing gear hight	2.5	m

3.4.1 Two DOF third order stable/unstable region

Since it was proven in Section 3.3.1.1, eigenvalues and the Routh-Hurwitz method were not derived again using both methods. The graph was created using only one method. The e-V plane can only be used during the design phase, while the F_z-V plane can also be used during the operational phase.

3.4.1.1 Two DOF third order shimmy model e-V plane stability status

In this section, caster length (e) and aircraft speed (V) are defined as variables. The stability and instability conditions of the system will be investigated based on these variations. While plotting the e-V plane, for different rotational stiffness coefficient (k_Ψ) values are used. The other parameter values are taken from Table 3.4.

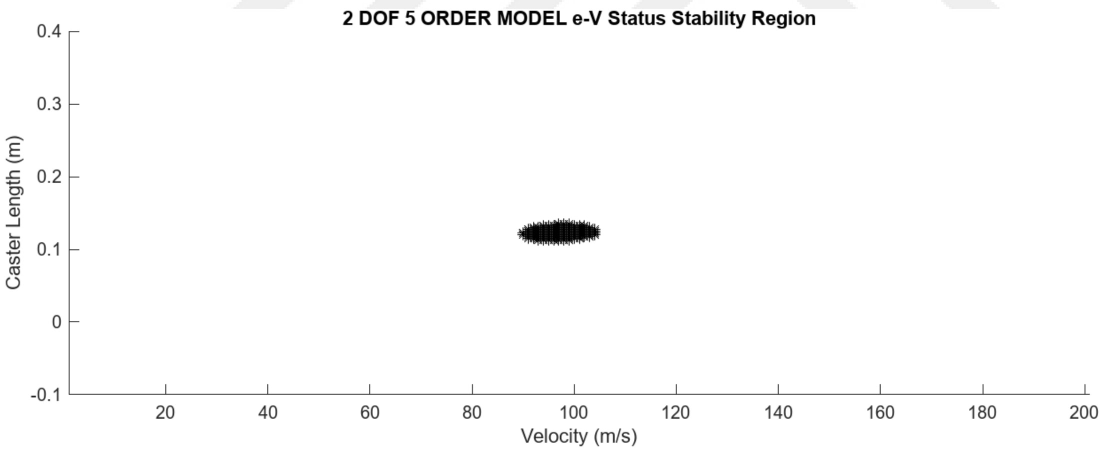

Figure 3.33 : 2 DOF Stability region of e-V plane for k=100000 Nm/rad.

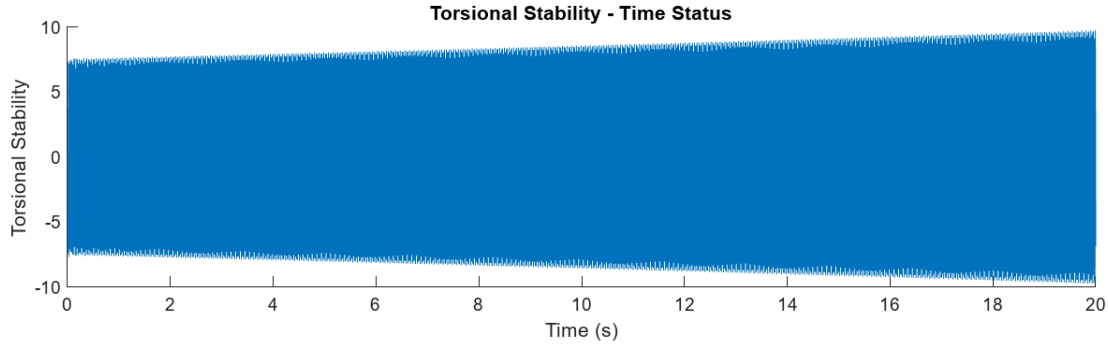

Figure 3.34 : 2 DOF Torsional stability for k=100000 & V=103 m/s & e=0.125 m (unstable).

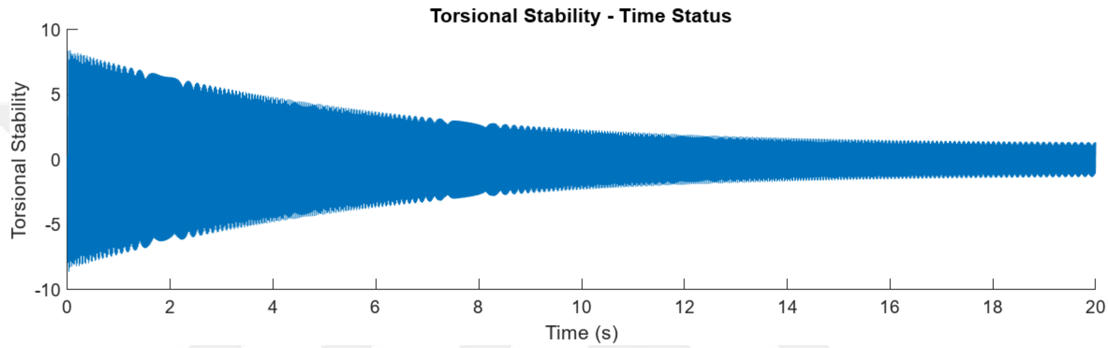

Figure 3.35 : 2 DOF Torsional stability for k=100000 & V=85 m/s & e=0.125 m (stable).

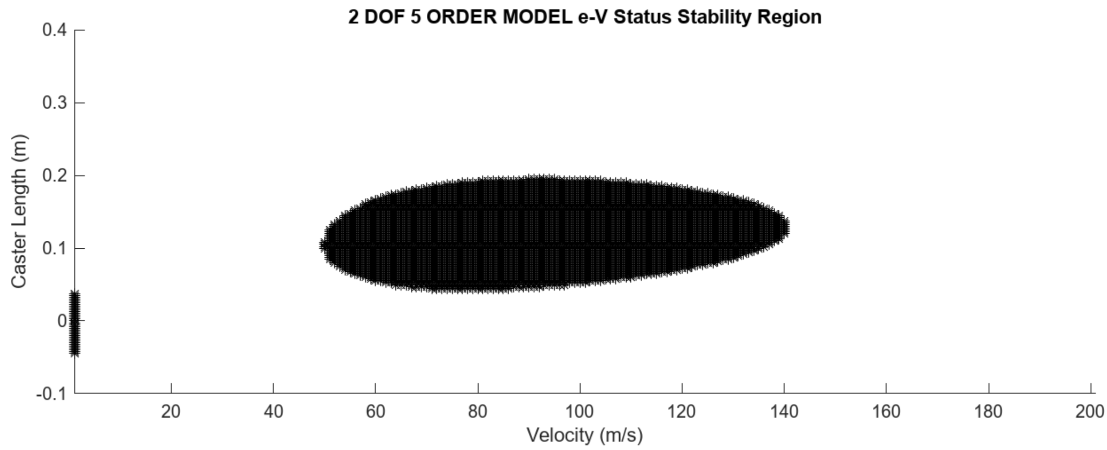

Figure 3.36 : 2 DOF Stability region of e-V plane for k=75000 Nm/rad.

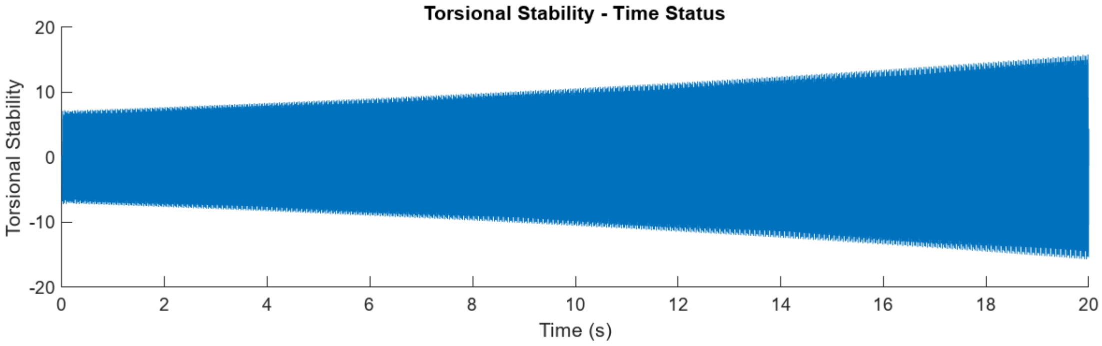

Figure 3.37 : 2 DOF Torsional stability for k=75000 & V=140 m/s & e=0.13 m (unstable).

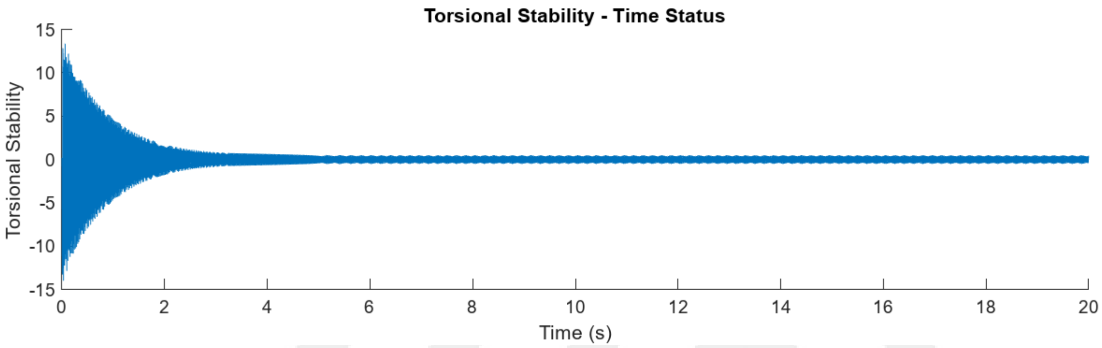

Figure 3.38 : 2 DOF Torsional stability for k=75000 & V=47 m/s & e=0.13 m (stable).

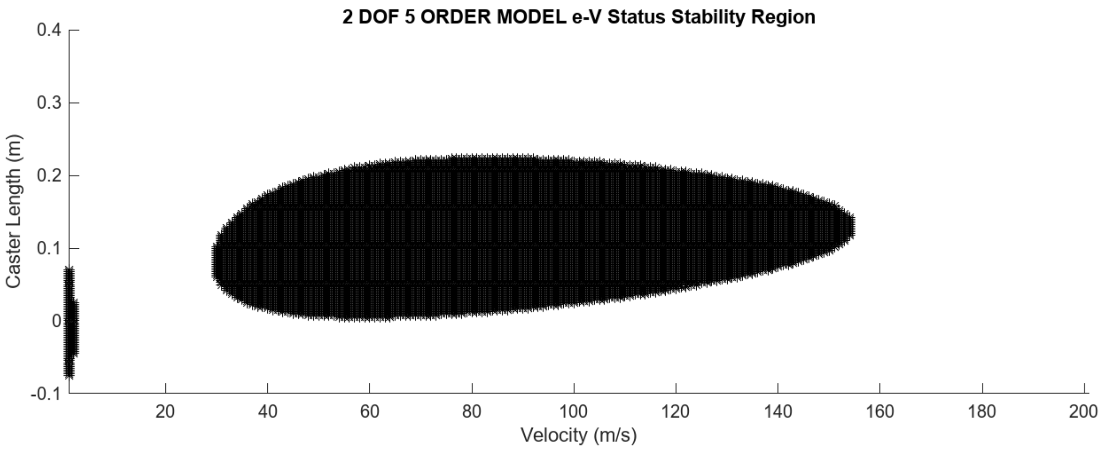

Figure 3.39 : 2 DOF Stability region of e-V plane for k=50000 Nm/rad.

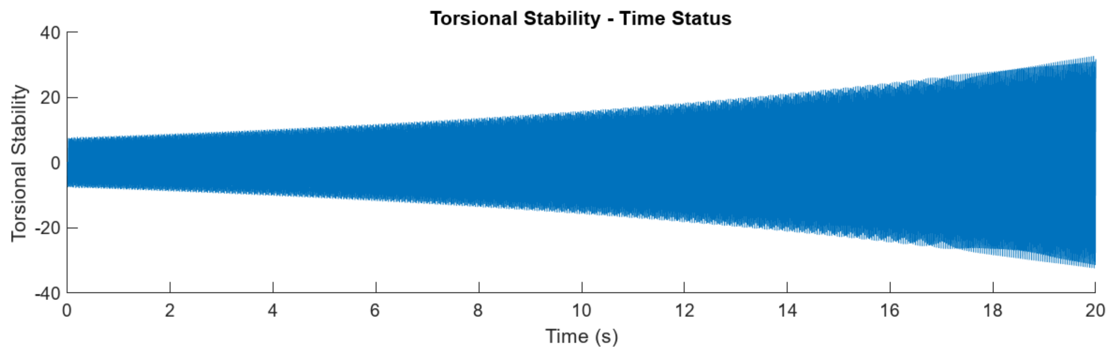

Figure 3.40 : 2 DOF Torsional stability for k=50000 & V=154 m/s & e=0.13 m (unstable).

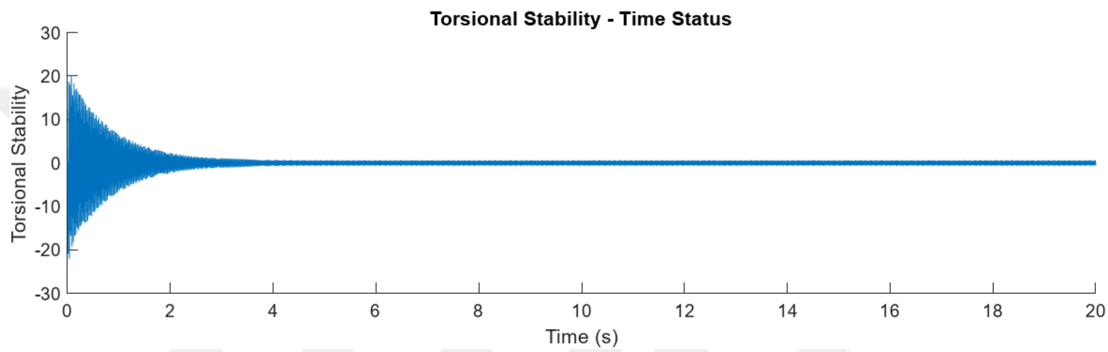

Figure 3.41 : 2 DOF Torsional stability for k=50000 & V=30 m/s & e=0.13 m (stable).

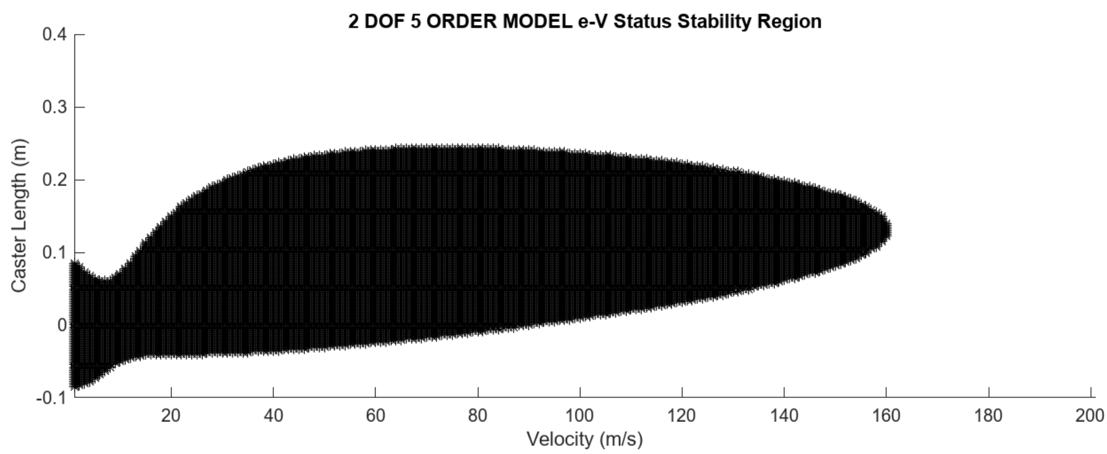

Figure 3.42 : 2 DOF Stability region of e-V plane for k=25000 Nm/rad.

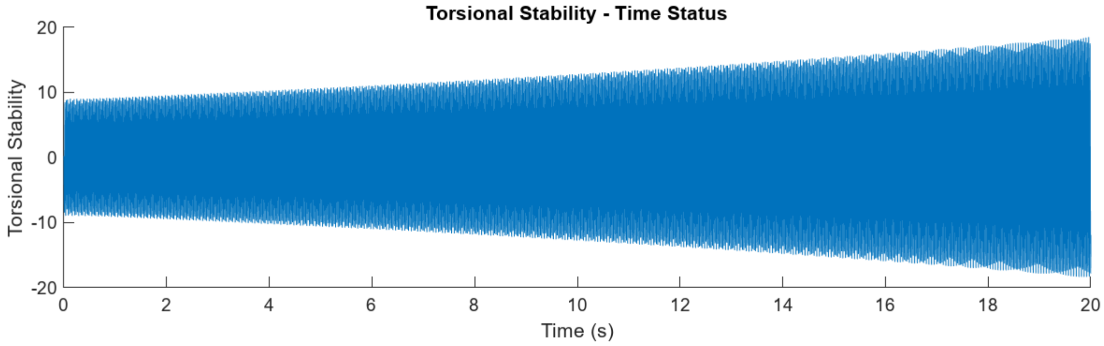

Figure 3.43 : 2 DOF Torsional stability for k=25000 & V=160 m/s & e=0.13 m (unstable).

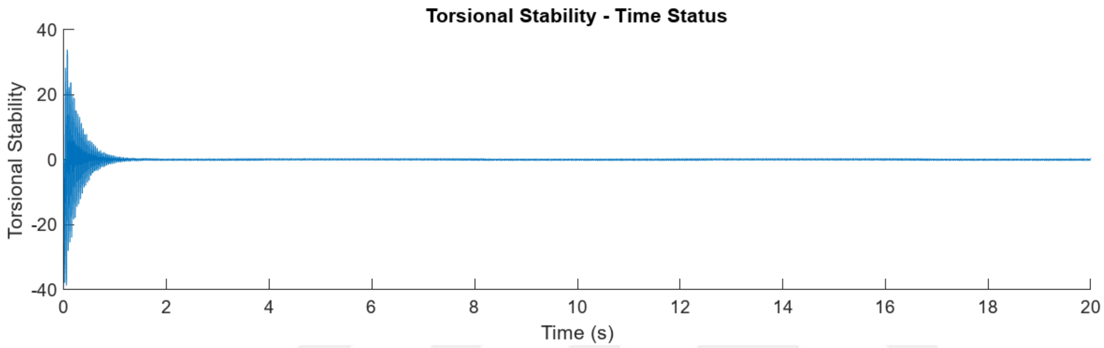

Figure 3.44 : 2 DOF Torsional stability for k=25000 & V=14 m/s & e=0.13 m (stable).

Conclusion;

- In Figures 3.33, 3.36, 3.39, and 3.42, the stable region is observed. In these graphs, the variables are caster length and aircraft speed..
- As seen in Figures 3.34-3.35, 3.37-3.38, 3.40-3.41, and 3.43-3.44, both stable and unstable conditions were created. Closely spaced values were selected to examine the critical conditions while generating the curves.
- Table 4.5 shows that as the normal tire force increases, stability decreases. Conversely, as the rotational stiffness coefficient increases, stability also increases.
- A similar situation to the One DOF third-order model applies to this model as well. However, the stability rates are different. Therefore, it is appropriate to consider both when a design or operational condition arises.

Table 3.5 : 2 DOF 5 order the effect of F_z change on e-V plane.

e=-0.1-0.4 m	Rotational Stiffness Coefficient			
V=1-200 m/s	k=100000 Nm/rad	k=75000 Nm/rad	k=50000 Nm/rad	k=25000 Nm/rad
Fz=10000 N	89.13 % stable	79.64 % stable	70.29 % stable	60.58 % stable
	55.71 % increment	53.21 % increment	51.81 % increment	46.79 % increment
Fz=12500 N	67.74 % stable	61.23 % stable	54.48 % stable	47.53 % stable
	18,34 % increment	17.80 % increment	17.67 % increment	15.17 % increment
Fz=15000 N	57.24 % stable	51.98 % stable	46.30 % stable	41.27 % stable
Fz=17500 N	50.56 % stable	46.03 % stable	40.58 % stable	37.30 % stable
	11.67 % decrement	11.45 % decrement	12.35 % decrement	9.62 % decrement
Fz=20000 N	45.76 % stable	41.71 % stable	36.85 % stable	34.55 % stable
	20.06 % decrement	19.76 % decrement	20.41 % decrement	16.28 % decrement

3.4.1.2 Two DOF third order shimmy model F_z-V plane stability status

In this section, normal tire force (F_z) and aircraft speed (V) are defined as variables. The stability and instability conditions of the system will be investigated based on these variations. While plotting the F_z-V plane, for different rotational stiffness coefficient (k_Ψ) values are used. The other parameter values are taken from Table 3.4.

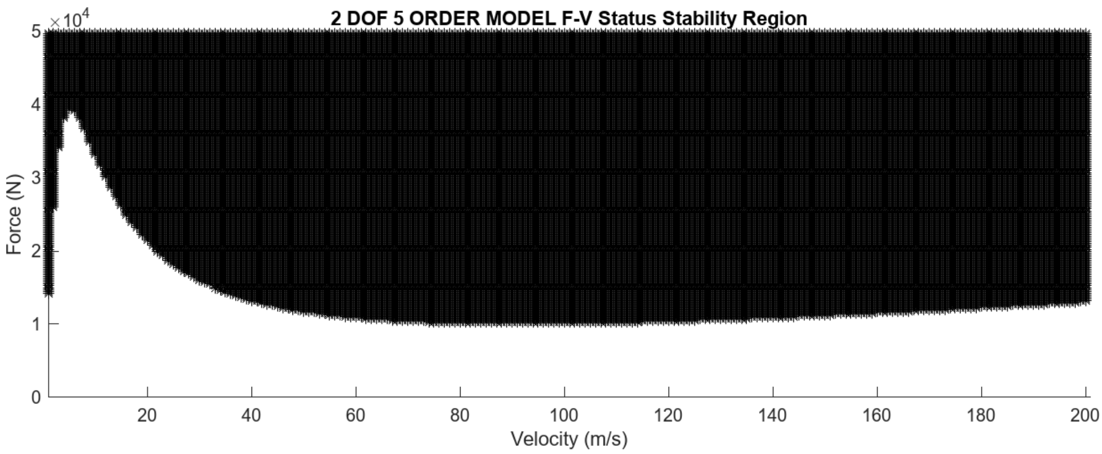

Figure 3.45 : 2 DOF Stability region of F_z-V plane for k=100000 Nm/rad.

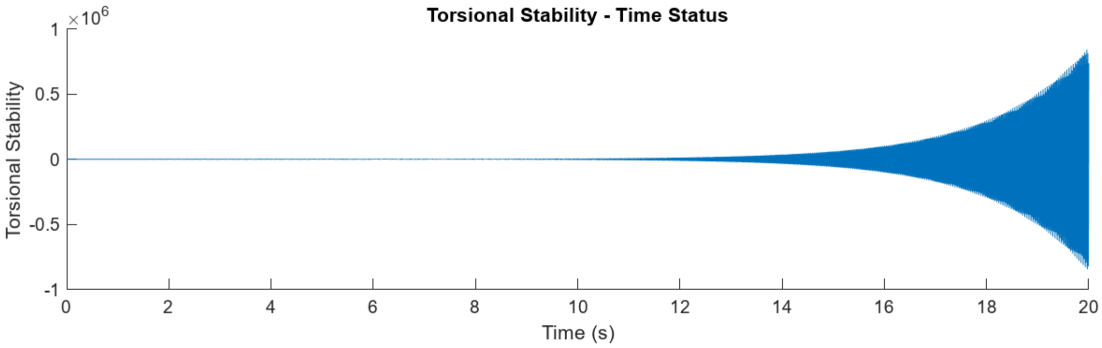

Figure 3.46 : 2 DOF Torsional stability for k=100000 & V=24 m/s & Fz=19000 N (unstable).

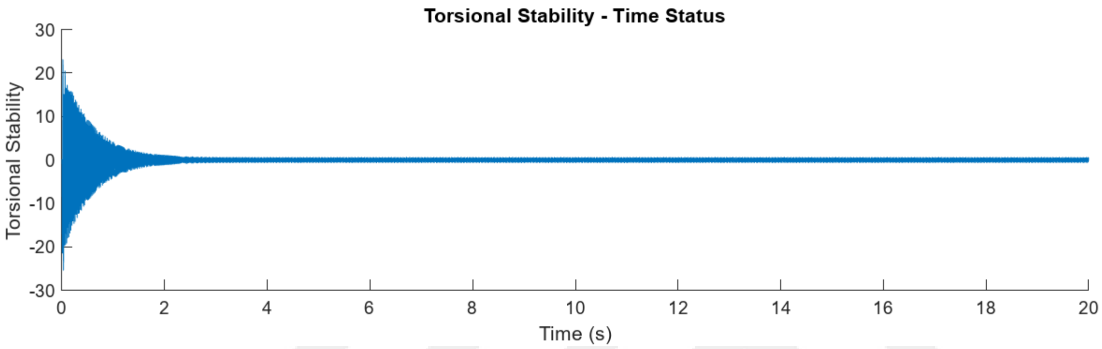

Figure 3.47 : 2 DOF Torsional stability for k=100000 & V=22 m/s & Fz=19000 N (stable).

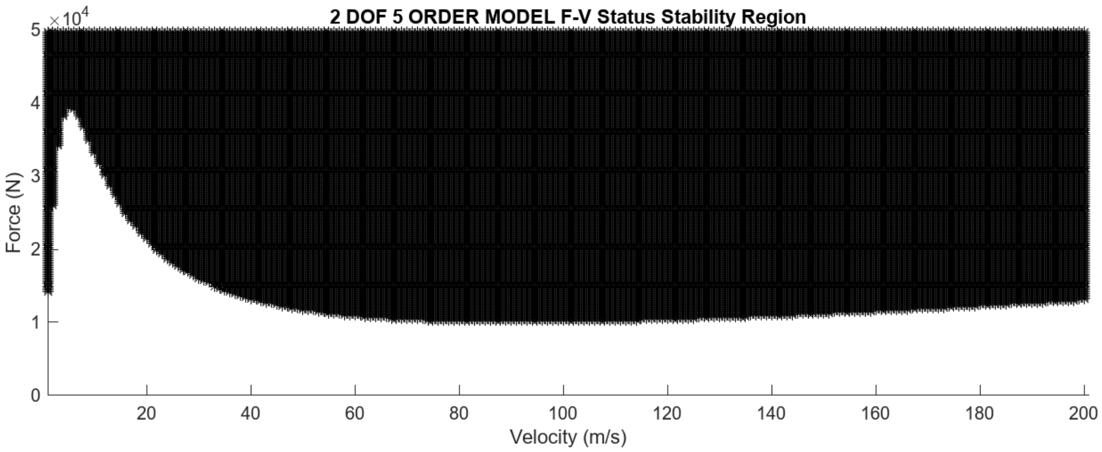

Figure 3.48 : 2 DOF Stability region of F_z-V plane for k=75000 Nm/rad.

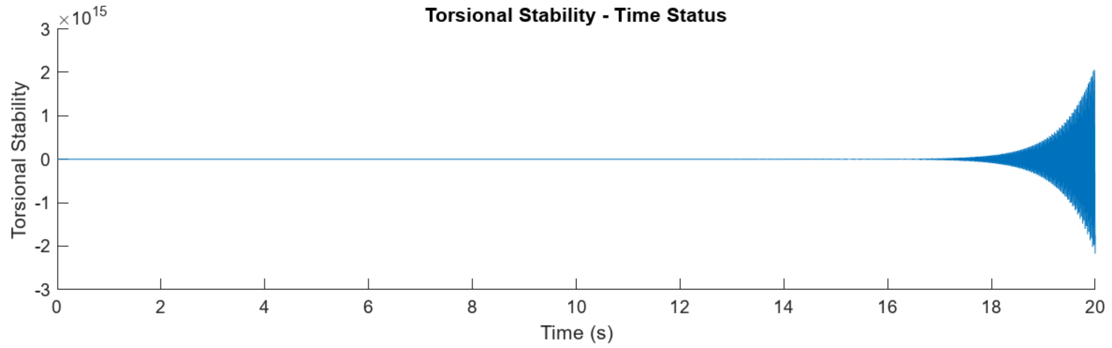

Figure 3.49 : 2 DOF Torsional stability for k=75000 & V=17 m/s & Fz=19000 N (unstable).

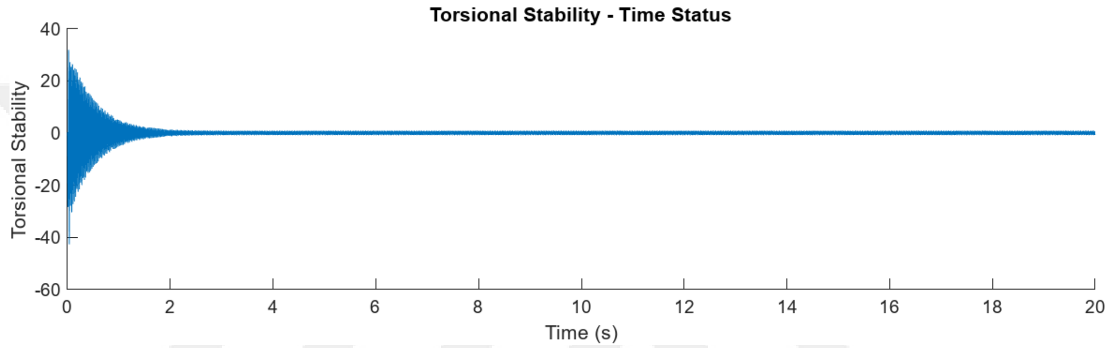

Figure 3.50 : 2 DOF Torsional stability for k=75000 & V=17 m/s & Fz=19000 N (stable).

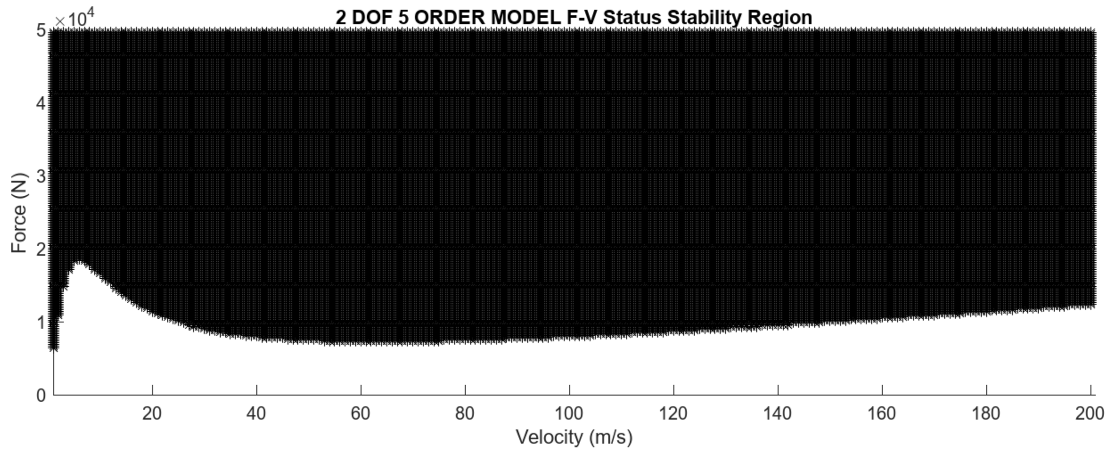

Figure 3.51 : 2 DOF Stability region of F_z-V plane for k=50000 Nm/rad.

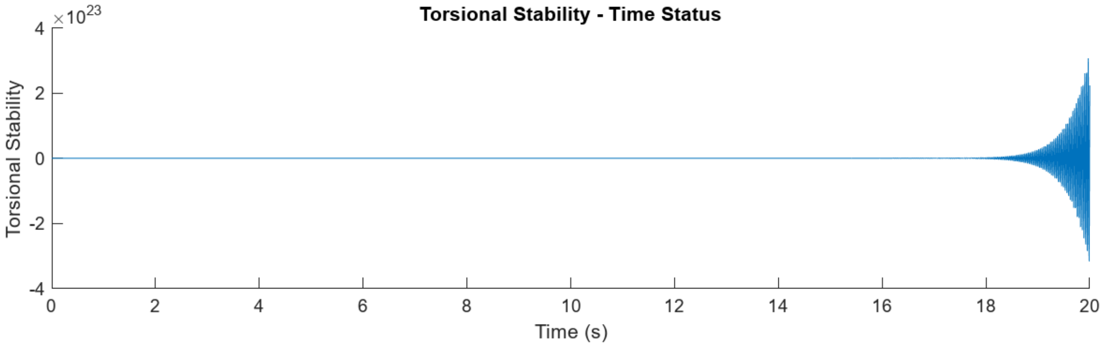

Figure 3.52 : 2 DOF Torsional stability for k=50000 & V=7 m/s & Fz=19000 N (unstable).

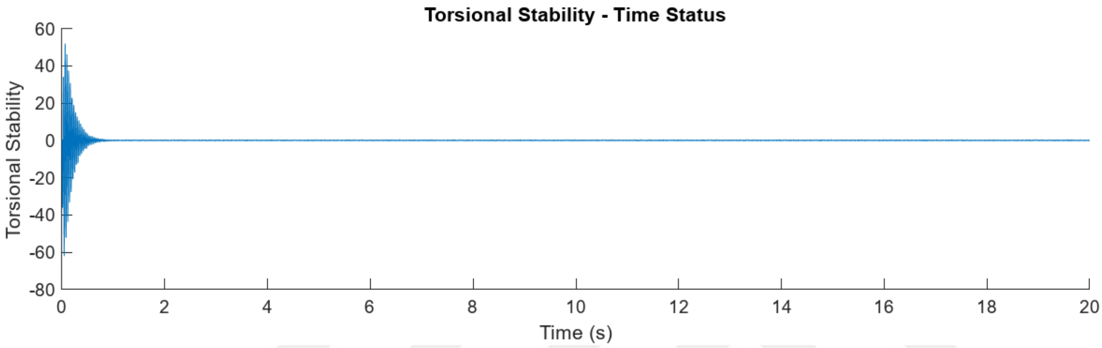

Figure 3.53 : 2 DOF Torsional stability for k=50000 & V=7 m/s & Fz=17000 N (stable).

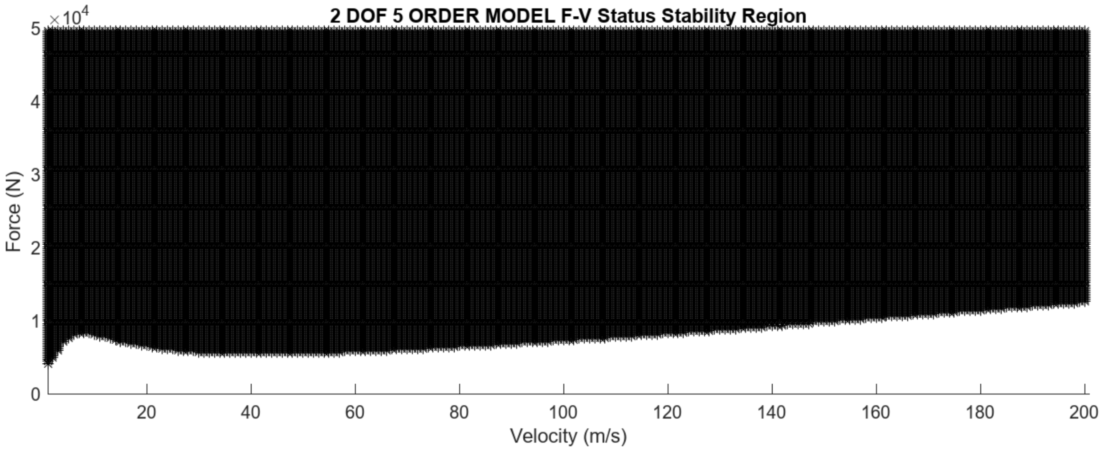

Figure 3.54 : 2 DOF Stability region of F_z-V plane for k=25000 Nm/rad.

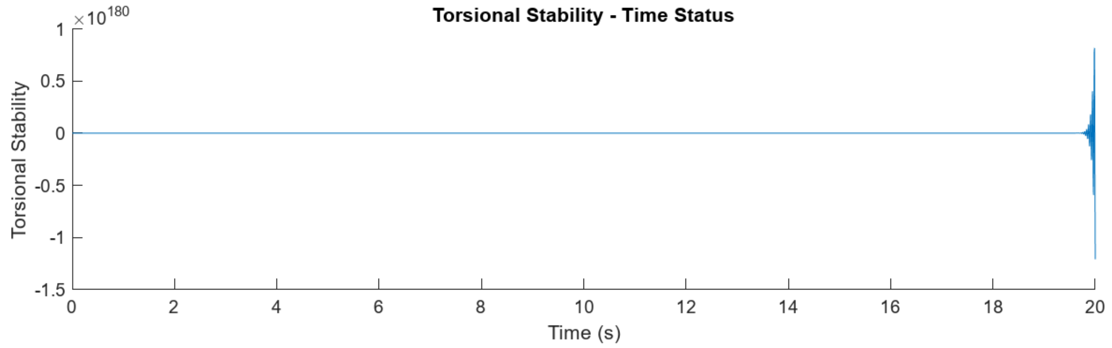

Figure 3.55 : 2 DOF Torsional stability for k=25000 & V=7 m/s & Fz=19000 N (unstable).

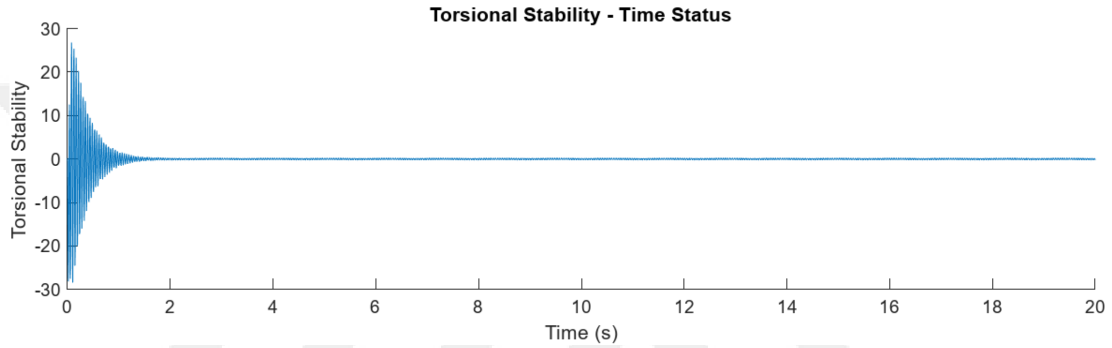

Figure 3.56 : 2 DOF Torsional stability for k=25000 & V=8 m/s & Fz=7500 N (stable).

Conclusion;

- In Figures 3.45, 3.48, 3.51, and 3.54, the stable region is observed. In these graphs, the variables are normal tire force and aircraft speed..
- As seen in Figures 3.46-3.47, 3.49-3.50, 3.52-3.53, and 3.55-3.56, both stable and unstable conditions were created. Closely spaced values were selected to examine the critical conditions while generating the curves.
- Examining Table 4.6, it is evident that an increase in caster length (e) expands the stability region. Similarly, an increase in the rotational stiffness coefficient also expands the stability region.

  As seen from the graphs and tables, the characteristics of the 1 DOF and 2 DOF shimmy models are similar. However, there are differences between them. While the stability rates may be very close under certain conditions, this is not always the case.

Table 3.6 : 2 DOF 5 order the effect of e change on F_z-V plane.

Fz=0-50000 N	Rotational Stiffness Coefficient			
V=1-200 m/s	k=100000 Nm/rad	k=75000 Nm/rad	k=50000 Nm/rad	k=25000 Nm/rad
e=0.26 m	46.45 % stable	43.64 % stable	40.75 % stable	37.87 % stable
	30.91 % increment	32.71 % decrement	34.76 % decrement	37.09 % decrement
e=0.28 m	54.71 % stable	52.00 % stable	49.24 % stable	46.55 % stable
	18.62 % decrement	20.81 % decrement	21.17 % decrement	22.67% decrement
e=0.30 m	67.23 % stable	64.85 % stable	62.46 % stable	60.20 % stable
e=0.32 m	87.04 % stable	85.59 % stable	84.19 % stable	83.02 % stable
	29.47 % increment	31.98 % increment	34.79 % increment	37.91 % increment
e=0.34 m	100 % stable	100 % stable	100 % stable	100 % stable
	48.74 % increment	54.20 % increment	60.10 % increment	66.11 % increment

4. LANDING GEAR SHIMMY CONTROL

First of all controller is a device or a set of algorithms designed to manage, command, direct, or regulate the behavior of other devices or systems. It is an essential part of a control system, which includes sensors, actuators, and other components that interact to achieve a desired performance. There are various types of controllers used in control systems, each designed for specific applications and performance criteria. Here are some of the main types: PID Controller (Proportional-Integral-Derivative, Feedforward Controller, On-Off Controller, Adaptive Controller, Optimal Control, Robust Control, Sliding Mode Controller, Model Predictive Control (MPC). Linear Quadratic Regulator (LQR) has been selected as one of the optimal control types because it is important to minimize the time in shimmy phenomenon.

4.1 Linear Quadratic Regulator (LQR)

The Linear Quadratic Regulator (LQR) is an optimal state-feedback control method specifically designed to calculate the most effective control input by using performance indices and state variables to minimize a predefined cost function. This technique, a part of modern control theory, utilizes state-space representations for analyzing the system it's applied to. The main goal in the LQR control system is to derive the gain matrix K by minimizing the cost function.

$$u = -Kx \tag{4.1}$$

$$J = \frac{1}{2}\int_0^\infty [x^T Q x + u^T R u] dt \tag{4.2}$$

J, is the cost function, is the objective function that the LQR controller aims to minimize. It typically represents the cumulative cost over time, accounting for both the states of the system and the control efforts. The Q and R matrices are known as weighting matrices and allow the control designer to adjust the weight values affecting the control inputs and state variables, thereby tuning their impact on system performance. The size of the Q matrix is defined by the number of state variables in the system. The extent of control performance allocated to a state variable is determined by the importance given to the first element of the Q matrix, and the deployment of control power is directly proportional to the magnitude of the element. The final LQR gain is calculated using the equation provided:

$$K = R^{-1}B^{T}P \tag{4.3}$$

The Algebraic Riccati Equation is used to determine the constant matrix P:

$$Q + A^{T}P + PA + PBR^{-1}B^{T}P = 0 \tag{4.4}$$

4.1.1 LQR controller design for 1 DOF system

An LQR design is implemented to control torsional stability in a 1 DOF 3rd order system. The graphs provided in sections 3.3.1.1 and 3.3.1.2 will demonstrate how unstable systems can be stabilized. The Q and R matrices necessary to determine the K gain have been chosen based on simulations as follows:

$$Q = \begin{bmatrix} 100 & 0 & 0 \\ 0 & 300 & 0 \\ 0 & 0 & 100 \end{bmatrix} \tag{4.5}$$

$$R = \{0.025\} \tag{4.6}$$

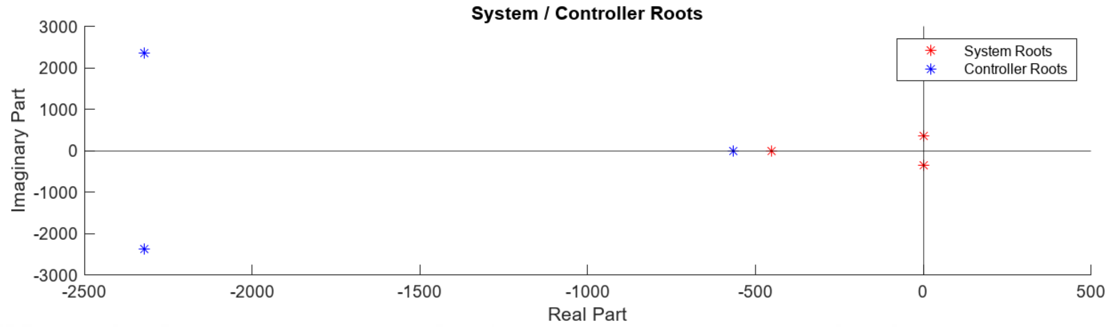

Figure 4.1 : 1 DOF Stability region of e-V plane for k=100000 Nm/rad & V=120 m/s & e=0.1325 m (Roots).

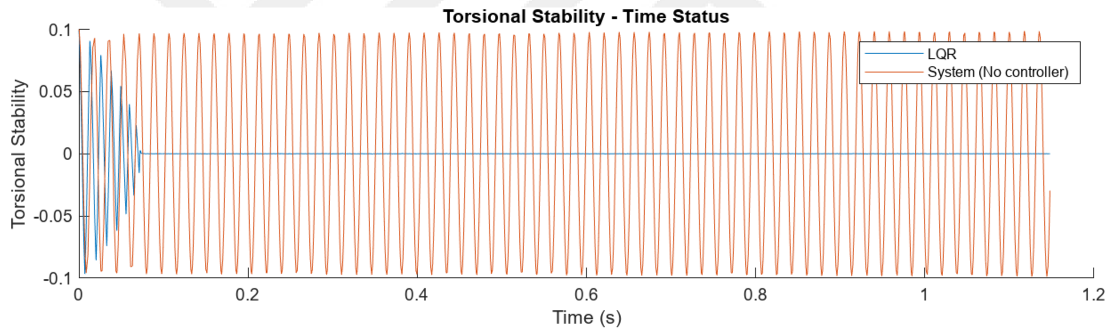

Figure 4.2 : 1 DOF Stability region of e-V plane for k=100000 Nm/rad & V=120 m/s & e=0.1325 m (System/LQR).

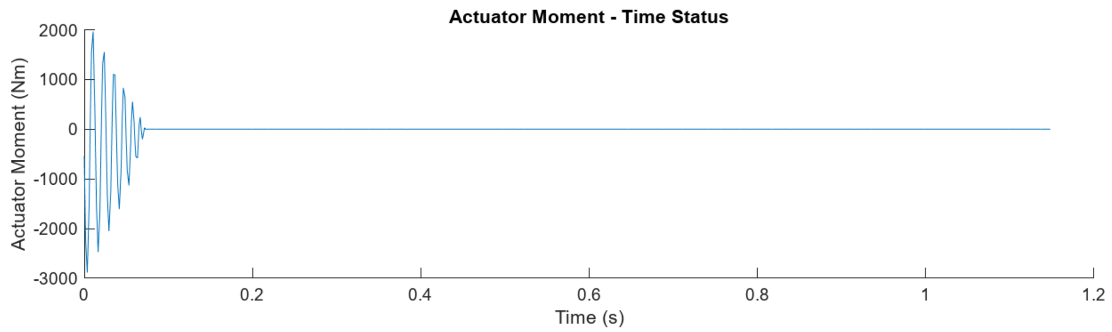

Figure 4.3 : 1 DOF Stability region of e-V plane for k=100000 Nm/rad & V=120 m/s & e=0.1325 m (Actuator moment).

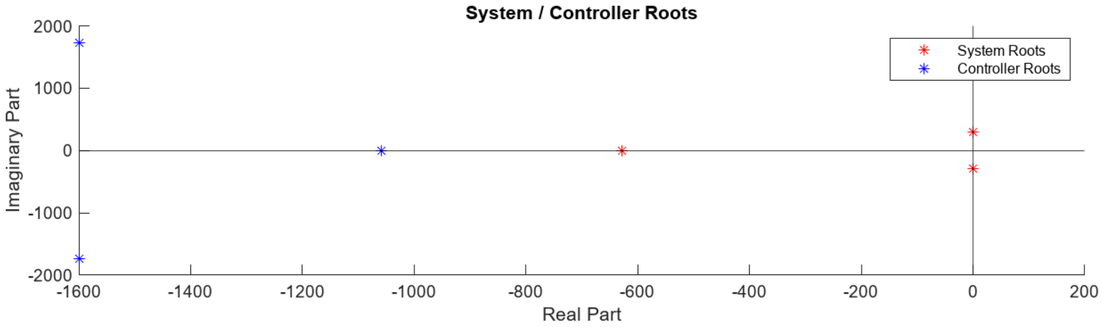

Figure 4.4 : 1 DOF Stability region of e-V plane for k=50000 Nm/rad & V=173 m/s & e=0.14 m (Roots).

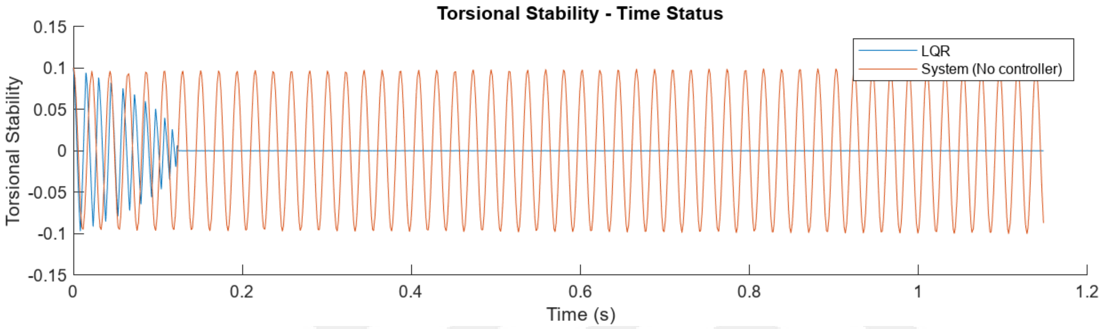

Figure 4.5 : 1 DOF Stability region of e-V plane for k=50000 Nm/rad & V=173 m/s & e=0.14 m (System/LQR).

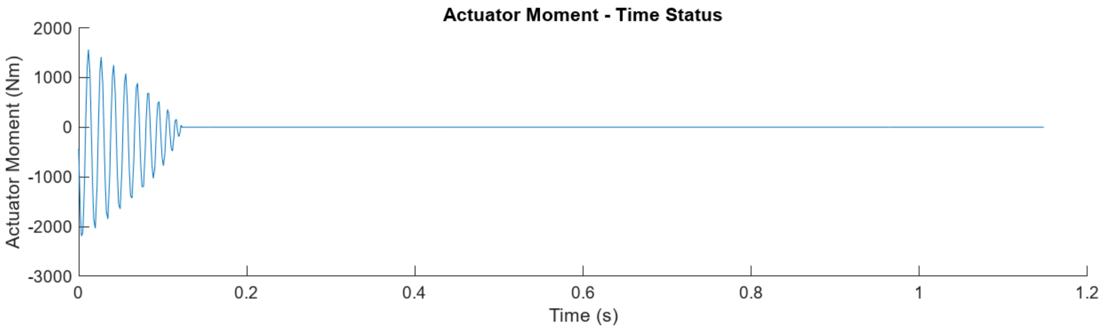

Figure 4.6 : 1 DOF Stability region of e-V plane for k=50000 Nm/rad & V=173 m/s & e=0.14 m (Actuator moment).

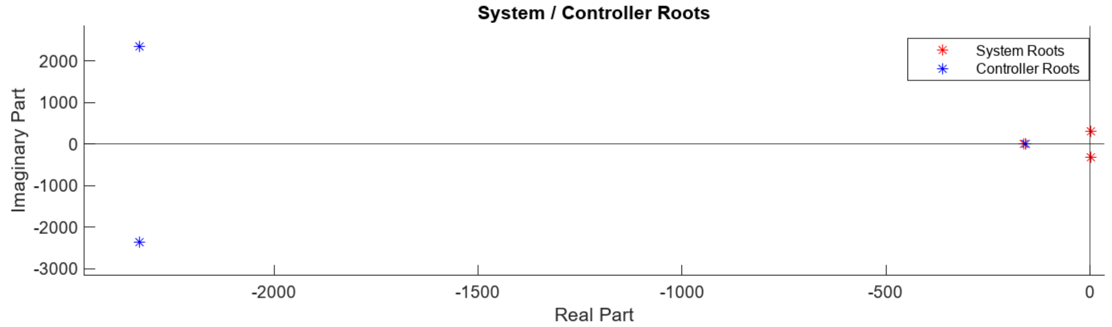

Figure 4.7 : 1 DOF Stability region of F_z-V plane for k=100000 Nm/rad & V=30 m/s & F=19000 N (Roots).

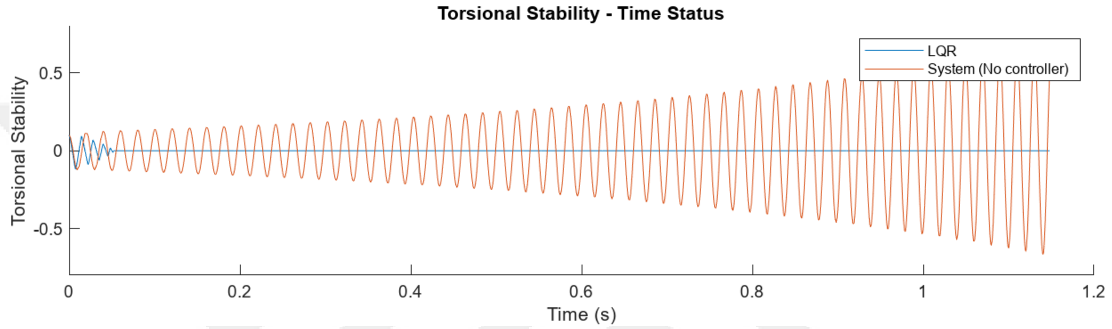

Figure 4.8 : 1 DOF Stability region of F_z-V plane for k=100000 Nm/rad & V=30 m/s & F=19000 N (System/LQR).

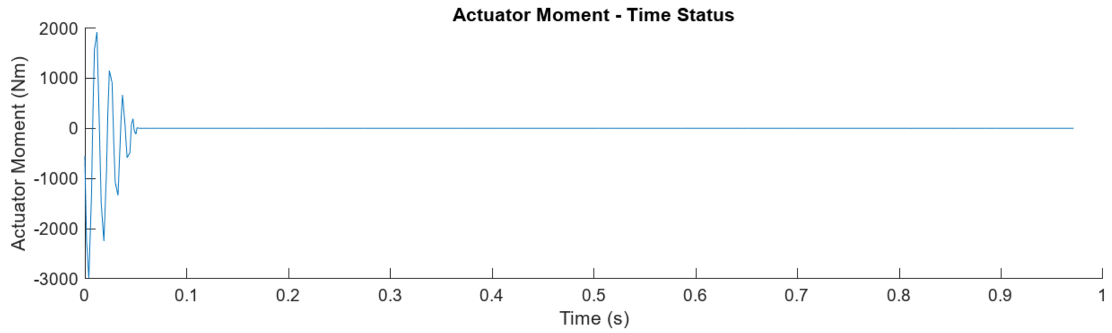

Figure 4.9 : 1 DOF Stability region of e-V plane for k=100000 Nm/rad & V=30 m/s & F=19000 N (Actuator moment).

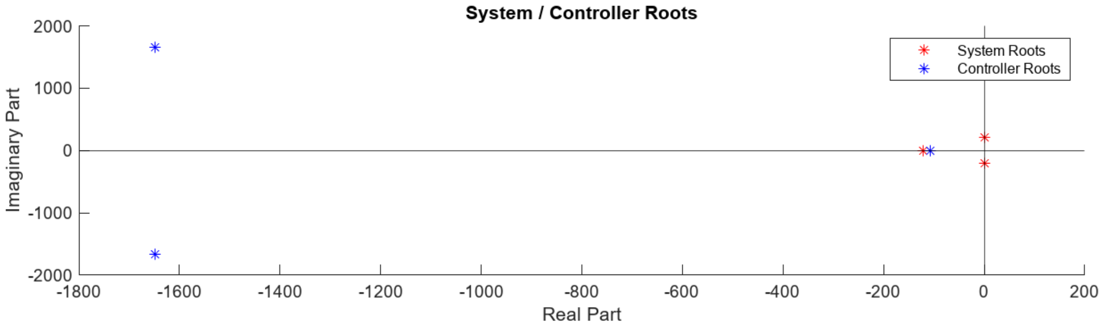

Figure 4.10 : 1 DOF Stability region of F_z-V plane for k=50000 Nm/rad & V=15 m/s & F=19000 N (Roots).

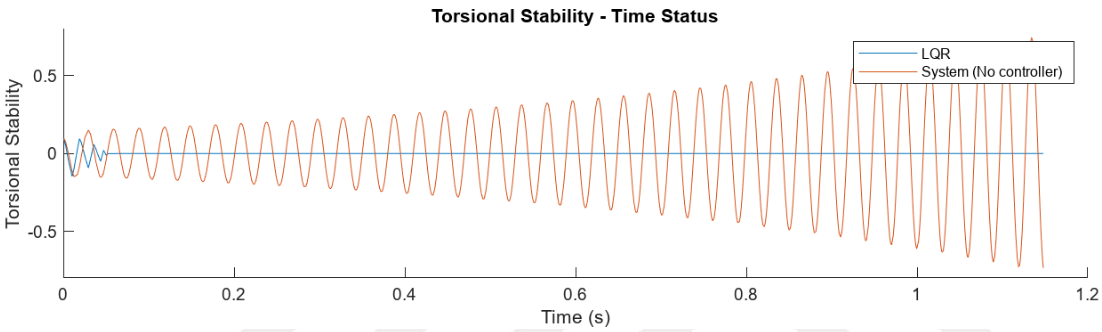

Figure 4.11 : 1 DOF Stability region of F_z-V plane for k=50000 Nm/rad & V=15 m/s & F=19000 N (System/LQR).

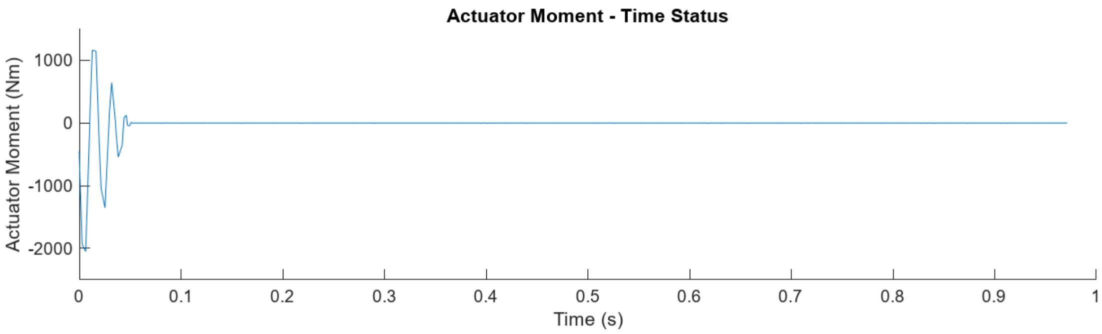

Figure 4.12 : 1 DOF Stability region of e-V plane for k=50000 Nm/rad & V=15 m/s & F=19000 N (Actuator moment).

4.1.2 LQR controller design for 2 DOF system

An LQR design is implemented to control torsional stability in a 1 DOF 3rd order system. The graphs provided in sections 3.4.1.1 and 3.4.1.2 will demonstrate how unstable systems can be stabilized. The Q and R matrices necessary to determine the K gain have been chosen based on simulations as follows:

$$Q = \begin{bmatrix} 100 & 0 & 0 & 0 & 0 \\ 0 & 300 & 0 & 0 & 0 \\ 0 & 0 & 100 & 0 & 0 \\ 0 & 0 & 0 & 100 & 0 \\ 0 & 0 & 0 & 0 & 100 \end{bmatrix} \tag{4.7}$$

$$R = \{0.025\} \tag{4.8}$$

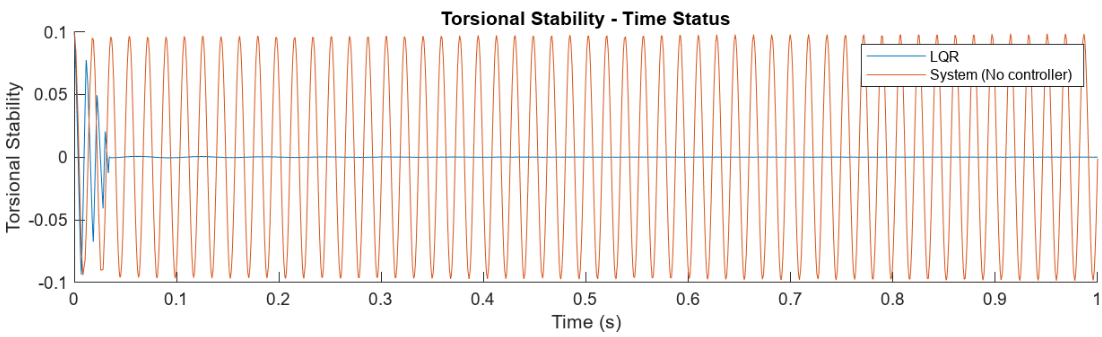

Figure 4.13 : 2 DOF Stability region of e-V plane for k=100000 Nm/rad & V=103 m/s & e=0.125 m (System/LQR).

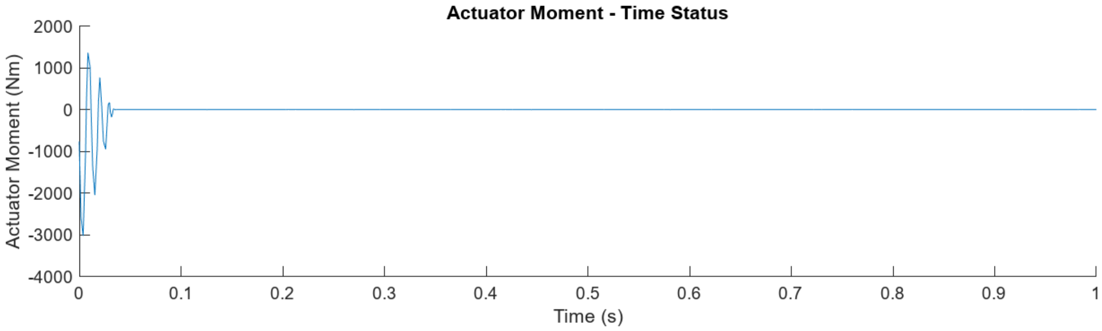

Figure 4.14 : 2 DOF Stability region of e-V plane for k=100000 Nm/rad & V=103 m/s & e=0.125 (Actuator moment).

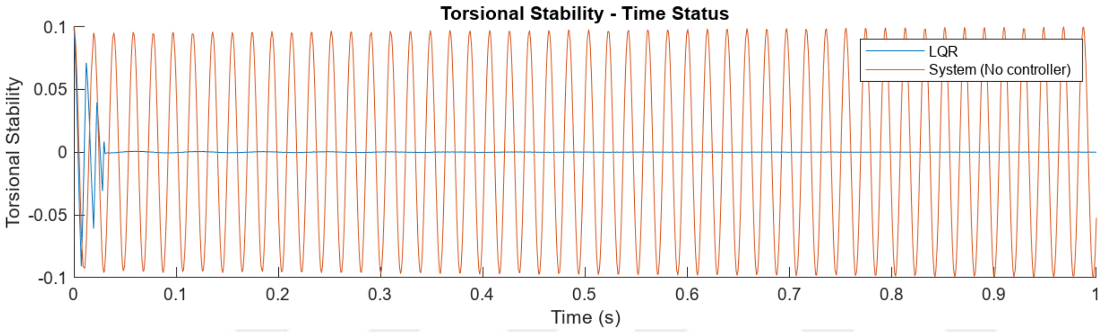

Figure 4.15 : 2 DOF Stability region of e-V plane for k=75000 Nm/rad & V=140 m/s & e=0.13 m (System/LQR).

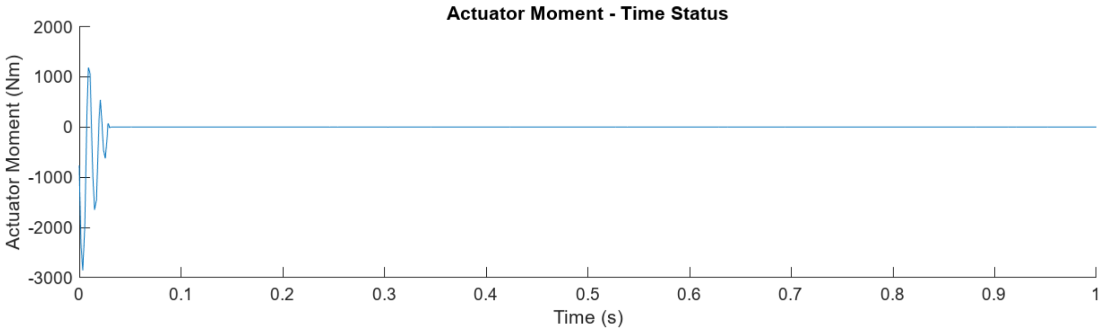

Figure 4.16 : 2 DOF Stability region of e-V plane for k=75000 Nm/rad & V=140 m/s & e=0.13 (Actuator moment).

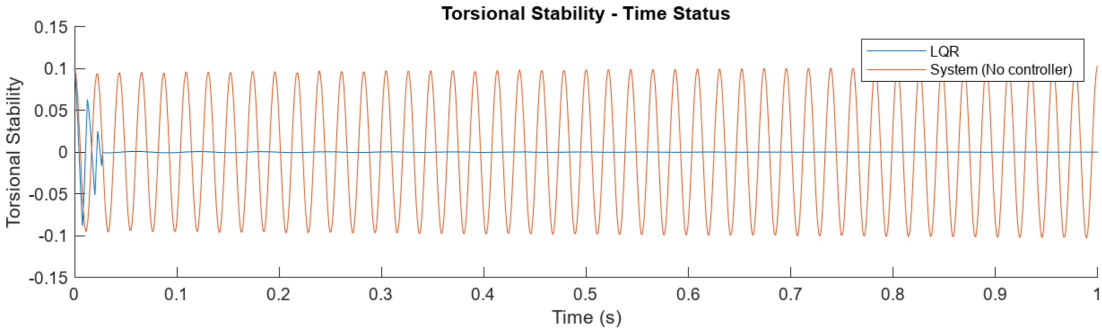

Figure 4.17 : 2 DOF Stability region of e-V plane for k=50000 Nm/rad & V=154 m/s & e=0.13 m (System/LQR).

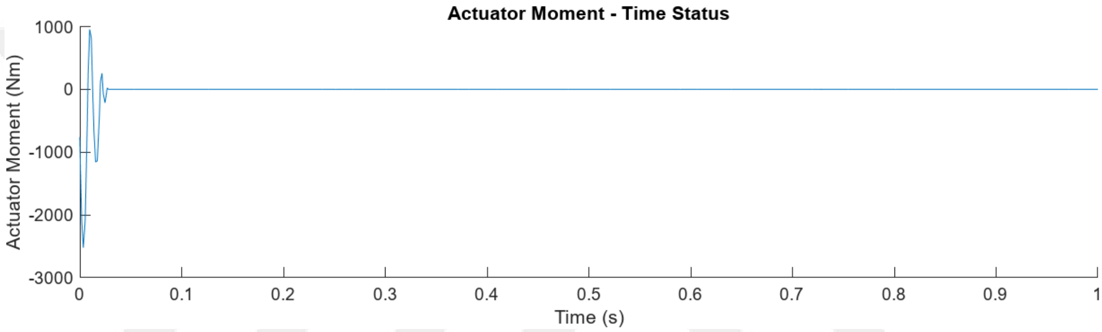

Figure 4.18 : 2 DOF Stability region of e-V plane for k=50000 Nm/rad & V=154 m/s & e=0.13 (Actuator moment).

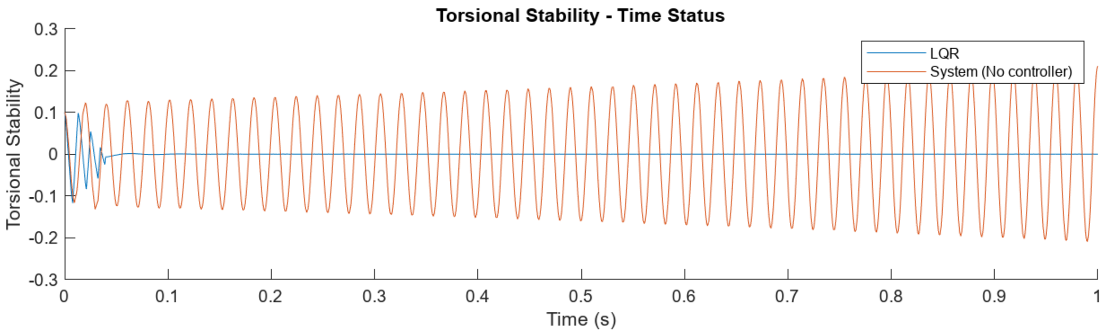

Figure 4.19 : 2 DOF Stability region of F_z-V plane for k=100000 Nm/rad & V=24 m/s & F_z=19000 N (System/LQR).

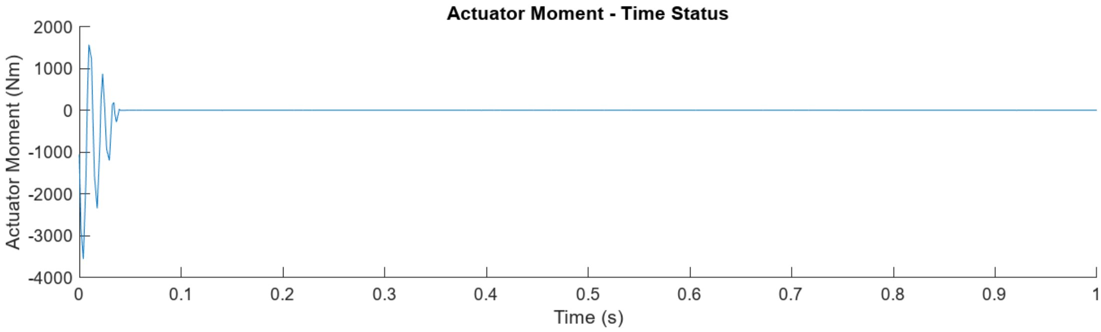

Figure 4.20 : 2 DOF Stability region of F_z -V plane for k=100000 Nm/rad & V=24 m/s & F_z =19000 N (Actuator moment).

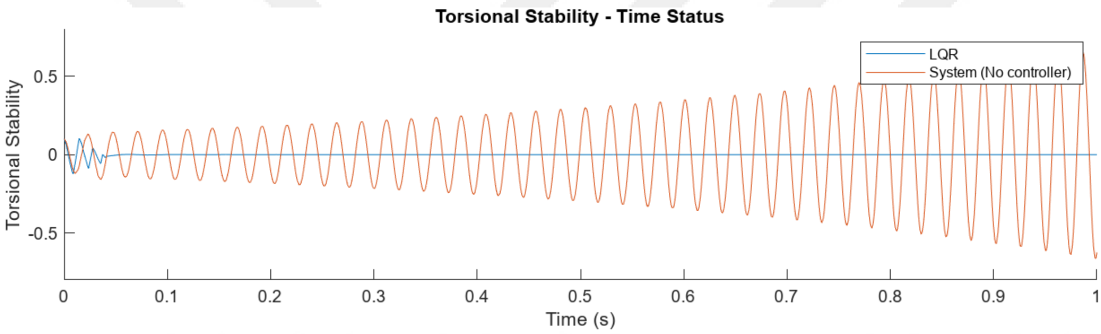

Figure 4.21 : 2 DOF Stability region of F_z-V plane for k=75000 Nm/rad & V=17 m/s & F_z=19000 N (System/LQR).

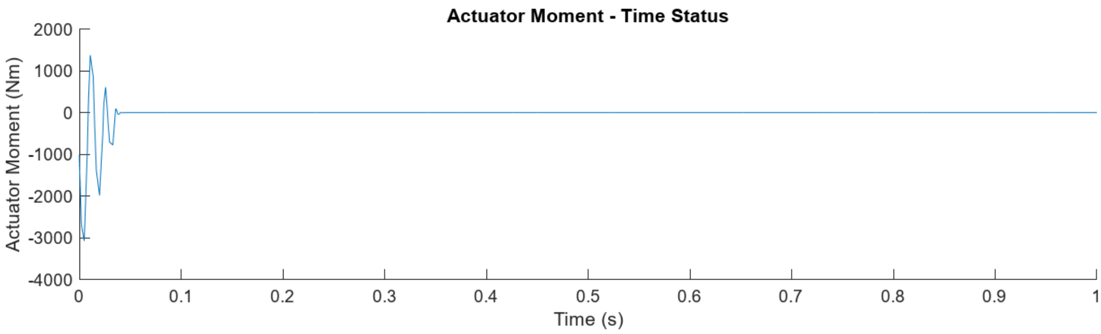

Figure 4.22 : 2 DOF Stability region of F_z -V plane for k=75000 Nm/rad & V=17 m/s & F_z =19000 N (Actuator moment).

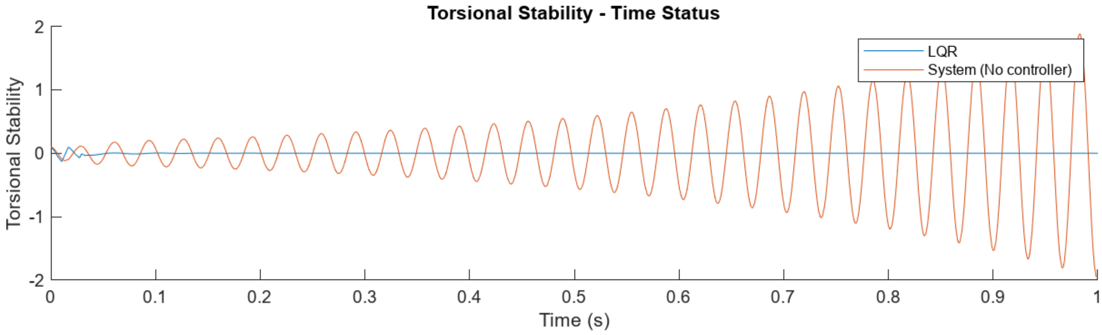

Figure 4.23 : 2 DOF Stability region of F_z-V plane for k=50000 Nm/rad & V=7 m/s & F_z=19000 N (System/LQR).

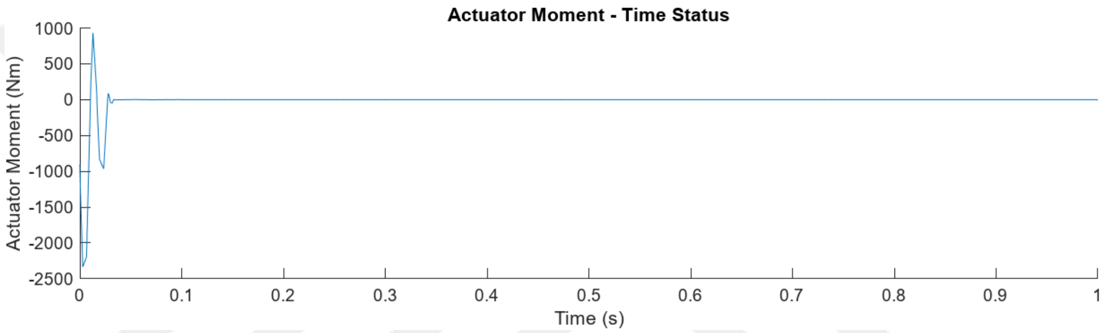

Figure 4.24 : 2 DOF Stability region of F_z -V plane for k=50000 Nm/rad & V=7 m/s & F_z =19000 N (Actuator moment).

Shimmy oscillation is a highly dangerous phenomenon that can lead to accidents if not properly addressed. Thus, it requires thorough analysis. In previous sections, a linear controller was designed to stabilize conditions that were identified as unstable. As shown in Figures 4.1, 4.4, 4.7 and 4.10 the roots of the uncontrolled systems have positive real roots, indicating instability. However, in the same graphs, it can be observed that the designed controller shifts the real roots of these roots to the negative side, stabilizing the system. This stabilization is clearly demonstrated in Figures 4.2, 4.5, 4.8, 4.11, 4.13, 4.15, 4.17, 4.19, 4.21 and 4.23. Moreover, for the designed controller to take action, an actuator is necessary. The moment values of this actuator are provided in Figures 4.3, 4.6, 4.9, 4.12, 4.14, 4.16, 4.18, 4.20, 4.22 and 4.24. The moment values do not exceed 3500 Nm, which is within the capabilities of actuators currently available on the market. This consideration was taken into account during the controller design process.

5. LANDING GEAR SHIMMY APPLICATION DESIGN (LaGeSh)

The shimmy phenomenon depends on many parameters, and controlling these parameters is quite challenging. Therefore, to facilitate a better understanding of this phenomenon, an application named LaGeSh was developed in this thesis. This application possesses numerous capabilities. It can be used to identify potential shimmy scenarios during the design phase or for an already designed landing gear. The application is composed of five tabs. In the first tab, as shown in Figure 5.1, the parameters used for either the 1 DOF third order or 2 DOF fifth order model are listed, along with their meanings and units. The necessary parameters for the selected model type are displayed accordingly.

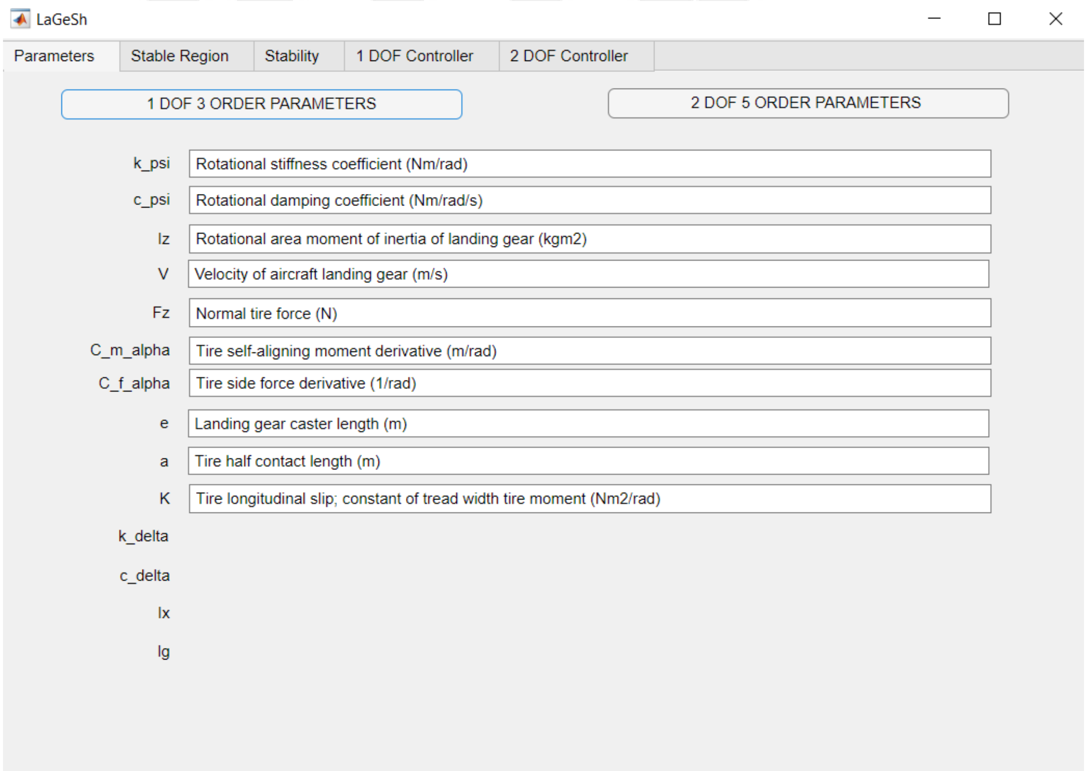

Figure 5.1 : LaGeSh parameters table.

The second tab, Figure 5.2, is where you can examine the stable regions. In this tab, depending on the selection of 1 DOF or 2 DOF, the required parameters become visible. After the parameters are displayed, you need to choose between the V-e (Velocity-Caster Length) or V-Fz (Velocity-Normal Tire Force) options. Based on the selection, you must enter the desired working ranges. Once these parameters are entered, you can select the method to generate the graph, either the eigenvalue method or the Routh-Hurwitz method, by pressing the corresponding button. The desired graph will then be generated.

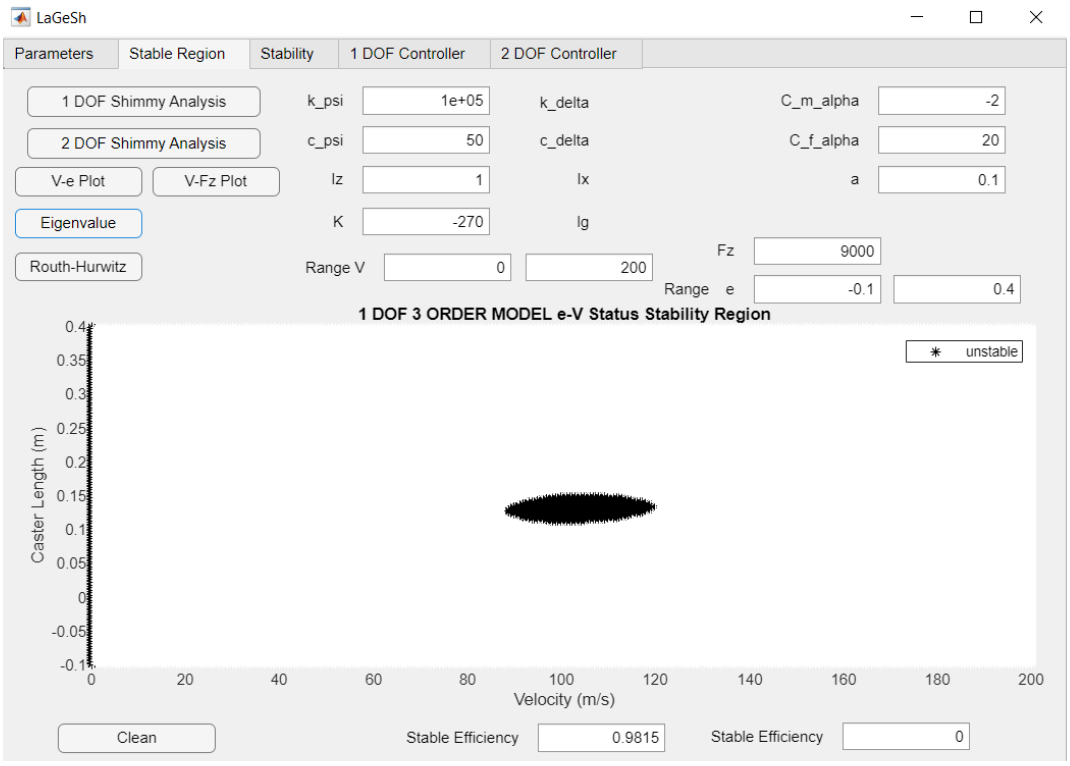

Figure 5.2 : LaGeSh stable region table.

In the tab shown in Figure 5.3, similar to the previous tab, you need to select either the 1 DOF or 2 DOF model. Based on the selected model, its parameters will become visible. In this tab, you enter the values for these parameters and set the runtime. After that, the system is run, and the results are displayed in the plot screen below.

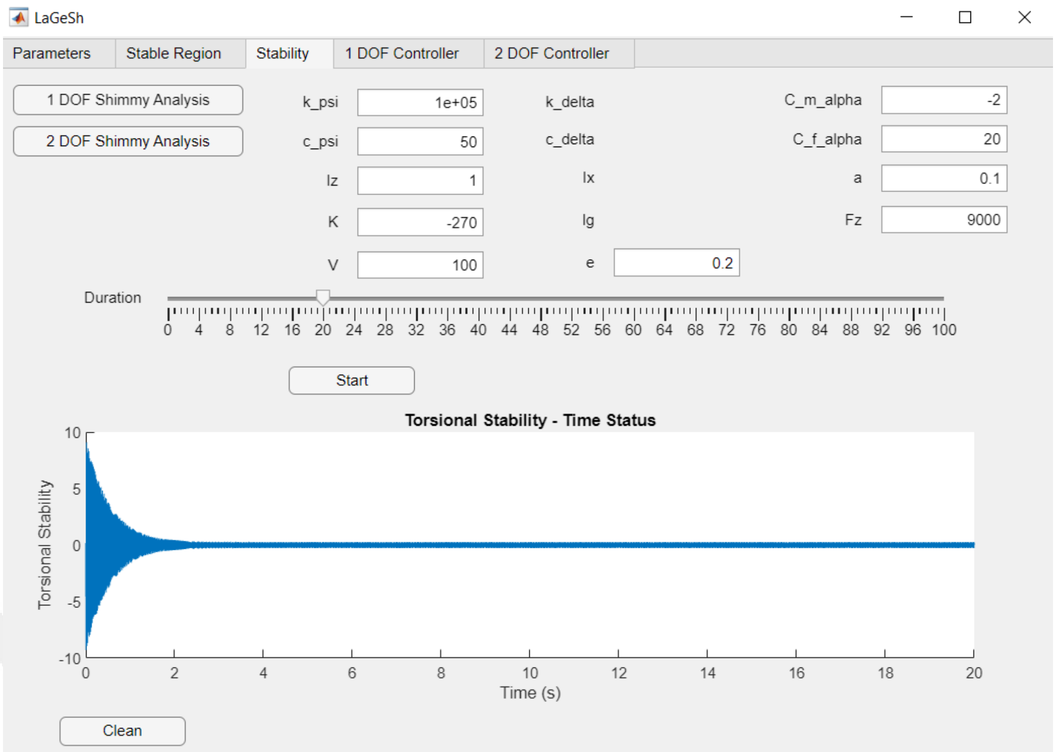

Figure 5.3 : LaGeSh stability table.

We can evaluate the last two tabs together. The fourth tab is used for 1 DOF controller design, and the fifth tab is for 2 DOF controller design. Figure 5.4 and Figure 5.5 show the tab layouts. In the top left corner of the opened screen, there are three types of controller operations available. This thesis discusses the design of an LQR controller. Depending on the selected controller, the required parameters become visible. Once the desired values are entered into the system, three buttons appear. The 'Start' button provides the torsional stability-time curve without a controller and with the selected controller. The 'Roots' button shows the roots of the system, displaying the roots for both the system and the designed controller. Finally, the 'Moment' button indicates the amount of torque required by the system according to the designed controller.

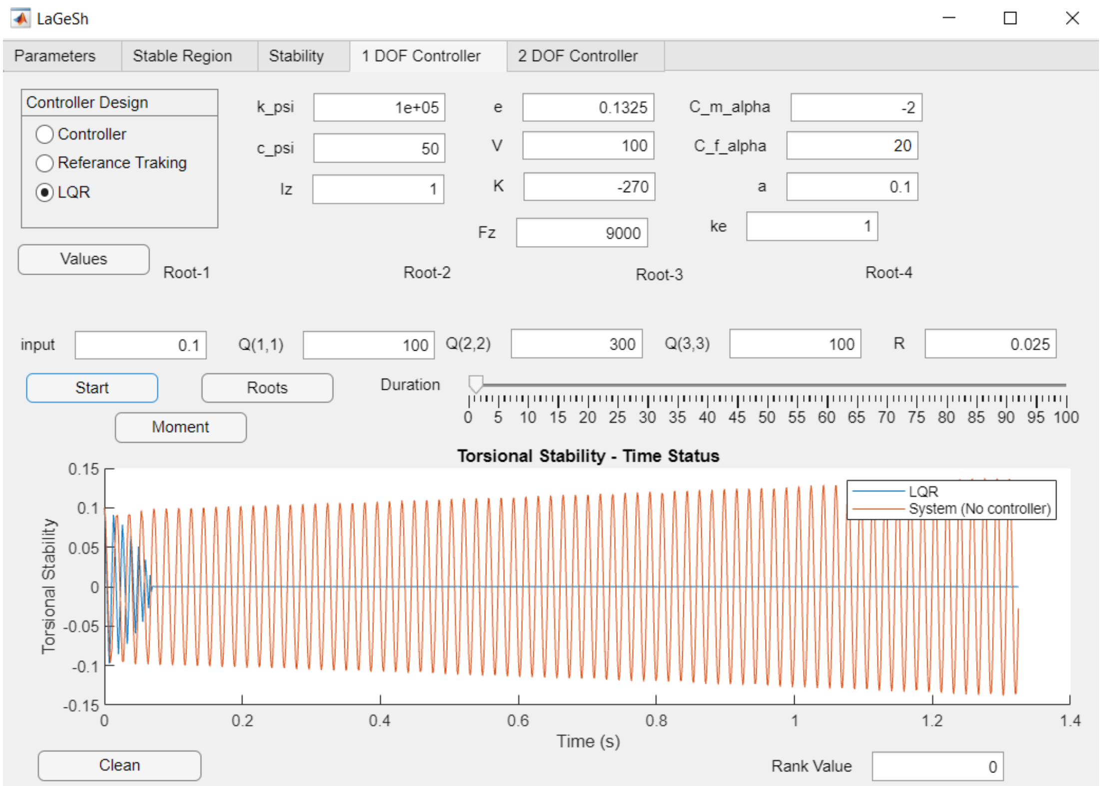

Figure 5.4 : LaGeSh 1 DOF Controller table.

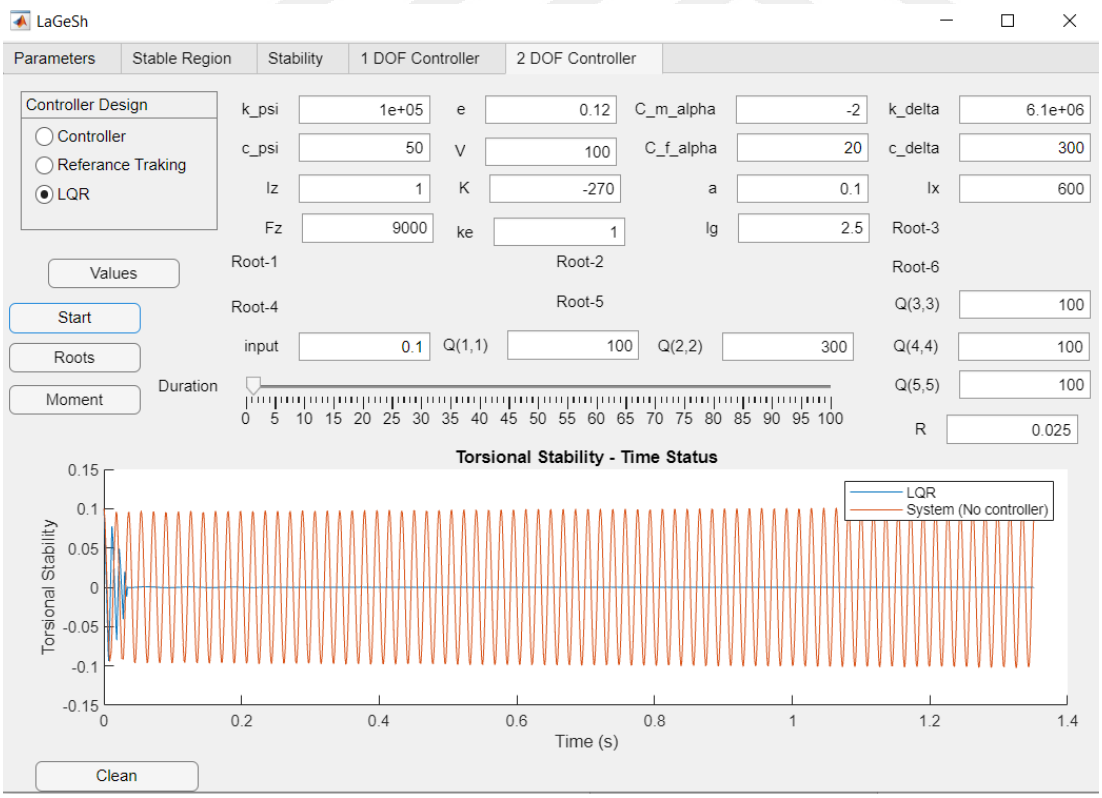

Figure 5.5 : LaGeSh 2 DOF Controller table.

6. CONCLUSION AND FUTURE WORK

This study presents a comprehensive investigation into the phenomenon of shimmy oscillations in aircraft landing gear systems. By focusing on both 1-DOF and 2-DOF models, the thesis presents a detailed analysis of the factors contributing to this instability. The results obtained through this research have demonstrated the critical importance of understanding shimmy oscillations for ensuring aircraft safety and performance. Key findings include the importance of considering the relationship between caster length and aircraft speed during the design phase. For existing aircraft, reducing the normal tire force by adjusting the aircraft's center of gravity is recommended. The study also revealed that increasing rotational stiffness and reducing normal tire force can enhance system stability.

Furthermore, the analysis showed that the system's stability is influenced by a combination of caster length, aircraft speed, and rotational stiffness. Controller designs were successfully implemented to stabilize unstable conditions. The development of the LaGeSh application facilitated comprehensive parameter analysis, providing valuable insights for landing gear design and optimization.

To ensure research reliability, eigenvalue analysis, Routh-Hurwitz criteria, and Simulink models were employed in specific cases.

6.1 Future Recommendations

Building upon the results of this study, future research should include developing and analyzing nonlinear models, conducting in-depth studies on various landing gear types (articulated, semi-articulated, cantilevered), and modeling the entire aircraft to assess its impact on shimmy characteristics. Additionally, incorporating friction into the model, examining the effects of braking, and conducting rigorous testing to refine system parameters are essential for improving model accuracy. Exploring different controller designs and conducting stability analysis without the rank angle assumption can provide valuable insights for optimizing landing gear performance.

REFERENCES

[1] **B. von Schlippe, & R. Dietrich** (1941). Shimming of a pneumatic wheel.

[2] **Moreland, R. J.** (1954). The Story of Shimmy, *Journal of the Aeronautical Sciences*, ***21***, 12, 793-.

[3] **Pacejka, H. B.** (1966). *The Wheel Shimmy Phenomenon* (Dissertation), Delf University of Technology

[4] **Roger L. C.** (1972). Theoretical tire equations for shimmy and other dynamic studies, AIAA Journal of Aircraft, 585-589

[5] **Grossman, D**. **T**. (1980). F-15 nose landing gear shimmy, taxi test and corrective analyses, *SAE technical paper 801239*

[6] **Somienski, G.** (1997). Shimmy Analysis of a Simple Aircraft Nose Landing Gear Model Using Different Mathematical Methods, Aerospace Science and Technology, 545-555

[7] **Besselink, I. J. M.** (2000). *Shimmy of Aircraft Main Landing Gears* (Dissertation), Technical University of Delft.

[8] **Long, S. H.** (2006). *Active Control of Shimmy Oscillation in Aircraft Landing Gear* (Dissertation), Concordia University.

[9] **Atabay E.** (2012) Dynamics of a Landing Gear Mechanism (Dissertation), Istanbul Technical University.

[10] **Buts D., & Kogan, A.** (2010). Helicopter Landing Gear Shimmy Analysis, *Conferance*, San Francisco, California, USA

[11] **Abba A., Carrera E., & Grossini, M.** (2001). Dynamic Models for Shimmy Analysis of Helicopter Landing Gear, *EUROMECH-427*

[12] **Çakır U., Sezer S.** (2019). Burun İniş Takımında Meydana Gelen Shimmy Titreşim Hareketinin PID ve LQR ile Kontrolü. TOK'2019 Otomatik Kontrol Ulusal Toplantısı, Muğla.

[13] **Özgen S., Middle East Technical University, Aerospace Engineering.** (2017). *Aeronautical Engineering Design I Landing Gear Sizing and Placement* [PowerPoint slides]. Retrieved from http://www.ae.metu.edu.tr/~ae451/lecture10_landing_gear.pdf

[14] **Arreaza, C.** (2015). *Linear Stability Analysis, Dynamic Response, and Design of Shimmy Dampers for Main Landing Gears* (Dissertation), University of Toronto

[15] **Ünlüsoy Y. S.,** Middle East Technical University, Mechanical Engineering. *Vehicle Dynamics* [PowerPoint slides].

[16] **Roskam J.,** (1989). Airplane design. Part IV layout design of landing gear design analysis and research

[17] **Currey N. S.,** (1988). Aircraft Landing Gear Design: Principles, AIAA Education Series

[18] **Barve S., & Menghani R., & Patel J., & Shetty D.**(2017). Optimization of an Oleo-Pneumatic Shock Absorber for Main Landing Gear of a Commercial Aircraft, International Conference on Advances in Thermal Systems, Materials and Design Engineering (ATSMDE2017)

[19] **Schmidt R. K.,** (2021). The Design of Aircraft Landing Gear, SAE Interinational

[20] **Farroni F.,** (2014) DEVELOPMENT OF A GRIP & THERMODYNAMICS SENSITIVE TYRE / ROAD INTERACTION FORCES ESTIMATION PROCEDURE EMPLOYED IN HIGH-PERFORMANCE VEHICLES SIMULATION (Dissertation), Universita’ Degli Studi Di Napoli Federico II

[21] **Krüger W. R, Morandini M.,** (1989). Numerical Simulation of Landing Gear Dynamics: State-of-the-art and Recent Developments

[22] **Tourajizadeh H., Zare S.,** (2015). Robust and optimal control of shimmy vibration in aircraft nose landing gear, Aerospace Science and Technology

APPENDICES

APPENDIX A: Landing Gear Shimmy Controller Design Graphics

APPENDIX A

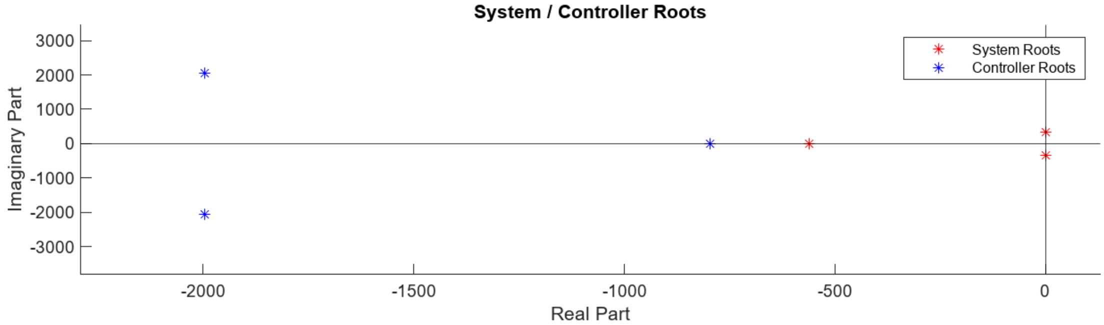

Figure A.1 : 1 DOF Stability region of e-V plane for k=75000 Nm/rad & V=153 m/s & e=0.135 m (Roots).

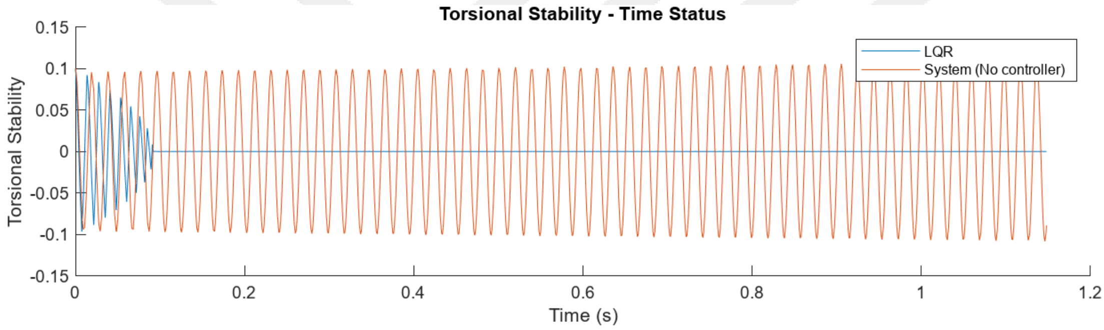

Figure A.2 : 1 DOF Stability region of e-V plane for k=75000 Nm/rad & V=153 m/s & e=0.135 m (System/LQR).

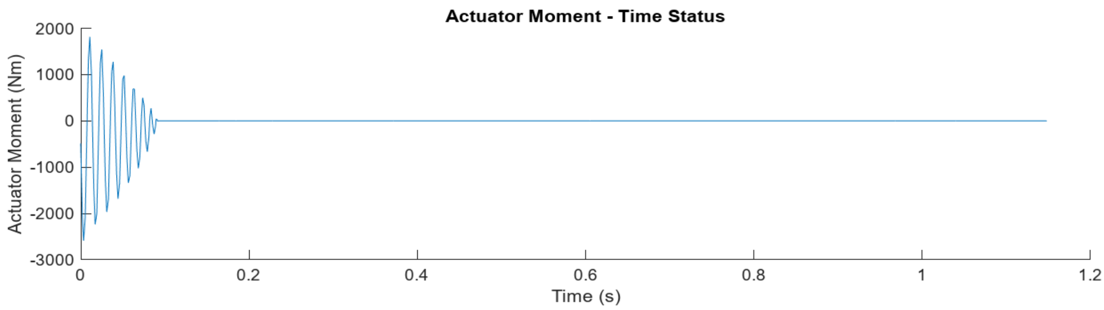

Figure A.3 : 1 DOF Stability region of e-V plane for k=75000 Nm/rad & V=153 m/s & e=0.135 m (Actuator moment).

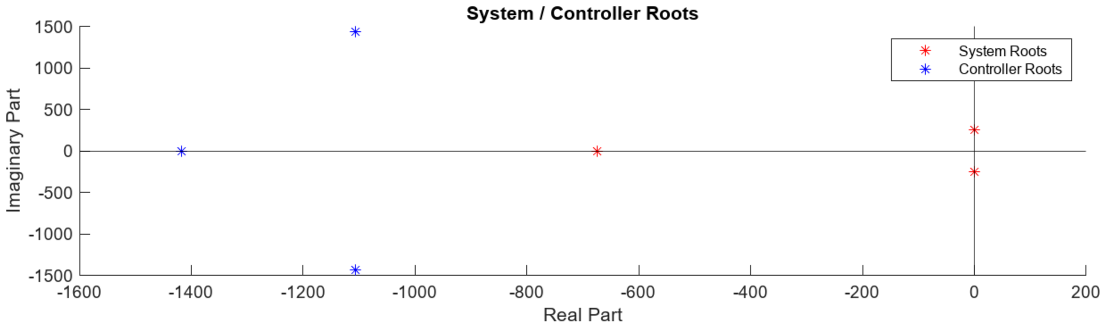

Figure A.4 : 1 DOF Stability region of e-V plane for k=25000 Nm/rad & V=187 m/s & e=0.14 m (Roots).

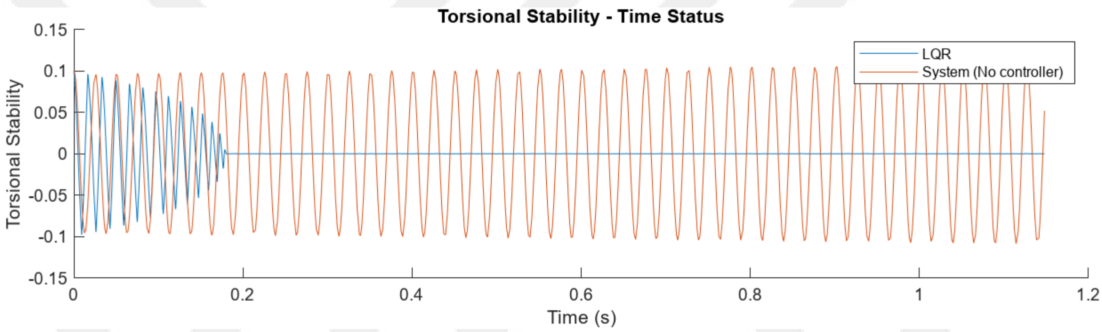

Figure A.5 : 1 DOF Stability region of e-V plane for k=25000 Nm/rad & V=187 m/s & e=0.14 m (System/LQR).

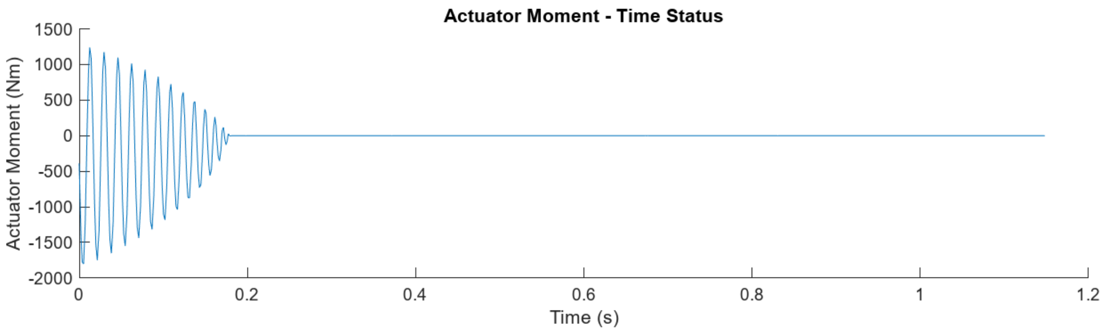

Figure A.6 : 1 DOF Stability region of e-V plane for k=25000 Nm/rad & V=187 m/s & e=0.14 m (Actuator moment).

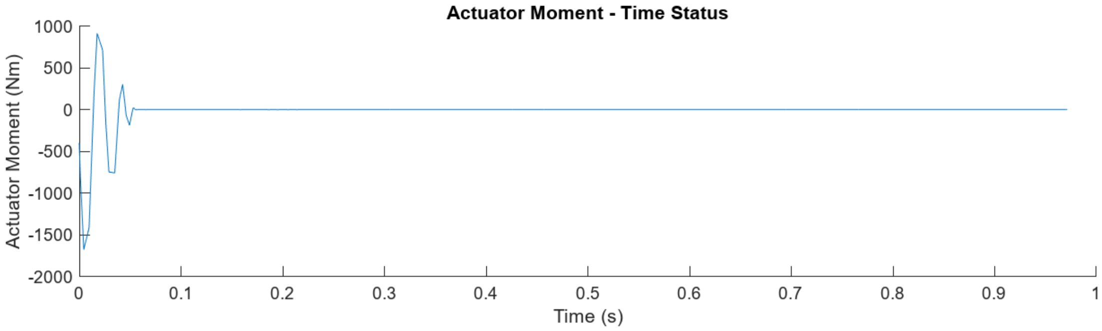

Figure A.7 : 1 DOF Stability region of F_z-V plane for k=25000 Nm/rad & V=8 m/s & F=19000 N (Roots).

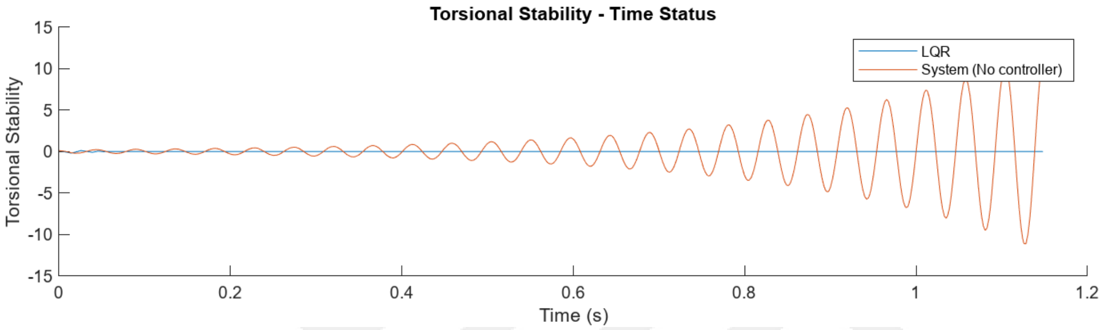

Figure A.8 : 1 DOF Stability region of F_z-V plane for k=25000 Nm/rad & V=8 m/s & F=19000 N (System/LQR).

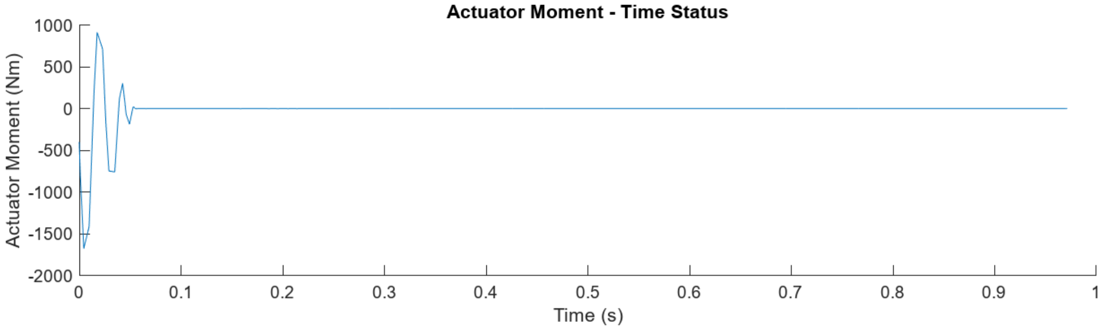

Figure A.9 : 1 DOF Stability region of e-V plane for k=25000 Nm/rad & V=8 m/s & F=19000 N (Actuator moment).

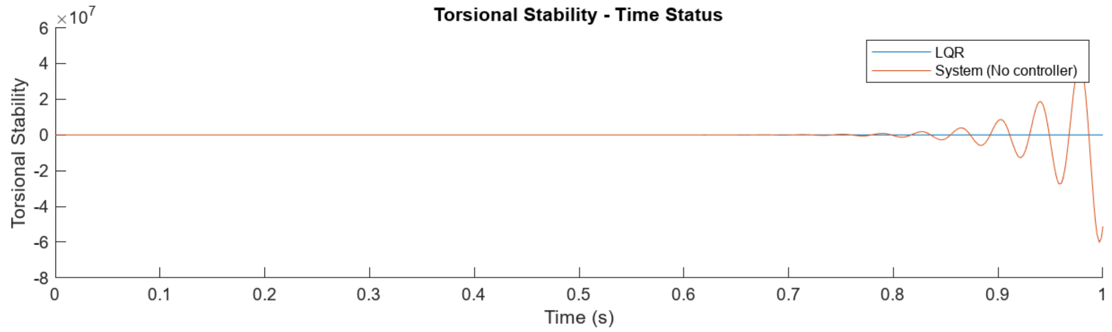

Figure A.10 : 2 DOF Stability region of F_z-V plane for k=25000 Nm/rad & V=7 m/s & F_z=19000 N (System/LQR).

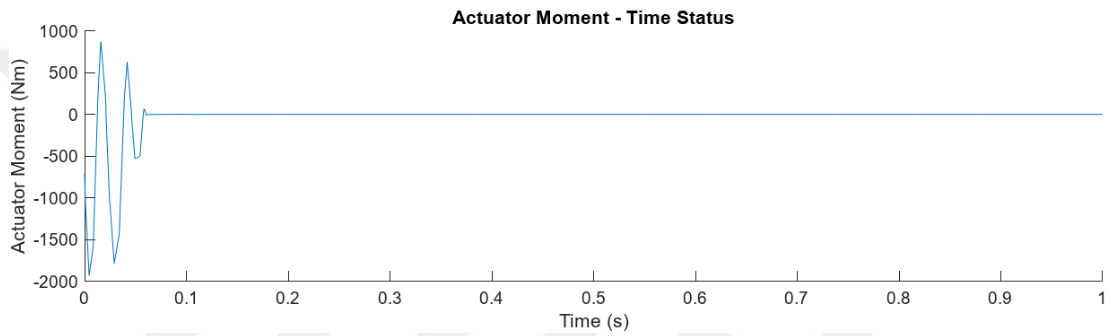

Figure A.11 : 2 DOF Stability region of F_z -V plane for k=25000 Nm/rad & V=7 m/s & F_z =19000 N (Actuator moment).

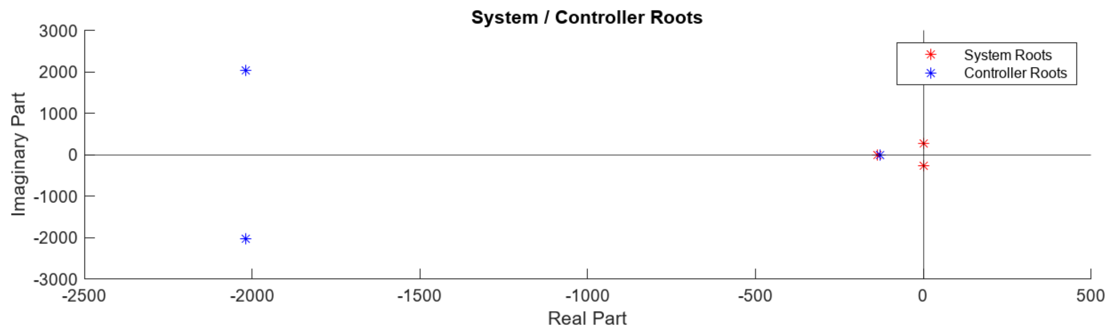

Figure A.12 : 1 DOF Stability region of F_z-V plane for k=75000 Nm/rad & V=22 m/s & F=19000 N (Roots).

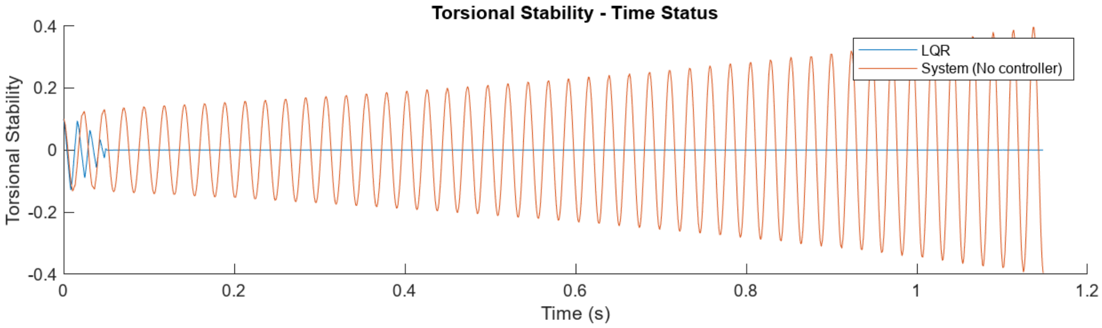

Figure A.13 : 1 DOF Stability region of F_z-V plane for k=75000 Nm/rad & V=22 m/s & F=19000 N (System/LQR).

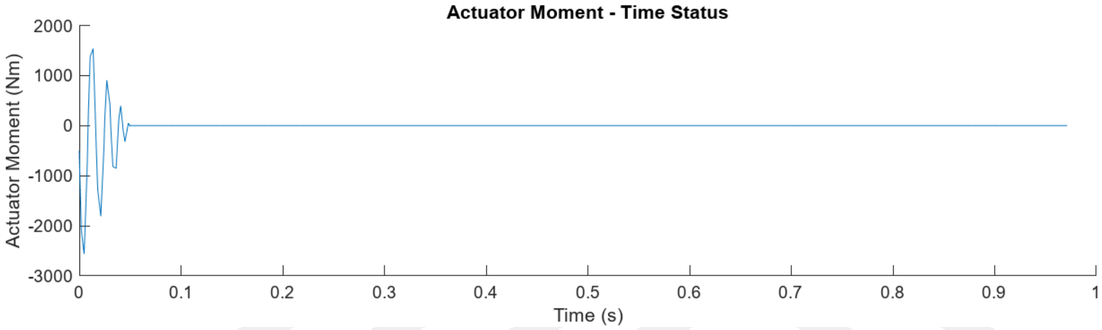

Figure A.14 : 1 DOF Stability region of e-V plane for k=75000 Nm/rad & V=22 m/s & F=19000 N (Actuator moment).

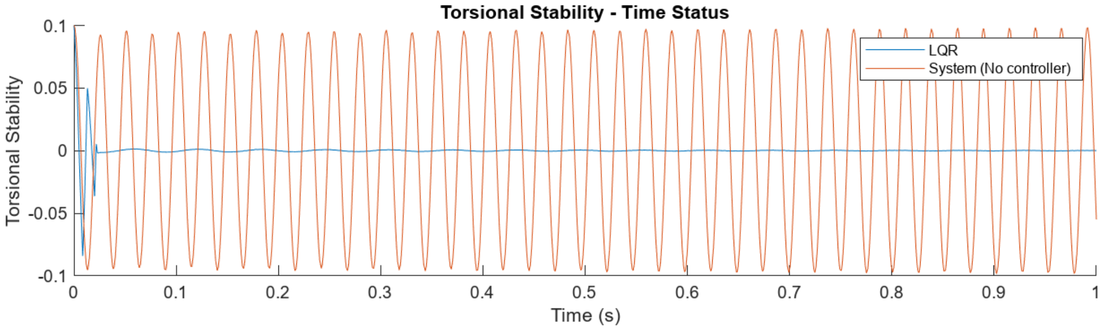

Figure A.15 : 2 DOF Stability region of e-V plane for k=25000 Nm/rad & V=160 m/s & e=0.13 m (System/LQR).

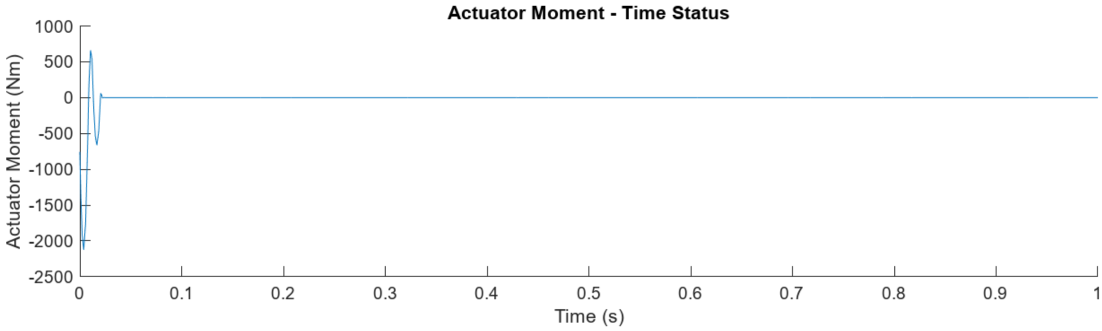

Figure A.16 : 2 DOF Stability region of e-V plane for k=25000 Nm/rad & V=160 m/s & e=0.13 (Actuator moment).

CURRICULUM VITAE

Name Surname : Kemal OKUYAN

EDUCATION :

- **B.Sc.** : 2020, Yildiz Technical University, Mechanical Faculty, Mechanical Engineering

PROFESSIONAL EXPERIENCE AND REWARDS:

- 2021-[Present] TUSAŞ (Turkish Aerospace Industries)

PUBLICATIONS, PRESENTATIONS AND PATENTS ON THE THESIS:

- Eken S., **Okuyan K.** 2024: Modelling-Control of Shimmy Oscillations in Aircraft Landing Gear Application Design. 3rd International Graduate Research Symposium, May 8-10, 2024 Istanbul, Turkey.